PHYSIK - DEPARTMENT

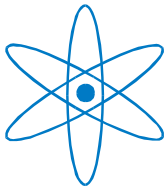

Living Cells and Cytoskeletal Model Systems: Mechanics and Responses to Dynamic Shear

Dissertation
von

Matthias Maier

TECHNISCHE UNIVERSITÄT
MÜNCHEN

TECHNISCHE UNIVERSITÄT MÜNCHEN

Lehrstuhl für Zellbiophysik E27

Living Cells and Cytoskeletal Model Systems: Mechanics and Responses to Dynamic Shear

Matthias Maier

Vollständiger Abdruck der von der Fakultät für Physik der Technischen Universität München zur Erlangung des akademischen Grades eines

Doktors der Naturwissenschaften (Dr. rer. nat.)

genehmigten Dissertation.

Vorsitzender:	Univ.-Prof. Dr. M. Zacharias
Prüfer der Dissertation:	
	1. Univ.-Prof. Dr. A. Bausch
	2. Univ.-Prof. Dr. M. Rief

Die Dissertation wurde am 11.02.2014 bei der Technischen Universität München eingereicht und durch die Fakultät für Physik am 27.05.2014 angenommen.

Summary

In order to proceed through cell cycle and particularly mitosis, living cells need a complex system known as the cytoskeleton to live up to multiple tasks raised by nature. One part of this cytoskeleton is the dynamic bio-polymer actin and its manifold additional regulatory proteins. This actin cytoskeleton offers mechanical stability and is the source for force generation in dynamic processes like mechanotransduction, cell migration and division. One way to generate such forces shows up in the interaction with motor proteins, which step along the actin filaments. These complex cytoskeletal actions are located in a small region at the cell membrane called the actin cortex. While fundamental functions of actin binding proteins have been revealed in measurements with well-defined reconstituted approaches, it is so far unknown yet how cells manage the heterogeneous cytoskeleton in time and space. Crucial findings that may lead to a better understanding of cytoskeleton-dependent regulation processes could be achieved by investigating reconstituted actin networks and cell mechanics. To this end, it is necessary to explore effects of external mechanical stimuli on such minimal actin systems and cells in various cell cycle stages.

For a living cell, the control of binding affinities of actin cross-linkers is of high importance concerning the transition from a in-motile into an motile state. In the case of cancer cells, the transformation into a more motile and invasive type of cells is a major key point in creating metastases. Here, dynamic structures called filopodia come into play. Filopodia dynamics depend on mechanics of actin and fascin structures. Therefore, changing the affinities of actin binding proteins plays an important role in understanding cancer cells on a molecular basis. The first part of this thesis focuses on the effect of mutations in fascin's binding domains on the mechanical and structural properties of *in vitro* actin networks. By combining macrorheology with fluorescence microscopy, it is demonstrated that different mutations in both binding domains lead to an effective shift of linear and nonlinear mechanical properties to higher molar ratios R - while the obtained bundle structures remain wild-type-like and similarly shift.

As polar cross-linkers, fascin and espin form straight bundles within actin networks. These networks incorporate transiently cross-linked bundles, where the thermal fluctuations of the bundle positions and reorganizations within the network are still observable. Nevertheless, there are completely static networks created by the cross-linker filamin that remain unchanged over the course of days. In the second part of this thesis, the very first characterization of structural and mechanical properties of actin-EPLIN networks will be presented. Similar to actin-filamin networks, two pronounced regimes emerge: Low molar ratios of EPLIN to actin lead to a filamentous phase where EPLIN may cross-link single actin filaments. Here, a unique feature is seen for low actin concentration in the formation of actin-EPLIN ring-like structures. At high EPLIN concentrations, a purely

bundled network is formed that exhibits branched bundles. For even higher molar ratios R_{EPLIN}, bundle clusters are observed, which depend less on the actin concentration as in the case of filamin. Rheological data are in good agreement with the bundle onset and formation, but a filamin-like structural saturation is not observed. Here, a difference in network formation processes may occur in comparison to filamin: aggregation may not control the network formation in actin-EPLIN networks to the same extent as in those of actin-filamin.

While reconstituted actin networks provide a powerful tool for a better understanding of the cytoskeleton, *in vivo* mechanical measurements remain an important necessity. Moreover, a comparison of *in vitro* results and *in vivo* cellular behavior is a crucial step in determining biological relevant mechanisms. In this thesis, shear deformations are imposed via a novel developed monolayer shear apparatus, which allows a groundbreaking way of mechanical stimulation of cells in interphase and mitosis. The setup also enables experimenters to measure forces and observe the cells with high quality microscopy. In contrast to 2D mechanostimulation with elastic rubber membranes, no volume changes occur in shear experiments. Furthermore, a full control of adhesive conditions is possible: albumin coated glass prevents cell adhesion during mechanostimulation - which in principal provides a kind of integrin "knock-down" situation. Other coatings with fibronectin or different extracellular matrix compounds are also applicable. With this method, a large quantity of cells can be analyzed and is subjected to molecular inhibitors, which allows to interfere at the molecular level to gain further insight in mechanical properties and outside-in mechanical information processing of the actin cytoskeleton.

At first, this novel setup is introduced to characterize mechanotransduction via high throughput mechanomics: a combination of gene expression analysis with force measurements of a large amount of cells. Both techniques, the mechanostimulation by dynamic shear and gene analysis method qPCR are refined. Cell monolayer rheology is used together with high quality microscopy, while qPCR data is normalized with cell culture data which enables in a unique way to extinguish influences of gene expression before experiments. β-actin, the standard reference gene, is revealed to be unsuitable as a reference due to large variations in gene expression of untreated cells. Myoblasts are sheared and tested on gene regulation and stress-strain relation but no reproducible mechano-induced signal is found. Cells seem to respond very incoherently throughout the experiments. Surprisingly, no adaption to external mechanical stimuli is revealed in terms of gene expression and mechanical properties of cells. Results, methods and pitfalls are critically discussed.

In the last part of this thesis, it is demonstrated how cells in mitosis resonate to dynamic shear forces. In contrast to cells in interphase, gene regulation is inactive and a central cytoskeletal structure emerges prior cell division: the mitotic spindle. Here, cell division of mitotic RPE1, MDCK and MC3T3 cells is revealed to be perpendicular to the external force. The preferred orientation of the division axis seems to be a direct result of force-induced cell and spindle elongation. These coupled elongation processes are mechanically nonlinear, time- and actomyosin-dependent. In addition, spindle elongation depends on microtubule dynamics. Cell elongation of 15% already suffices to align mi-

totic spindles and particularly, it can be uncoupled from spindle elongation by abolishing microtubule dynamics. Spindle elongation seems to lead to a direct coupling of the actomyosin cortex to the spindle poles with astral microtubules vanishing. Here, a previously proposed mechanical coupling model is refined with inclusion of contractile actions by the actin cortex. External forces may propel actin cortex remodeling - which is indicated by higher myosin II intensity in immunofluorescence images at the cell pole than at the cell equator. All in all, cell division under external forces stays uncompromised and proceeds normally, which may imply that these phenomena provide biological tasks - even it may be utilized to guide in-vitro buildup of artificial tissues and replacement organs in the future.

In conclusion, well-defined reconstituted systems follow a bottom-up approach. This is a highly effective tool to reveal the function of cytoskeletal proteins and basic cellular processes - while living cells provide the counterpart of high complexity yet governed by detectable and quantifiable dynamics under cytoskeletal mastery. The results shown denote that future studies that join advanced *in vitro* procedures with the suitable *in vivo* experiments. They will help essentially to improve our understanding of mitosis plus other dynamic cellular processes and its cytoskeletal regulation mechanisms, which are part of the astonishing intricacy of living cells.

Contents

1 Introduction

Mechanotransduction is known as the conversion of mechanical forces into biochemically relevant information. It is involved in multiple developmental, physiological and pathological processes [Orr et al., 2006]. Mechanical factors such as applied forces or the rigidity of the extracellular matrix affect form and function of cells and organisms. Bone and muscle's development and pathobiology strongly relies on mechanical forces from weight and muscle contraction, while lung physiology and disease is influenced by forces from inflation [Burger and Klein-Nulend, 1999, Raisz, 1999, Orr et al., 2006, Liu et al., 2010]. The rigidity of the extracellular environment governs the differentiation of mesenchymal stem cells [Engler et al., 2006] and myotubes in cell culture [Engler et al., 2004]. A complete picture of mechanotransduction is still missing, although progress has been made towards a better understanding. A future concept may include force-induced changes of rates of key subcellular processes to influence cell function: cells may function as a multiband pass filter in which time-dependent stimuli activate individual signaling pathways that change cell fate [Hoffman et al., 2011, Vogel, 2006]. An ultimate understanding of mechanotransduction and its key processes may be achieved by measuring forces and gene expression in one experiment. Although cell mechanics have been studied comprehensively over the years with various technical approaches [Evans and Yeung, 1989, Bausch et al., 1998, Pelham and Wang, 1999, Fabry et al., 2001, Trepat et al., 2004, Trepat et al., 2007, Ragsdale et al., 1997, Smith et al., 2005, Guck et al., 2001, Fernández et al., 2007, Fernández and Ott, 2008], a combination of extensive gene analysis and stress-strain measurements via dynamic shear has not been used so far in a mechanotransduction context. Several studies in this context mainly used fluid shear or membrane stretching techniques so far [Garcia-Cardena et al., 2001, Tzima et al., 2002, Simmons et al., 2003, Grote et al., 2003].

While interphase cells are motile and are able to regulate their gene expression, mitotic cells exhibit a different behavior: in mitosis, cells round up and segregate pairs of chromosomes via mechanical processes to the nascent daughter cells. The inevitable forces for these processes are generated at the molecular level by motor proteins and other cytoskeletal compounds like microtubules or actin. The orientation of a mitotic spindle defines the plane of cell division [Gachet et al., 2004, Fishkind and Wang, 1995]. The daughter cells will accomplish different fates when cell-type determinants are variably distributed along the spindle axis due to intracellular polarity or asymmetric external cues [Betschinger and Knoblich, 2004]. The importance of these asymmetric cell divisions in the development of multicellular organisms has been discovered in many invertebrate and vertebrate systems [Betschinger and Knoblich, 2004, Strauss et al., 2006, Siller and Doe, 2009]. The most basic cue which dictates spindle orientation is cell shape - thus, cells division occurs along long cell axis naturally [Honda, 1983].

Spindle position and orientation is achieved via a complex balance of mechanical forces that still lacks understanding. When the cell shape is altered with a micro-pipette, the spindle supervises and responds to externally inflicted variations in cell morphology [O'Connell and Wang, 2000]. Two mechanisms have been described which show an external force-induced orientation of the division axis - that are alterations in cell shape and mechanosensitive reactions triggered at certain adhesion spots. It is poorly understood how cells integrate these mechanical cues. They could antagonize or act together - essentially, it may rely on an interplay of adhesive conditions, geometry and timescale of the mechano-stimulus.

In metaphase, not only spindle orientation but also spindle length is controlled in diverse ways. Spindle length determination is far from being solved and multiple mechanisms are postulated in literature for systems like yeast, C. elegans, Xenopus and others [Dumont and Mitchison, 2009b, Goshima and Scholey, 2010]. There are some quantitative length control models like slide-and-cluster models for anastral Xenopus spindles [Burbank et al., 2007] or force-balance models for astral spindles of Drosophila embryos [Goshima et al., 2005] and mammalian cells [Ferenz et al., 2009]. Mitotic cells in tissues are constantly under external forces, thus it is natural to think of experiments impose external forces on mitotic cells to mimic *in vivo* scenarios and to evoke cellular responses. Investigations in a more dynamic external context are missing so far and could provide more insight into the mechanical coupling of actomyosin cortex to the mitotic spindle and therewith, into the organization of length and orientation of cells and their corresponding spindles.

While it is of essential importance to explore the biological processes mechanotransduction and mitosis *in vivo*, it is necessary to lower the complexity of biological systems to understand and learn to control the biophysical mechanisms and identify key properties of key players. Using a bottom-up approach [Bausch and Kroy, 2006], reconstituted actin networks still prove to be a magnificent tool to explore basic biological processes *in vitro*. A key process in rigidity sensing is the modulation of cellular contractility [Hoffman et al., 2011]. Structures that generate and endure cellular forces are part of force-sensing [Orr et al., 2006]. Cytoskeletal proteins such as actin with actin binding proteins (ABP) for example fascin, EPLIN and tubulin are essential in the mediation of external mechanical inputs in almost all systems [Chen, 2008]. Two important structures have been recently extensively studied: focal adhesions and filopodia - both important in mechano- and rigidity sensing. One of those basic constituents of such actin-based structures has been recently drawn into focus: the LIM domain containing actin-binding protein EPLIN [Maul and Chang, 1999]. LIM domain proteins are potential tension sensors in focal adhesions because of a myosin II dependent recruitment [Schiller et al., 2011]. EPLIN contains a potential mechanosensitive LIM domain [Kadrmas and Beckerle, 2004, Schiller et al., 2011]. Moreover, mechanosensory machinery have been found at the interface EPLIN α-catenin which performs as a tension transmitter [Taguchi et al., 2011, Chervin-Pétinot et al., 2012]. It is also an essential component of the actin cortex while cytokinesis [Chircop et al., 2009].

Filopodia are known to be force and rigidity sensors of the ECM and to be important

in cancer cell invasion [Kureishy et al., 2002, Vignjevic et al., 2007]. They are hairlike protuberances in migrating cells that essentially consist of ordered actin-fascin bundles. The dynamics and mechanics of filopodia of cells are essential for guidance of cellular movement. Filopodia turn out to be created due to the sensing of external mechanical cues [Tse et al., 2012]. While the detailed mechanism of the assembly and disassembly of filopodia is still unclear, the major constituents have been identified [Mattila and Lappalainen, 2008]. The actin bundle structure is determined by fascin [Faix and K.Rottner, 2006]. Fascin is the main cross-linking protein, which organizes actin filaments into polar bundles of hexagonal structure [Claessens et al., 2008, Aratyn et al., 2007]. Due to the *in vivo* roles of ABPs, it is of high interest to achieve a deeper understanding of the parameters, which control the structure of actin networks which contain EPLIN or fascin. Further interest lies in how these structures are connected to the mechanical properties, which lead to mechanosensing and various cellular states *in vivo*. The impact of different cross-linking ABPs on the mechanical properties of actin networks has been examined over the last decade by reconstituting and simulating *in vitro* model systems of diverse intricacy [Bausch and Kroy, 2006, Kasza et al., 2007, Heussinger and Frey, 2007, Head et al., 2003, Schmoller et al., 2010]. In former studies the effect of the geometry of crosslinking proteins on the structural and mechanical properties of *in vitro* actin networks has been examined [Wagner et al., 2006], yet the effect of the binding site mutations on the *in vitro* structure and mechanics is still unknown.

In this thesis, diverse cross-linked and bundled cytoskeletal networks are studied using an *in vitro* and *in vivo* approaches - the latter with living cells concerning gene expression changes mediated by the cytoskeleton and its special importance in mitosis (fig. 1.1). Chapter 3 focuses on the effect of mutations in fascin's binding domains and the mechanical and structural properties of *in vitro* actin networks. By combining macrorheology with fluorescence microscopy, it is demonstrated that different mutations in both binding domains lead to an effective shift of linear and nonlinear mechanical properties to higher molar ratios R - while the obtained bundle structures remain wild-type-like and similarly shift. With the same techniques, the first characterization of structural and mechanical properties of actin-EPLIN networks is revealed in chapter 4. In chapter 5 and 6 a novel setup is introduced to characterize cells in interphase rheologically and morphologically by a monolayer shear device that is combined with microscopy. In chapter 5, this setup is used for evaluation of mechanotransduction via high throughput mechanomics: a combination of gene expression analysis with force measurements of a large amount of cells. Both techniques, the mechanostimulation by dynamic shear and gene analysis method qPCR are refined. In chapter 6, cell division of mitotic RPE1, MDCK and MC3T3 cells is revealed to be perpendicular to the external force, while the overall cell division is not compromised. The preferred orientation of the division axis seems to be a direct result of force-induced actomyosin-dependent cell and spindle elongation. Moreover, these imposed forces may propel overall actin cortex remodeling and direct coupling of the cortex to the spindle - which is indicated by higher myosin II intensity in immunofluorescence images at the cell pole than at the cell equator and abolished astral microtubules.

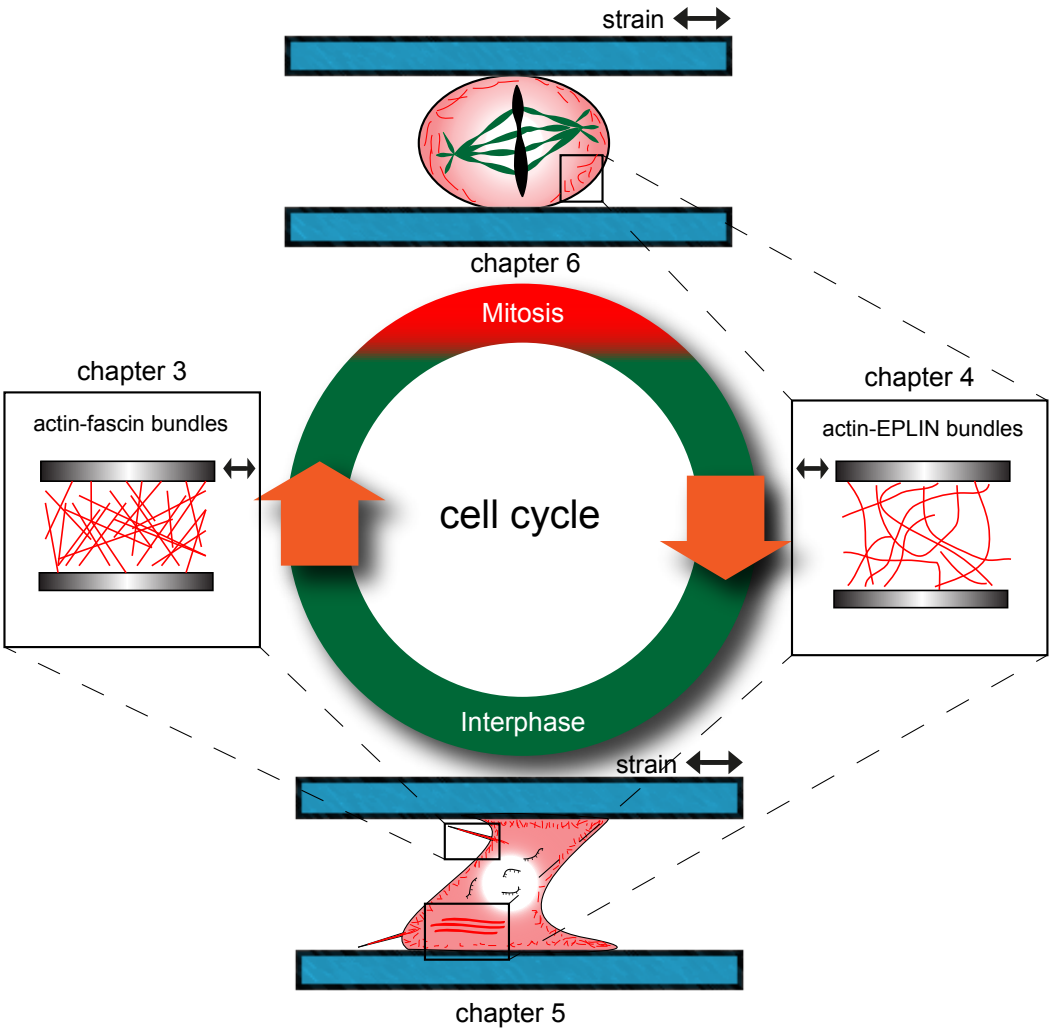

Figure 1.1: Dynamic mechanostimulation of living cells in different cell cycle stages: Dynamic shear is imposed on cells in mitosis (M-phase) by analyzing the mitotic spindle and interphase by gene expression analysis. Especially, the role and properties of the actin cytoskeleton by manifesting as the actin cortex *in vivo* and bottom-up assembled *in vitro* including actin binding proteins. Chapter 3 focuses on the effect of mutations in fascin's binding domains and the resulting mechanical and structural properties of *in vitro* actin networks. By combining macrorheology with fluorescence microscopy, it is demonstrated that different mutations in both binding domains lead to an effective shift of linear and nonlinear mechanical properties to higher molar ratios R. With the same techniques, the very first characterization of structural and mechanical properties of actin-EPLIN networks is revealed in chapter 4. In chapter 5 and 6 a novel setup is introduced to characterize cells rheologically and morphologically by a monolayer shear device that is combined with high-resolution microscopy. In chapter 5, this setup is used for evaluation of mechanotransduction via high throughput mechanomics: a combination of gene expression analysis with force measurements of a large amount of cells. In chapter 6, cell division of mitotic RPE1, MDCK and MC3T3 cells is revealed to be perpendicular to the external force, which seems to be a direct result of force-induced actomyosin-dependent cell and spindle elongation

2 Materials and methods

2.1 Cell culture

2.1.1 Cell types

For gene expression studies, mouse C2C12 myoblasts, NIH3T3 fibroblasts and MC3T3-E1 osteoblasts are used and attained from [DSMZ, 2010]. C2C12 cells are able to differentiate after days into muscle-like myotubes by addition of 2% horse serum to normal cell medium [Portier et al., 1999, DSMZ, 2010]. Moreover, they are also capable to transform into osteoblast-like cells [Nishimura et al., 1998, Katagiri et al., 1994]. For mitosis projects, human RPE-1 cells are supplied by Zuzanna Storchova (MPI Biochemie, Martinsried). The spindle length experiments are performed with mCherry-tubulin-alpha transfected and non-transfected MDCK II dog cells kindly provided by Christoph Klingner and Roland Wedlich-Söldner (MPI Biochemie, Martinsried). These cells are grown in DMEM-Glutamax (Gibco) with 10% FBS (PAA, Austria) and supplemented with hygromycin (Roche) for stable expression of mCherry-tubulin. Cell media and bovine serum are purchased at PAA (Austria) and at Invitrogen (now Life technologies). Passaging, storage and overall handling is performed using standard protocols [DSMZ, 2010, Lindl, 2008].

2.1.2 Cell division, cell cycle synchronization and preparation

In order to divide itself, a cell has to go through the cell cycle where it doubles its DNA in interphase. In the M-phase, cells form their mitotic spindle and segregate mechanically their chromosome pairs to the daughter cells. Multiple techniques are used to synchronize cells for mitotic experiments. Mitotic shake-off is used as an inhibitor-free method to collect mitotic cells direct from the cell culture flask for the spindle rotation studies with phase contrast imaging. Cells become round during the M-phase and therefore are less adhesive to the flasks. Mild tapping and shaking is sufficient for harvesting mitotic cells, but huge flasks have to be used to get a large quantity of cells. After shake-off cells are store-able for several hours at 4°C, while no mitotic progress is achieved. For metaphase experiments, a proteasome inhibitor MG132 is added to the cells ($c = 20$ µM, Sigma-Aldrich), which then enter metaphase within half an hour when stored at 37°C. They do not leave this mitotic phase due to blocking cyclin D1 by MG132 [Clute and Pines, 1999]. Another way to assemble a whole flask of mitotic cells is by adding the microtubule-depolymerizer nocodazole ($c = 300$ nM, Sigma-Aldrich) to the cells flasks 20 hours prior to experiments [Zieve et al., 1980]. This is mainly used for the spindle length experiments to attain a large amount of cells in a short time. In this way cells do

not lose their mCherry-labeled tubulin by growing too many passages over several weeks in the incubator. Cell fixation and staining of metaphase cells is performed after shear experiments by using standard protocols (see B.1).

2.2 Proteins and biochemical inhibitors

2.2.1 Actin

In cells, G-actin is a globular 42 kDa ATP-dependent protein and has multiple important roles in cellular processes. By adding ions ($MgCl_2$) and ATP, actin polymerizes into a filamentous form called F-actin. Polymerized actin is one of the three major ingredients of the cytoskeleton and moreover, in muscle cells an important part of the contractile apparatus. In this thesis, G-actin is prepared from rabbit skeletal muscle [Spudich and Watt, 1971] and stored lyophilized at -80°C or in G-buffer at 4°C (2 mM Tris/HCl (pH 8), 0.2 mM $CaCl_2$, 0.2 mM ATP, 0.2 mM DTT). Polymerization was induced by adding 10-fold F-buffer at room temperature (pH 7.5, 20 mM Tris/HCl, 5 mM ATP, 20 mM $MgCl_2$, 2 mM $CaCl_2$, 1 M KCl, 2 mM DTT). Actin is stained via the small actin binding protein phalloidin, which stabilizes actin filaments against depolymerization. In this work, phalloidin-alexa488 (Invitrogen) is used for actin visualization and phalloidin-alexa647n (Invitrogen) for staining of cytoplasmic actin in fixed cells.

2.2.2 Cross-linking proteins

Proteins that bind actin are called actin-binding proteins. By this process, actin filaments can be reorganized in different structures and geometries. Cells attain highly varied structures and networks by combining different actin-binding proteins as cross-linkers, where every protein has its own special assignment for certain cellular purposes. A lot of work has been put into understanding how actin-binding proteins control the architecture of actin structures and networks [Lieleg et al., 2009b]. Nevertheless, the key parameters that govern the specific impact of a certain actin-binding protein are still poorly understood.

Fascin

Fascin is an actin-binding 55kDa protein and contributes to filopodia structures by actin bundling as a monomer [Vignjevic et al., 2006]. *In vitro*, fascin and actin organize in polar, hexagonally packed bundles with a maximum size of about 20 filaments [Claessens et al., 2008]. In this work, recombinant human fascin and its mutants were expressed in E. coli and purified via GST-columns (GE Healthcare Life Sciences). The GST-tag was cut off by thrombin incubation overnight at room temperature. Fascin is stored in "fascin puffer" (pH 7.4, 2 mM Tris/HCl, 150 mM KCl) at 4°C and for longtime storage at -80°C. The molar ratio of fascin to actin ($R = c_{fascin}/c_{actin}$) determines how much fascin was added prior the experiments. Point mutations were performed with the Quick change kit (Qiagen) after carefully designing the appropriate primers following the kit instructions.

Accomplished mutants of wild type fascin, that are used in this work, are summed up in fig. 3.1. The focus is on constructing mutants for both actin binding domains, disabling or reducing actin binding capacity, thus changing the actin-fascin network structure and mechanical properties.

EPLIN

α-EPLIN (Epithelial protein lost in neoplasm) is a LIM domain containing 67kDa protein, that may form dimers and oligomers and is down-regulated in various cancers [Maul and Chang, 1999, Karaköse, 2012]. *In vivo*, it is predominantly observed in focal adhesions and adherens junctions [Chervin-Pétinot et al., 2012, Taguchi et al., 2011, Abe and M.Takeichi, 2008, Schiller et al., 2011]. Moreover, EPLIN has been described as an integral part of the contractile ring in cell division [Chircop et al., 2009]. An important role in mechanosensing processes and structures in epithelial cells has recently been discovered [Taguchi et al., 2011, Gulino-Debrac, 2013]. Furthermore, α-EPLIN is able to bind and bundle actin via two binding domains, which can be disabled by phosphorylation [Maul et al., 1999]. By actin-binding, it inhibits depolymerization of actin filaments and the branching of actin filaments driven by the Arp2/3 complex [Maul et al., 1999].

For this thesis, α-EPLIN-flag and -his vectors are kindly provided by Esra Karaköse from the Reinhard Fässler group (MPI Biochemie, Martinsried). Purification is obtained by using his-columns (GE Healthcare Life Sciences) and FLAG-beads (Invitrogen) with standard protocols. The FLAG-tag was not cut off due to its small size and location on α-EPLIN's C terminus. Furthermore, no interaction of the FLAG-tag with actin or obstruction with bundling is reported or seen in experiments. α-EPLIN is always prepared freshly and stored at $4^{\circ}C$ in TBS puffer (pH 7.4, 150 mM KCl, 100 mM Tris/HCl). In this work, only α-EPLIN is used and therefore, the abbreviated name *EPLIN* will be utilized in chapter 4.

2.2.3 Biochemical inhibitors

In mitosis experiments the role of several cytoskeletal key proteins has to be deduced (see chapter 6). For this purpose the following biochemical inhibitors are used: taxol stabilizes microtubules and reduces their dynamics [Schiff et al., 1979, Schiff and Horwitz, 1980]. The unspecific dynein inhibitor vanadate is able to block motor activity (300 µM). At higher concentrations, kinesins are also influenced in their activity [Abal et al., 2005]. In this work, low concentrations are used to rule out any effects on kinesins like kinesin-5 (Eg-5). To block kinesin-5 activity, 25 µM of monastrol (Sigma-Aldrich) is added and leads in most cases to monopolar mitotic spindles [Mayer et al., 1999, Kapoor et al., 2000]. Ciliobrevin D (Merck Millipore) is a novel, specific dynein inhibitor, which leads to defocusing of mitotic spindles (at 40 µM) in metaphase and prevention of the kinetochore-microtubule attachment [Firestone et al., 2012]. Furthermore, it is able to block dynein-dependent microtubule gliding and ATPase activity *in vitro*. Y27632 inhibits the ROCK kinase that regulates myosin II activity and thereby

reducing the actin cortex stiffness in L9 29 fibroblasts by 50% at $c = 10$ µM [Tinevez et al., 2009]. Nocodazole (300 nM, Sigma-Aldrich) abolishes astral microtubules and can be used for cell synchronization before mitosis [Mitchison et al., 2005, Zieve et al., 1980]. Latrunculin A depolymerizes actin filaments and bundles, thereby leading to cell apoptosis at high concentrations [I. Spector and Groweiss, 1983]. Blebbistatin (50 µM, Sigma-Aldrich) is known for direct inhibition of myosin II activity [Kovács et al., 2004, Limouze et al., 2004]. Most inhibitors are only soluble in DMSO, hence control experiments with high contents of DMSO (0.1%) are always carried out. With this concentration being higher than in any other drug experiment, it is made clear that no special effects on cells or artifacts are measured by using this solvent.

2.3 Experimental techniques

2.3.1 Real-time Polymerase Chain Reaction

Real-time polymerase chain reaction (qPCR) is a fast way of analyzing gene expression of a large number of cells, living tissues or verifying viral and bacterial diseases. In contrast to normal polymerase chain reaction where DNA proliferate exponentially, real-time measurements of DNA contents allow quantitative studies of different initial amounts of all kinds of nucleic acids. SYBR Green is used as an unspecific intercalating dye with an excitation of 492 nm and emission of 516 nm, that binds to double stranded DNA. DNA can be transformed from messenger RNA (mRNA), which is produced by the living object of interest. In this work the overall RNA content including mRNA is isolated with Qiashredder and RNeasy Plus mini kit (Qiagen). A RNase inhibitor (RNAsin, Promega) is added to minimize RNA degradation. Concentrations of the isolated RNA are measured with a Nanodrop (Thermo Scientific) and the integrity of RNA samples is always checked by RNA gel electrophoresis: two sharp rRNA bands at 28 S and 18 S with no smear should be visible for undegraded RNA. Isolated mRNA is transformed into the complementary DNA (cDNA) by reverse transcription with the SuperScript III kit (Invitrogen). All cDNA and RNA samples are stored at -80°C. For a well of 25 µl qPCR reaction, 1 µl of 1 : 10 diluted cDNA is pipetted together with 1 µl of left and right Oligo(dT) primers (see A) without creating air bubbles for all 96 wells. All mixed gently with the master-mix of Quantitect SYBR green PCR kit (Qiagen) is then put in the qPCR cycler (Stratagene). SYBR green fluorescence is measured after each cycle.

The qPCR run protocol can be divided in three segments (fig. 2.1a): (I) First of all, PCR gets initiated by heating up to $95^{\circ}C$. Here, the polymerase is activated. (II) Then 40 cycles of the following steps are performed: at first, denaturation above the melting point at 94°C is achieved to ensure no dye is bound to the DNA. Secondly, annealing at approximately 3-8°C below T_m (usually around 55°C) of the Oligo(dT) primers is taking place. At last, extension of the DNA fragment is achieved at 72°C for 30 s. At the end of this step, fluorescence data collection is performed and the next cycle starts by heating up. (III) The last segment consists of recording a dissociation curve by denaturation with a slow cooling afterwards. The derivative of melting data (fig. 2.2) is then utilized to

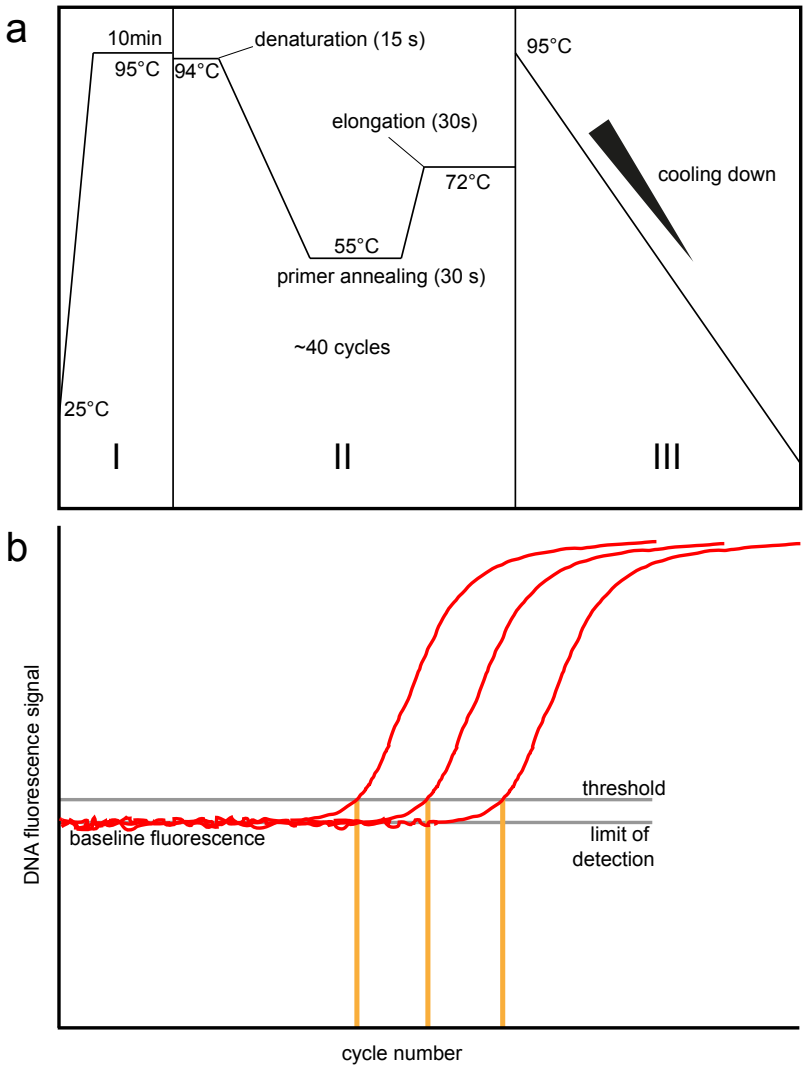

Figure 2.1: Overview over qPCR cycle progression: In (a) cycle schematics of a typical qPCR run are shown with primer pair specific annealing temperature. (b) Schematic diagram of a typical real-time polymerase chain reaction curves for three independent wells with threshold cycle C_t (arrow).

control genomic DNA contamination and amplified fragment length, which is calculated beforehand. Contamination results in shoulders or additional peaks in the melting curve.

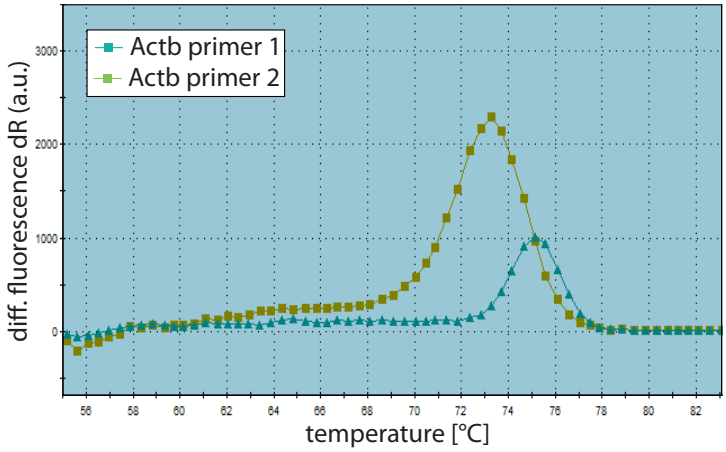

Figure 2.2: Melting curve after qPCR run: For two different primer pairs of beta-actin two different peaks are present which depends on genomic contamination and amplified fragment length

All samples are performed as triplets with water controls run additionally. A passive reference dye ROX ensures no leakages of wells and gives a baseline to normalize the SYBR green fluorescence data (fig. 2.1b). Furthermore, threshold cycles C_t are determined by applying a threshold line to the exponential data plot in the early exponential phase of similar growth rates of intensities (fig. 2.1b). The C_t data for three wells of the gene of interest (GOI) are relative quantity normalized (dRn) using GAPDH as reference gene for different initial amounts of RNA. This reference normalization is necessary, because cell numbers always differ from experiment to experiment. Without reference genes, even small differences in cell numbers may lead to high errors due to the exponential amplification in qPCR. β-actin is not used as a reference because of high noise for different cell culture conditions (fig. 5.1) despite being the overall standard reference in literature (see chapter 5). Gaussian error propagation is utilized for pooling of data of multiple experiments. Afterwards, the data is normalized with the cell culture values of gene expression from cells picked prior to the experiment. Developed in this thesis, this is a novel and essential step for qPCR analysis and so far, not a part in standard protocols (see 5). At the end, the relative change of gene expression of shear experiments to control experiments is calculated:

$$\Delta\Delta C_t = (C_{t,GOI} - C_{t,norm})_{control} - (C_{t,GOI} - C_{t,norm})_{exp} \tag{2.1}$$

$$R = 2^{-\Delta\Delta C_t} \tag{2.2}$$

After finishing all normalization steps, the fold change - the logarithm of relative quantity R with basis 2 - sums up the change in expression for a gene.

2.3.2 Rheology with cells

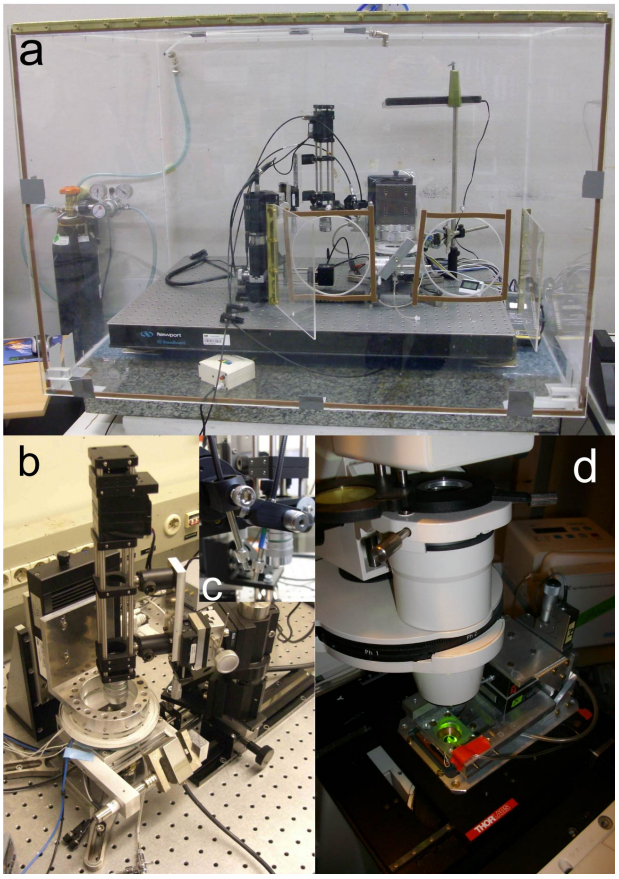

Figure 2.3: Setup for cell shear experiments: (a) Self-made cell shear apparatus in a Plexiglas chamber for standard incubator (5% CO_2) conditions. (b) Setup used for gene expression studies. (c) Spectrometer and light source for gap measurements. (d) Smaller version of cell shearer for mitotic cells for visualization on conventional microscopes.

Strain-controlled shear setups are self-made for cell stimulation via dynamic shearing. For stress-strain measurements, a force sensor (Futek, USA, LCF300 25 lb) is calibrated and read out, while the strain is positioned by the a piezo using an own-written C++ program. A spectrometer for visualizations of interferences of visible light (fig. 2.3c, fig. 2.4b) and optical cell diameter calculation are used for gap measurements. Gap is maintained by micrometer screws and a piezo stage in z-direction for mitotic experiments and with a DC motor (Physik Instrumente, Germany) for gene expression studies. A CO_2 chamber with a gas feedback controller, a pump for cell medium flushing and a heating device (37°C) are used for incubator-like conditions (fig. 2.3a). To shear every cell the same amount, one has to ensure that the glass plates are parallel. To control the tilting angle of the upper plate, special plate to plate calibration techniques were developed by looking at the interference fringes and minimizing their emergences after multiple

cleaning steps of the plates. Cleaning is done with hot hellmanex (∼ 15 s), ethanol and extensive millipore water washing steps with soft wipes suited for optical lenses. Afterwards, a metal holder with motor stage is bonded with an adhesive to the upper plate by UV-light illumination. Cell shearing is performed via piezo motors in x- and y-direction controlled by a computer or oscilloscopes.

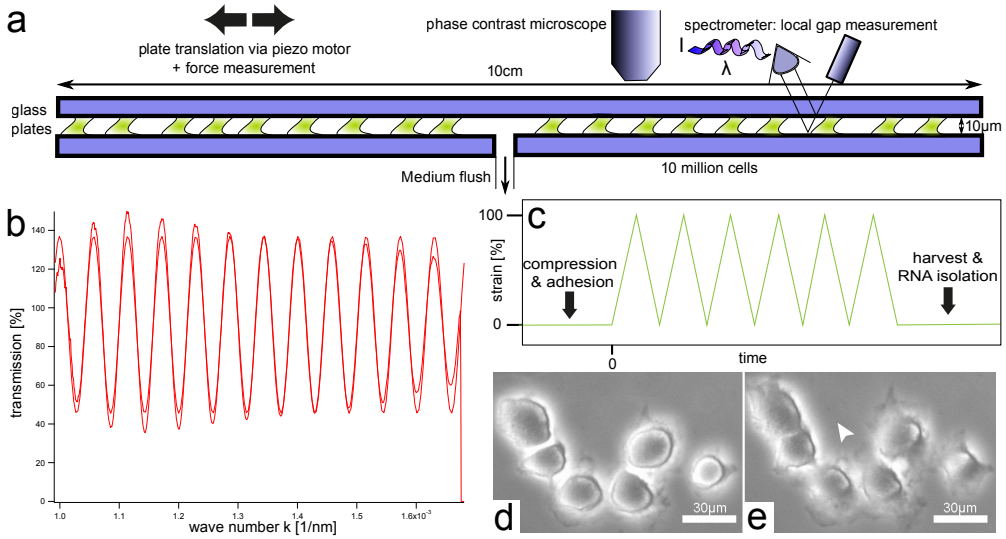

Figure 2.4: Setup for cell shear experiments with corresponding force measurements: (a) Big glass plates (⌀ = 10 cm) are used to squeeze homogeneously a large quantity of cell (10^7) while piezo motors are used for shearing. Flush of medium ensures oxygen and fresh medium. Gap distance is controlled via spectrometer measurements and fitting of interference data of visible light spectra (b). (c) Experimental scheme of applied strains and basic steps of cell treatment. Cells are shown without strain in (d) and with applied strain $s = 10$ µm in (e) (scale bar 30 µm). (d and e taken from [Maier, 2008])

About ten million cells are put between the plates by using a syringe at a gap of 30 µm to reduce air bubbles and cell clumping because of excessive fast medium flow. Less cells are used for mitotic experiments with a smaller setup. The medium flow during the experiment was set to 6 µl/min. An own built phase contrast microscope is utilized to look at cells for control and cell viability concerns. At the end of the experiment, PBS and trypsin is flushed through to detach cells smoothly. Afterwards, the harvest is centrifuged for RNA extraction (see 2.3.1).

For mitosis experiments, several hundred thousand cells are brought onto the glass plates by pipetting and then gently squeezed. Plates are kept at 37°C from the beginning for mitotic cells synchronized in metaphase. In the case of mitotic shake-off, the setup is warmed up after the compression of cells. After 20 minutes of waiting time in a compressed and confined state, mechanical stimulation is performed. For confocal imaging of stained cells, the control and sheared cells are fixed on the setup (see B.1). A x-y motorized stage (Thorlabs) is used for visualization of multiple positions during cell stimulation and controlled by a *Labview* program.

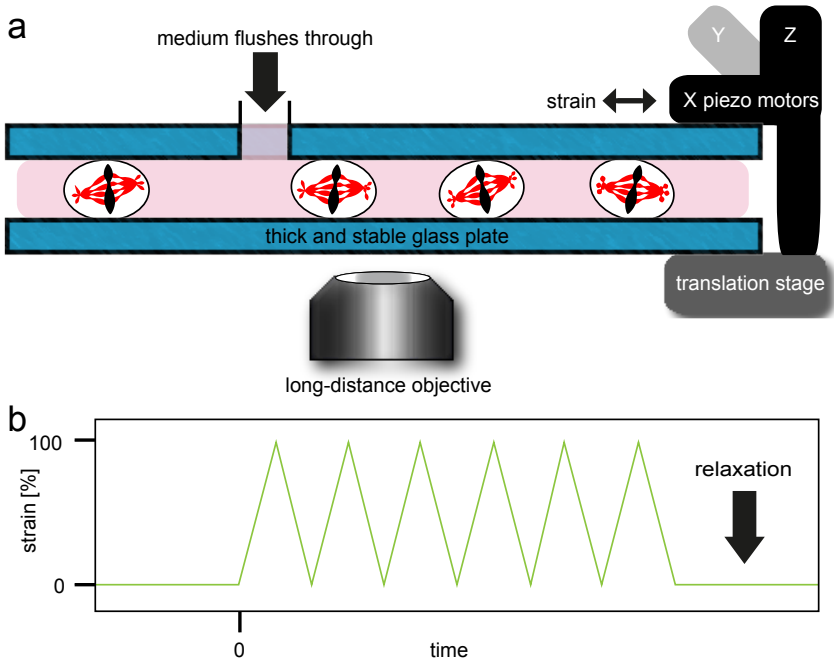

Figure 2.5: Setup for mitotic cell shear experiments: (a) Tubulin-labeled cells in metaphase are squeezed between two thick glass plates and can be imaged on a fluorescence microscope for data acquisition. A flow of fresh medium ensures supply of oxygen and nutrients while keeping the pH constant. Shear stimulation is achieved by moving one plate with piezo stages in x- or y-direction. Multiple areas of interests can be observed by using a x-y translation stage which translocates the whole setup allowing measurements of large quantities of cells. Due to this translation, only long-distance objectives can be used with adjustable working distance to overcome the thickness of the glass plate. (b) Protocol for applied strains: After initial compression of the cell monolayer and environmental adaption for 20 min, cells are sheared with various amplitudes and frequencies for 10 or 30 minutes. Afterwards, relaxations of spindle and cell shape are investigated

2.3.3 Macrorheology with actin networks

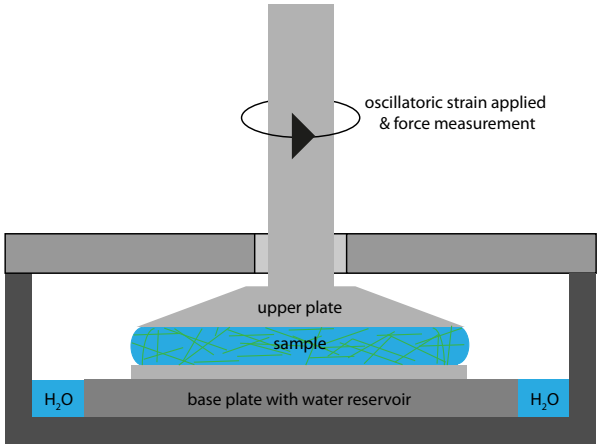

Figure 2.6: Setup for rheology with actin networks: Unpolymerized sample is placed under the plates, which is protected against dehydration by water surroundings and a mental cover cage.

Macrorheology is a good way to analyze the mechanical properties of reconstituted actin networks both in the linear (small deformations) and nonlinear regime (high deformations). In opposition to microrheology, which mechanically characterizes the sample on the microscopic scale, macrorheology measures mechanical properties on a length scale, which is larger than the characteristic length scales of the probe [Bausch and Kroy, 2006, Kasza et al., 2007]. Nevertheless, actin bundles can have persistence lengths of millimeters [Claessens et al., 2006], thereby the characteristic length scale exceeds the gap distance. Here, the gap distance is the smallest dimension of the macrorheological machinery.

In this thesis, rheological measurements are performed with a stressed controlled macrorheometer (Physica MCR 301, Anton Paar, Graz, Austria) at a gap distance of 160 µm at 21°C. Plane plate geometry is used with a diameter of 50 mm. A sample volume of 450 µl is gently pipetted put onto the base plate. After polymerizing for one hour, a frequency sweep (10 mHz to 10 Hz) is performed by measuring the elastic modulus G' and loss modulus G". In the linear regime of small deformations, a frequency sweep lays out the viscoelastic properties depending on the timescale of the deformation for viscoelastic materials like actin networks. Measurements are done in a constant strain mode for better resolution. Therefore, the strain is chosen by measuring the polymerization curve with small torques. At last, to test the nonlinear behavior a constant shear rate $\dot{\gamma} = 5$ %/s is applied to look at response at high deformations. The stress-strain relation is recorded and the differential modulus K is calculated after carefully splining the data and performing a differentiation with *IGOR*. By analyzing the nonlinear regime, strain hardening or softening can be found for actin-fascin networks [Lieleg et al., 2007], while for certain cross-linkers cyclic hardening can occur [Schmoller et al., 2010] - all in all, revealing unique mechanical properties for polymers.

2.3.4 Microscopy

Low magnification phase contrast (PC) microscopy with 10x long distance objectives and an own built PC microscope with a 20x Leica objective is used for mitotic cell imaging. For confocal imaging (Leica Microsystems, Wetzlar, Germany), cells are fixed and stained before mounting the sample chambers on the microscope. A 63x oil immersion objective is used, while sensitive HyD detectors ensure good signals for multi-stained samples. Cell images are zoomed 10x and averaged over three scans. Epifluorescence based microscopy is utilized for imaging of stained cells, live cells and phalloidin-labeled actin networks. These networks are visualized using 63x and 100x objectives on an inverted microscope (Axiovert200, Zeiss, Oberkochen, Germany) with molar ratio of phalloidin to actin of $R_{phalloidin} = 0.01$ and actin concentration of $c_{actin} = 3$ µM. For molar ratios $R < 0.01$, labeled reporter filaments are added at a concentration of 0.3 µm. MCherry-tubulin transfected cells are imaged using long-distance 20x (numerical aperture = 0.8) and 40x objectives (Zeiss) on a x-y movable stage (Thorlabs). This feature of moving the setup and using long-distance objectives reduces the resolution of the images. Hence, extensive matlab analysis for flexible threshold pinning is carried out (see 2.4).

2.4 Matlab analysis of mitotic cells

The fluorescent images are taken with a 20x objective (Zeiss, Oberkochen, Germany) and split up into single cell movies for further analysis. To reduce image noise, mean filtering is performed smoothly with FIJI (ImageJ). Other cells than the target cell are removed by hand to minimize disturbance for the threshold finding and fitting process (fig. 2.7c). Since the background signals inside of the cells are of high intensity, a special matlab script is developed for this thesis to find the best threshold of a spindle for every frame of a single cell movie. By calculating the mean intensity for all thresholds of each frame with FIJI, one can perform third degree polynomial fits to the data with Matlab. This is done in the region, where the spindle intensity increase is to be suspected: a shoulder appears in the mean intensity data at high thresholds (fig. 2.7a). The corresponding threshold is then attained by performing a numerical differentiation to the fit (fig. 2.7b) and taking the minimum value as a threshold, which is then applied to the image, binarized (fig. 2.7e) and fitted with an ellipse. As a control, the fitted ellipse is overlayed with the original image (fig. 2.7f). Spindle orientation is defined by the major axis, spindle length as the whole length of the ellipse and spindle width as the ellipse width. Background fluorescence of unbound tubulin enables to attain information about the cellular shape. Because the shape of a mitotic cell is close to elliptic, it is possible by characterizing it in terms of the ellipse with the same moments as the cell body (fig. 2.7d). We can calculate the cell elongation as the ratio of major to minor axis. Threshold is calculated for single frames with the same method described before for spindle thresholding. Cell orientation is defined as the angle of the major axis. Arithmetical means and box-plots are calculated by using all cells from multiple experiments sheared under identical conditions. Because of the asymmetry of the distributions of lengths and orientations, box-plots are used to

demonstrate this behavior, while giving the median of the data. The boxes above and underneath the median correspond to 50% of the data with every box containing 25% of the data points (25th and 75th percentiles). The notch shows the 5% significance level of the median. The bars have a maximum length of 1.5×boxlength. By this, the maxima and minima of data points are shown, while outliers outside these bars are not displayed.

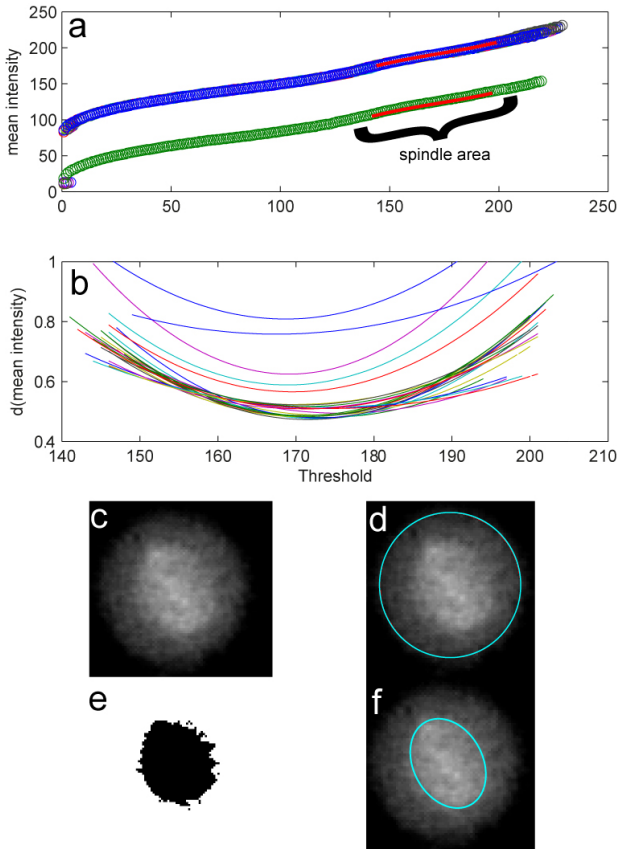

Figure 2.7: Threshold finding and spindle fitting: (a) Mean intensities for every frame of a single cell movie are summed up for all thresholds and fitted with a polynomial of the third degree. (b) Numerical differentiation yields a minimum for each frame of a single cell movie which determines the threshold to be applied. (c) Original image of a cell shows a mitotic spindle with high intensity, while the background fluorescence signal reveals the cell body. (d) Cell shape, orientation and elongation is obtained by fitting the cell edge with an ellipse similar to the spindle case. (e) A binary image is created after applying the threshold and then fitted with an ellipse to obtain spindle length, width and orientation. (f) The fitted ellipse (pale blue) is overlayed with the original image for control.

At last, to analyze myosin intensities of stained cells in chapter 6, stack images of a thickness of 3 µm at cell center are average projected and divided by shear direction (angle 0°) in four quadrants with Matlab algorithms (see 6.11). Then, these four quadrants are taken together under the assumption of symmetry of directed external forces and the shear stimulus. The average is then calculated for control and sheared cells.

3 Actin-fascin networks: interplay of mechanical properties and binding affinities

Filopodia are hairlike protuberances in migrating cells that essentially consist of ordered actin-fascin bundles. The dynamics and mechanics of filopodia of cells are essential for guidance of cellular movement. Filopodia turn out to be created due to the sensing of external mechanical cues [Tse et al., 2012]. While the detailed mechanism of the assembly and disassembly of filopodia is still unclear, the major constituents were identified [Mattila and Lappalainen, 2008]. In the filopodia tip complex, proteins are present that induce the polymerization and formation of the filopodia, molecular motors such as myosin-X seem to be responsible for the material transport. The actin bundle structure is determined by fascin [Faix and K.Rottner, 2006].

Fascin is the main cross-linking protein, which organizes actin filaments into polar bundles of hexagonal structure [Claessens et al., 2008, Claessens et al., 2006, Aratyn et al., 2007]. Fascin is also described to be important in cancer cell invasion [Kureishy et al., 2002, Vignjevic et al., 2007] and locates in invadopodia [Li et al., 2010, Jawhari et al., 2003]. The activity of fascin is regulated by a phosphorylation site in the binding pockets and an additional regulation can occur via a C-terminal region serine residue revealing a role for fascin beside actin bundling at the distal end of filopodia [Zanet et al., 2012]. The actin-binding domain 1 (ABD1) is described as a MARCKS sequence containing a phosphorylation site and three lysine residues [Ono et al., 1997]. *In vivo* and *in vitro* studies on mutated fascins showed reduced numbers of filopodia for a phosphomimicking mutant S39E [Vignjevic et al., 2006]. The actin-binding domain 2 (ABD2) was determined by electron microscopy and mutational studies [Jansen et al., 2011, Yang et al., 2013]. Transmission electron micro-graphs reveal an inability to bundle actin when R271E, K353E and K358E mutations are implemented in fascin's β - trefoil domain 3, while the number of filopodia is reduced in mouse melanoma cells [Jansen et al., 2011].

While there is *in vivo* a reduction of filopodia measurable, the functional consequence of such mutations on the mechanical function has not been addressed yet. In former studies the effect of the geometry of crosslinking proteins on the structural and mechanical properties of *in vitro* actin networks has been examined [Wagner et al., 2006], yet the effect of the binding site mutations on the *in vitro* structure and mechanics is still unknown. The off-rate of crosslinking proteins can be detected directly in the macroscopic rheological properties of actin networks [Lieleg et al., 2007, Lieleg et al., 2009a]. Thus it can be expected that also the altered binding sites of a bundling protein such as fascin

would have a direct consequence on the moduli. Nonlinear elasticity as reported in cross-linked actin-filamin networks [Kasza et al., 2009] may change when binding affinities of cross-linkers are reduced.

In this chapter, the effect of mutations in fascin's binding domains on the mechanical and structural properties of *in vitro* actin networks is determined. By combining macrorheology with fluorescence microscopy, it is demonstrated that different mutations in both binding domains lead to an effective shift of linear and nonlinear mechanical properties to higher molar ratios R - while the obtained bundle structures remain wild-type-like and similarly shift.

3.1 Mutating the actin binding domains of fascin

Fascin has two binding domains: ABD1 was identified as a MARCKS sequence, which lies in one of the beta-trefoil domains [Ono et al., 1997, Jansen et al., 2011] - ABD2 is located in another beta-trefoil domain [Jansen et al., 2011]. In both binding domains it turned out that a charged lysine is essential for its binding affinity. 8 mutants of fascin are constructed addressing both binding domains (fig. 3.1). The mutants 3, II and III have charged lysines replaced with uncharged methionines. This should obstruct binding to actin, because lysine is known for its importance and ability to bind actin [Tang and Janmey, 1996]. A direct way to modulate the actin binding ability is to mimic phosphorylation or de-phosphorylation (mutants 1, 2, I). Human wild-type and mutated fascin is expressed and purified from e.coli via a GST-tag, which is cut off with thrombin overnight (see 2). Two of these mutants (4 and IV - knockout mutants) have their affinities of the ABDs in such a way reduced that the reconstituted actin networks do not show any form of bundles. For control, a mutation in a non-binding region is used to clear out any effects of the process of mutagenesis itself. All rheological experiments are performed with $c_{actin} = 0.4$ mg/ml, fluorescence measurements are conducted with $c_{actin} = 0.133$ mg/ml. There are multiple *in vitro* and *in vivo* studies characterizing mutations of the fascin molecule [Ono et al., 1997, Jansen et al., 2011, Vignjevic et al., 2006, Yang et al., 2013].

3.2 Linear Response of actin-fascin mutants networks

First of all, the frequency dependent storage and loss modulus (G', G") for small deformations are determined. WT bundle phase starts at a molar ratio of R=R*=0.01. A pronounced minimum in G" is visible, which shifts to higher frequencies at higher molar ratios (fig. 3.2, [Lieleg et al., 2007]). This prominent minimum in WT fascin's and control mutant's G" (arrows, fig. 3.2a and b) is nearly lost in the sweep for mutants 1 and II (fig. 3.2c and d). This frequency dependent reduced viscous response is an example of how a small molecular change can affect macroscopic mechanical properties by changed affinities as in case with mutants 1 and II. It is not depending on the special kind of mutation. A lost or reduced minimum may result in a changed off-rate as seen before with mutant 2 (S39A) [Lieleg et al., 2011].

a

# mutant	ABD	mutation	characteristics	references
1	1	S39E	phospho-mimicking, addition of - charged aa	Vignjevic et. al.
2	1	S39A	de-phospho-mimicking	Ono et. al, Vignjevic et. al., Lieleg et. al.
3	1	K42M	end of MARCKS sequence, M: apolar and hydrophobic	-
4	1	K41/42M	end of MARCKS seq., M: apolar and hydrophobic, ABD KO	-
I	2	S357E	phospho-mimicking, addition of + charged aa	-
II	2	K358/359M	elimination of 2 + charged aa, M: apolar and hydrophobic	-
III	2	K358M	elimination of a + charged aa, M: apolar and hydrophobic	similar to Jansen et. al., Yang et. al
IV	2	S357E/K358/359M	M: apolar and hydrophobic, phospho-mimicking, ABD KO	-
control	-	K303M	control: outside of ABD regions, M: apolar and hydrophobic	-

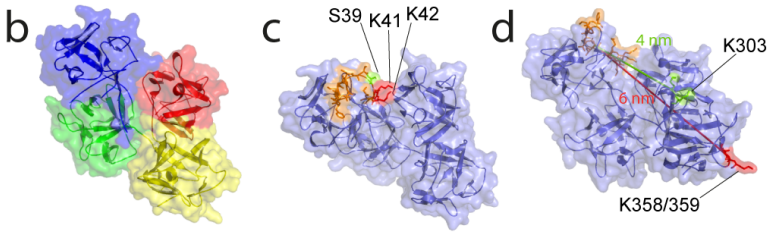

Figure 3.1: Overview of fascin mutants of both actin binding domains: (a) mutational targets include phosphorylation sites and positive charged lysines. A mutant with an amino acid exchange in a per se non-binding region was used as a control. The structural perspective of fascin's beta-trefoil domains are shown in (b) (PDB-entry 1DFC). The mutants' locations are pointed out in (c) for ABD1 and (d) for ABD2. The distance between the ABD regions is 6 nm. (b-d taken from [Köhler, 2012])

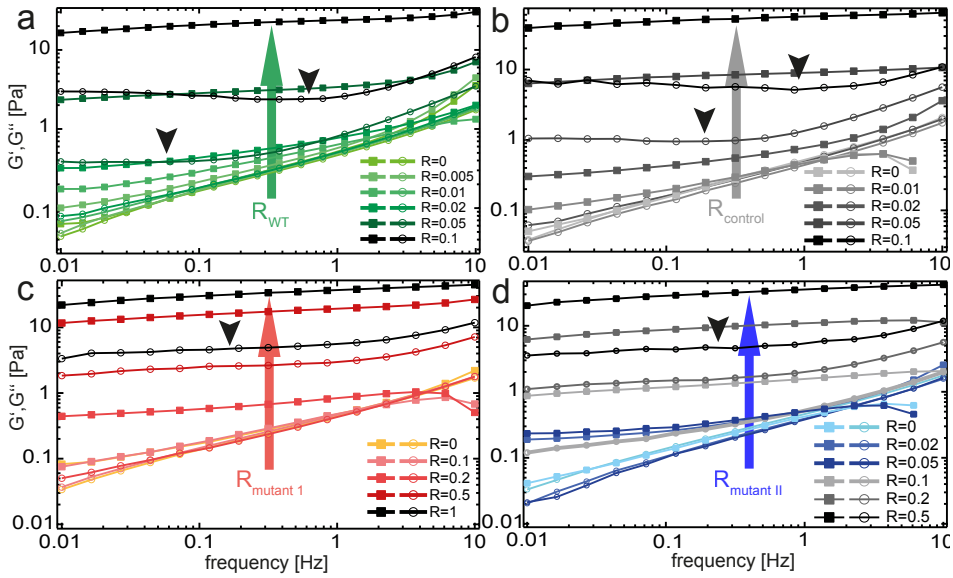

Figure 3.2: Storage modulus G' (filled squares) and loss modulus G" (open circles) increase with rising molar ratios R due to bundling: (a) wild-type fascin (green, $R = 0...0.1$), (b) control mutant (grey, $R = 0...0.1$), (c) constant inactive mutant 1 (red, $R = 0...1$) and (d) mutant II (blue, $R = 0...0.5$). WT fascin and the control mutant show a minimum in G" (black arrows) that shifts with higher Rs in contrast to affinity-reduced mutants 1 and II, who have lost that pronounced minimum in their frequency sweeps ($c_a = 9.5$ µM)

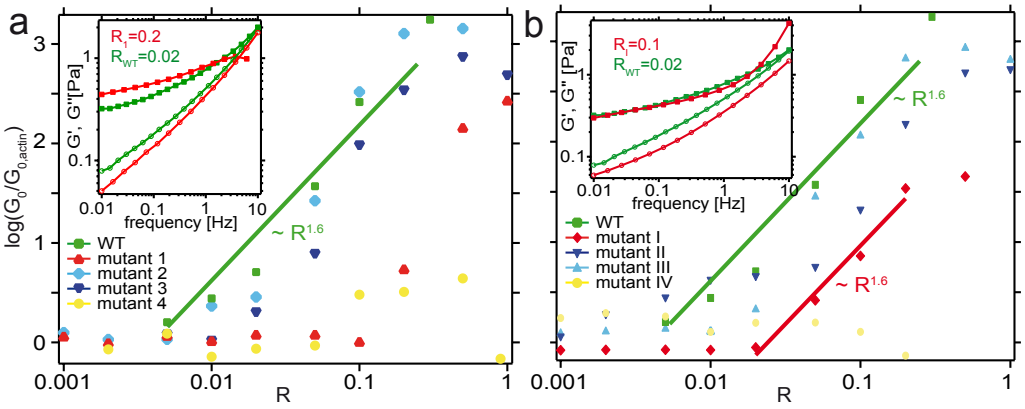

Figure 3.3: R-dependence of plateau moduli G'(10 mHz) reveals postponed bundling: (a) ABD 1: An extreme shift of the bundle phase onset for phospho-mimicking mutant 1 (red) from $R*_{WT} = 0.01$ to $R*_I = 0.1$ is visible, but it still reaches high moduli at high molar ratios R. Mutants 2 (pale blue) and 3 (dark blue) behave WT-like in terms of starting the bundling phase. Mutants 4 (yellow) for ABD 1 and IV for ABD 2 (yellow, b) have no significant rise in plateau moduli and therefore, no bundle properties can be measured. For ABD2 (b) mutant III (pale blue) behaves WT-like in contrast to I (red) and II (dark blue) which are shifted to higher Rs, while phospho-mimicking mutant I is reaching an early plateau for R>0.2. Only a shift to higher moduli and no change in G' (square) and G" (circle) curve shapes is revealed in the insets (a, mutant 1 (red, R=0.2) vs. WT (green, R=0.02); b, mutant I (red, R=0.1) vs. WT (green, R=0.02))

All mutants - except the knockout mutants - show similar behavior in the frequency sweep with rising moduli due to bundling with exception of R*, where the bundle phase begins. This is shifted in certain cases for the extracted plateau moduli $G_0 = G' = 10$ mHz (fig. 3.3): For phosphorylation-mimicking and thereby "inactive" mutants 1 and I, a delay of the bundle phase is visible without a change in bundle stiffness at high R for mutant I. For all other mutants, there are no drastic changes in bundling dependent on R (fig. 3.3). The maximum plateau modulus is reduced for ABD2 mutant I and therefore, bundle size could be affected (as seen with TEM measurements for a similar mutant [Jansen et al., 2011]). Blocking ABD 2 needs a phosphorylation mimicry in combination with lysine depletion in contrast to ABD 1, where multiple lysine exchanges to methionine are sufficient to impede actin binding. All in all, R* is shifted to higher R, when binding affinity is reduced without changing the overall shapes of the frequency sweep curves (insets, fig. 3.3a and b). Already discussed effects to G" in some cases are excluded. A change of the off-rate due to the lost minimum in G" of mutant 1 could be a reason for delaying bundle formation by changing the affinity with a point mutation.

3.3 Nonlinear response of actin-mutant fascin networks

A shear strain of 250% at a constant shear rate $\dot{\gamma} = 5$ %/s is applied for all studied mutants to quantify the nonlinear response of the actin-fascin network. WT fascin has a

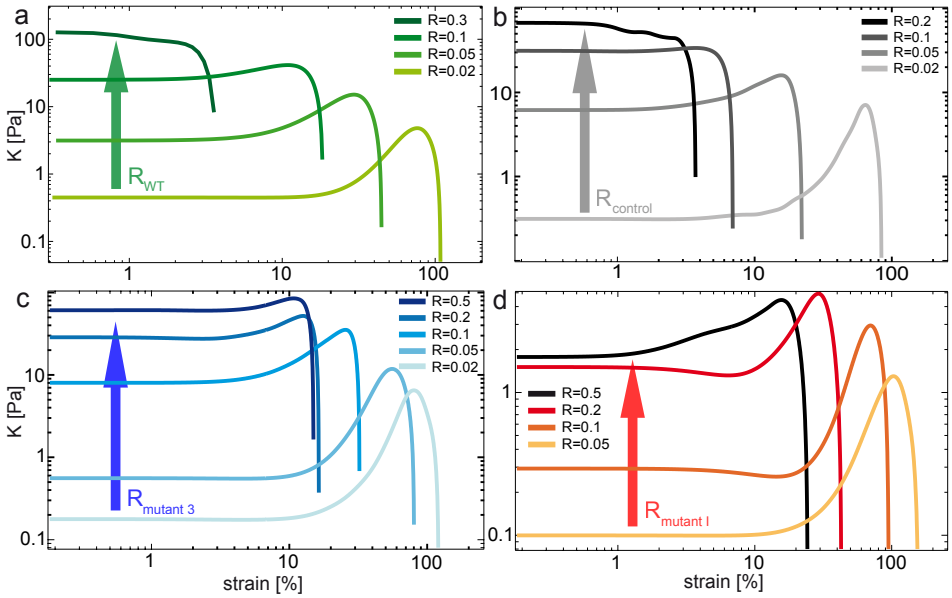

Figure 3.4: Nonlinear response of the AFN reveals affinity-dependent strain softening: stress-strain curves with differential moduli K calculated from the stress data ($\dot{\gamma} = 5$ %/s): (a) wild-type ($R = 0.02...0.3$) and (b) control mutant ($R = 0.02...0.2$) with strain hardening at low molar ratios R and strain softening at high R, (c) mutant 3 ($R = 0.02...0.5$) and (d) mutant I ($R = 0.05...0.5$) have strain hardening and no strain softening visible at high R.

characteristic behavior: at lower R strain hardening and at highest Rs strain weakening is observable in the stress-strain relation ([Lieleg et al., 2007, Lieleg and Bausch, 2007], fig. 3.4). This transition is attributed to the fact that at high fascin concentrations the macroscopic deformation will lead to forced unbinding of interconnecting fascin molecules even before nonlinear behavior of the bundles can be evoked. For all mutants with reduced binding affinities is observed that the non-linear rheological response resembles closely the characteristic response of the WT - yet only shifted to higher molar concentrations. This can be best seen by determining the critical strain (5% deviation from linear differential modulus) and the ratio of the differential moduli K_{max}/K_{lin} (fig. 3.5). Similar to G' in frequency sweeps (insets, fig. 3.3), strain-K curves only seem to be shifted to higher Rs while not changing the overall shape when being compared to WT curves (right insets, fig. 3.5a and b). ABD knock-out mutants 4 and IV behave pure actin-like (fig. 3.3). Likewise the control and the constitutively active mutant 2 is behaving like the WT.

The shift is about one order of magnitude in the linear properties such as G_0 of mutant 1 (R=0.2) compared to WT fascin (R=0.02). ABD2 mutant I's G_0 is shifted by a factor of 5. In the nonlinear regime, the characteristic response of mutant 1 are shifted by about a factor of 5 for $K_{max}/K_{lin} = K_{max/lin}(R_{WT} = 0.1) \simeq K_{max/lin}(R_1 = 0.5))$ and γ_{crit}. Mutant I's nonlinear response is shifted by a factor of 4 in the K_{max}/K_{lin} at $R_I = 0.2$ while about a factor of 5 for critical strains at $R_I = 0.5$.

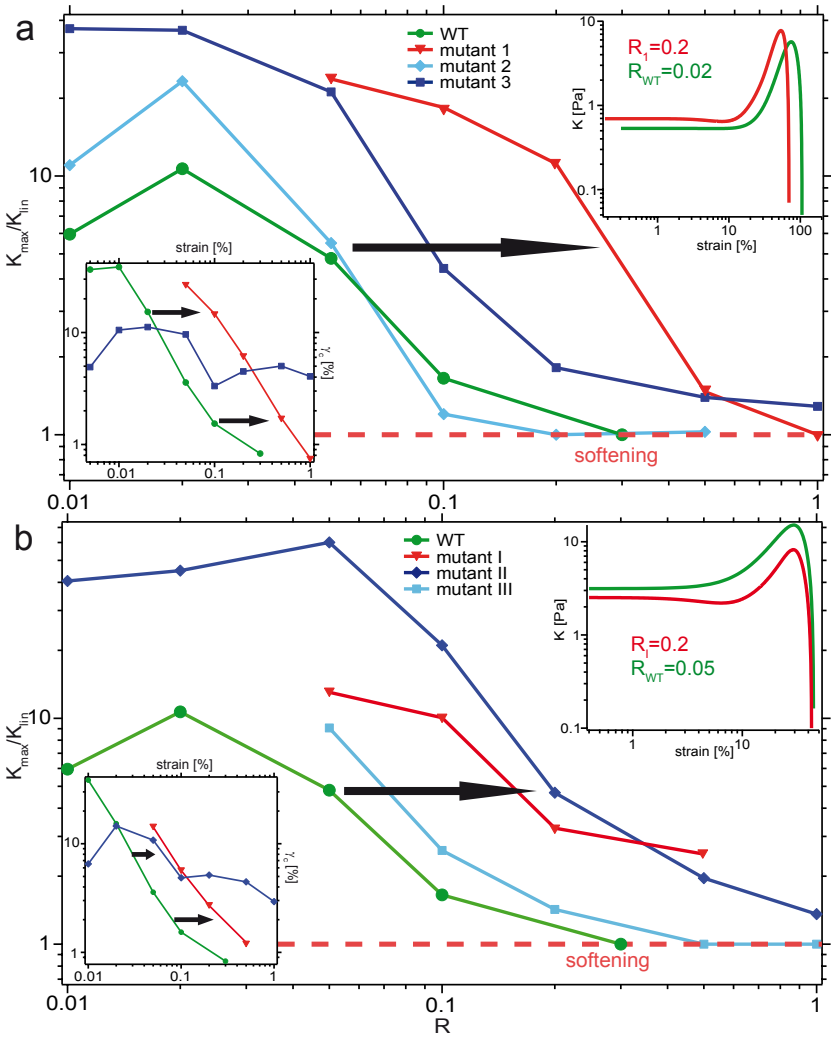

Figure 3.5: Non-linear measurements show shifted K_{max}/K_{lin} ratios and critical strains without changing the overall shape of the strain-K curves: K_{max}/K_{lin} is decreasing with higher molar ratios R: ABD1 (a) mutants show a shift with the exception of constant active mutant 2 (pale blue), whose maximum is higher than observable in WT AFN (green). Mutant 3 (dark blue, a) does not reach the softening regime defined by a value of 1. (b) ABD2 mutants show similar behavior with mutant II (dark blue) and I (red) not achieving a strain softening, while mutant III's softening (pale blue) occurs at a higher molar ratio. A shifting of the K_{max}/K_{lin} maximum to higher Rs is visible for all ABD 2 mutants. Critical strains γ_c reveal a shifting to higher Rs for mutant 1 (red, left inset, a) and mutant I (red, left inset, b), while maintaining a similar slope compared to the WT (serine-depleted mutants 1 and I). Furthermore, mutants 3 and II have less steep slopes. While critical strains and K_{max}/K_{lin} are shifted, strain-K curves of mutant 1 (R=0.2, red, right inset, a) and mutant I (R=0.2, red, right inset, b) do not change their appearance by shifting to higher molar ratios compared to the wild type (R=0.02, a; R=0.05, b, green)

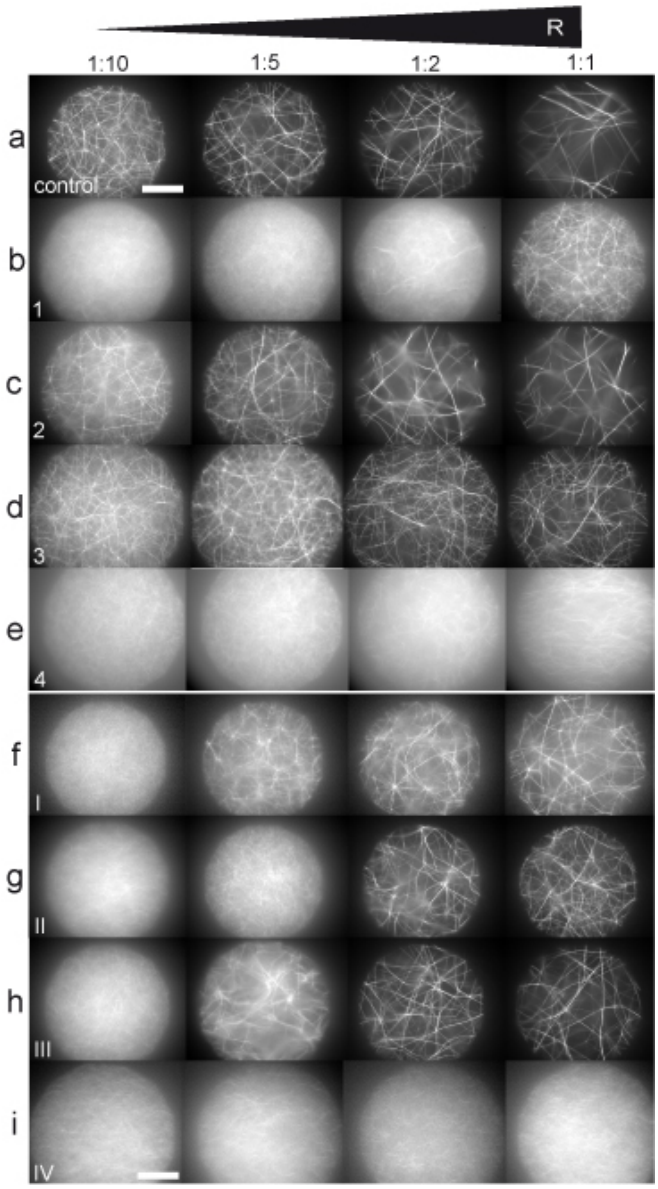

Figure 3.6: Fluorescence images of molar ratio series reveal shifted bundle regimes: (a) bundle thickness increases with R for the control mutant. Constant active mutant 2 (c) and single lysine-deprived mutant 3 (d) show similar bundle formation despite mutations. This is not the case for mutant 1 (b), I (f), II (g), III (h): The bundle phase is shifted to higher Rs with mutant 1's and II's bundle phase being the most postponed. Complete knock-out of binding domains with no visible bundles and reduced fluctuations is achieved with multiple lysines-substituted mutants 4 for ABD1 (e) and IV for ABD2 (i). Due to $c_{actin} = 3$ µM, there is an overall shift of bundling to higher R (see also [Lieleg et al., 2007]) compared to rheological experiments with $c_{actin} = 9.5$ µM (scale bar 3 µm, actin labeling with Alexa488-phalloidin)

3.4 Fluorescence imaging reveals a lag of bundle formation

Fluorescent micro-graphs reveal that a delay of bundle formation is observable for the studied mutations. The series of fluorescence images are taken at a concentration of actin $c_{actin} = 3$ µM. Wild-type fascin shows straight bundles formed with bundle thickness with increasing R until a maximum diameter [Claessens et al., 2008]. For mutant 1 (fig. 3.6b) and the ABD2 mutants (fig. 3.6f to h) straight bundle formation is shifted to higher concentration ratios in comparison to the control mutant (fig. 3.6a). The de-phospho-mimicking mutant 2 (fig. 3.6c) and the control mutant behave WT-like. For mutant 4 and IV - the complete ABD1 and ABD2 knockouts - no bundle phase emerge (fig. 3.6e and i): only filaments with less fluctuations than pure actin filament solutions are visible. This reduction results from binding the uncompromised second binding site of fascin. For similar mutants as mutants III and IV, electron microscope micro-graphs showed that changed bundle structures are observable with reduced bundle thickness using a R271E/K353/358E mutant at equimolar ratios of fascin to actin [Jansen et al., 2011].

3.5 Discussion

Systematic mutations in both binding pockets of the ABP fascin reduced effectively their affinities, leading to a detectable structural and mechanical change of the in vitro networks at a given concentration. For most mutants the effect of reduced affinities can be compensated by increasing the molar ratio of the cross-linking proteins - resulting to the same linear and nonlinear response of the network and its structure. Even the absolute value of the moduli can be obtained, which confirms that these networks are well equilibrated and in thermal equilibrium. This is in sharp contrast to α-actinin or filamin networks, where the binding propensity of the crosslinking proteins forces the networks into a kinetically trapped state [Schmoller et al., 2008b, Gardel et al., 2002].

The Actin-binding sites of fascin lie in the beta-trefoil domains 1 and 3. ABD1 was described as a MARCKS sequence [Ono et al., 1997] with a serine residue S39 and two lysine residues K41 and K42. S39E phospho-mimicking mutation (mutant 1) enables to shift fascin actin bundling activity to higher molar ratios. A constant active S39A mutant (mutant 2) shows WT behavior. The K41/42M fascin mutant (mutant 4) loses its actin bundling activity completely. This confirms the results about bundling behavior and MARCKS sequence being the actin binding site from earlier studies [Ono et al., 1997, Vignjevic et al., 2006]. The suggested binding site in β-trefoil domain 3 [Jansen et al., 2011] are acknowledged by combined mutations at S357, K358 and K359 (mutant IV). More mutations are needed to block out ABD2 than ABD1. For ABD1, substituting lysine residue K41 seems to be sufficient for loosing actin binding activity.

The actin-binding constant is reduced by phosphorylation of protein kinase Cα by an order of magnitude (from WT $3.5 \star 10^6$ 1/M to $< 0.5 \star 10^5$ 1/M) [Ono et al., 1997]. By looking at the plateau moduli G_0 plotted in fig. 3.3, the R* is shifted by one order of magnitude for the phospho-mimicking mutant 1. Thus affinity A_1 of mutant 1 could be

directly connected to the plateau modulus G_0 via the shift of the molar ratio dependence. The nonlinear response of mutant 1 is less shifted implicating less influences of changed binding sites to nonlinear properties. Here, reducing the lysine charges of ABDs may lead to a higher force dependence of the fascin off-rate. Therefore, faster unbinding of inter-bundle cross-links may happen under load rather than intra-bundle unbinding events.

The G_0-plot (see fig. 3.3) shows two regimes for the bundling mutants: Until a critical molar ratio R* the slope is small. Then with emerging bundling the slope increases without drastic differences between the mutants. R* only shifts to higher Rs, while not changing the overall highest plateau modulus except for mutant II. A reason for reaching those high plateau moduli despite reduced affinity could be that WT fascin and actin already maxes out at $R = 0.25$ [Claessens et al., 2008], while actin is still not totally coated by fascin. Thus binding sites for additional fascin remain. In the mutant situation, this additional binding sites of actin could be occupied by the mutants and add stability to the AFN. Reduced binding affinity for one binding domain could be countered by binding more fascin. The G_0 could increase therefore further until $R = 1$ (see fig. 3.3) - maybe limited by bundle twist and its entropic cost [Claessens et al., 2008]. If the images of wild-type and mutant 1 are compared, it can be seen that the mutant's bundle phase is shifted to higher R without basic changes in morphology of the AFN. Therefore bundle persistence length in AFN could depend on the amount of fascin (R) and the affinity of fascin's ABD. Here, the mutation contains a phosphorylation site and thereby a potential target for destabilization of bundles *in vivo* by kinases. By phosphorylation, the maximum G_0 for a certain molar ratio is reduced and the bundle persistence length should rise. Cells with that mutant may be able to create no filopodia at all or softer versions for an adequate environment and thereby, establish a way to destroy filopodia faster in order to reduce tissue invasion. The constant active mutant 2 could achieve a higher number of filopodia and therefore promoting the chance for tissue invasion.

The fast exchange of fascin in filopodia explains their stable and dynamic character. It is to be assumed the reason why filopodia form and bend without breaking - thereby having a rigid and soft mechanics. Fascin is an orientation selective cross-linker [Courson and Rock, 2010]. This property could have an influence on the coating process: high affinity binding site binds first and because it is a polar bundler all binding sites for high affinity connect to actin while the low affinity binding sites are unbound at first or dissociate much faster. The bundle formation by connecting two actin filaments is then governed by the low affinity binding sites. But the nucleation phase filament to filament binding [Yang et al., 2006] could also be unchanged. It could be prolonged and lead to longer bundle times which depend on actin lengths. After bundling of two filaments, entropic cost, which is a main criterion for actin-fascin bundling [Claessens et al., 2008], prevents from forming thicker bundles, thus G_0 is reduced, because there are more fluctuations as a result of higher dissociation rates for mutant fascin. Overall, when less thick bundles are formed, more bundles should form because of hangover material. This would confirm fluorescence data where bundle phase is shifted to higher molar ratios. More fascin is needed for mutant 1 to counter the energy cost of entropy and bun-

dle thickness should rise. For future considerations, the bundle thickness of actin-fascin networks could be measured by small angle scattering to determine the helical twist of actin-fascin mutant bundles. TEM experiments could be used for direct measurements of the bundle thickness to learn more about the molar ratio dependence.

In conclusion, the reduction of affinities of the ABP fascin to actin leads to a delay of bundle formation in fluorescent and rheological data. Macrorheology proves to be a good technique to examine protein network behaviors regulated by protein affinities. By obstructing the binding domains carefully, the structure of the actin-fascin networks and therefore its mechanical properties change, while maintaining its WT character with straight bundles and shifting properties to higher molar ratios. Direct annihilation of the ABD properties results in a loss of any actin binding potential in microscopical and rheological measurements. In a cellular context, this could be a major feature of the fascin molecule to steer its bundling behavior and filopodia mechanics. Cells adjust their mechanosensorial, motile and mechanical properties in concert with many other proteins of the cell. As a basic symmetric ABP with two ABDs without forming complicated multimers, fascin is a good and simple target for a cell to change its actin affinities by phosphorylation or regulatory proteins. The following chapter will focus on the mechanosensitive actin binding protein EPLIN. EPLIN is a nonpolar cross-linker and exhibits different mechanical and structural properties compared to the polar cross-linker fascin.

4 EPLIN: a mechanosensitive actin-binding protein

In the previous chapter, it has been shown how binding affinities evoke changes in mechanical and structural properties of the ABP fascin. As polar cross-linkers, fascin and for example espin form straight bundles within actin networks. These networks incorporate transiently cross-linked bundles, where thermal fluctuations of the bundle positions and reorganizations within the network are still observable [Schmoller, 2008, Lieleg et al., 2009b]. Nevertheless, there are completely static networks created by the cross-linker filamin, that remain unchanged over the course of days [Schmoller et al., 2008b]. Due to branched structures, these networks are interconnected with a high number of cross-links, thus multiple unbinding events would be needed to execute structural changes. Furthermore, this branching leads to kinetic trapping as in case of filamin and α-actinin, where networks are trapped in different meta-stable states depending on the history of network formation [Schmoller et al., 2008b, Lieleg et al., 2009b].

By using the non-equilibrium nature of these cross-linked actin networks, cells are able to form various meta-stable structures with changing mechanical properties while using the same building blocks. One of those basic constituents has been drawn into focus: the LIM domain containing ABP EPLIN (Epithelial Protein Lost In Neoplasm) [Maul and Chang, 1999]. It has been identified in proteomic analysis via mass spectrometry approaches as a component of focal adhesions [Schiller et al., 2011]. Furthermore, LIM domain proteins are potential tension sensors, because of a myosin II dependent recruitment [Schiller et al., 2011]. EPLIN is a compact actin-binding protein with two binding sites that bundle actin and inhibits the branching nucleation of actin filaments by the Arp2/3 complex [Maul et al., 1999]. A recent study on high density motility assays, in which polar and apolar cross-linkers are compared to EPLIN resulted in similar behavior of EPLIN to the branching cross-linkers filamin and α-actinin [Schaller et al., 2013]. However, differences manifest in more effective crosslinking in active systems, higher ability to stabilize actin networks under stress and maintenance of network integrity at low concentrations. Further reports show that *in vivo* EPLIN has been sighted as a mechanosensitive regulator of adherens junction remodeling by cooperation with vinculin, where tension is important at the EPLIN/α-catenin interface, which binds cadherin [Taguchi et al., 2011]. Due to the *in vivo* roles of ABPs, it is of high interest to achieve a deeper understanding of the parameters, which control the structure of actin networks. Further interest lies in how these structures are connected to the mechanical properties, which lead to mechanosensing and various cellular states *in vivo*. The impact of different cross-linking ABPs on the mechanical properties of actin networks has been examined over the last decade by reconstituting and simulating *in vitro* model

systems of diverse intricacy [Bausch and Kroy, 2006, Kasza et al., 2007, Heussinger and Frey, 2007, Huisman et al., 2007, Conti and MacKintosh, 2009, Head et al., 2003, Wilhelm and Frey, 2003, Astroem et al., 2008, Schmoller et al., 2010]. The high complexity of the actin cytoskeleton is tuned by each cross-linking protein via its own characteristic impact on structural and mechanical performances [Bausch and Kroy, 2006, Wagner et al., 2006, Schmoller et al., 2008b, Shin et al., 2004, Tseng and Wirtz, 2001, Tseng et al., 2004, Ward et al., 2008]. To learn more about the role of EPLIN in this concert of proteins and mechanics, the structural and mechanical characteristics have to be further determined. It has to be investigated whether EPLIN depicts a similar non-equilibrium character of kinetically trapped actin bundle networks as observed for actin-filamin structures [Schmoller et al., 2008b]. A first step to decipher EPLIN's structural and mechanical properties - that may be the basis for observed mechanosensing in cells [Taguchi et al., 2011] - consists of an investigation of the viscoelastic response in relation to the micro-structure.

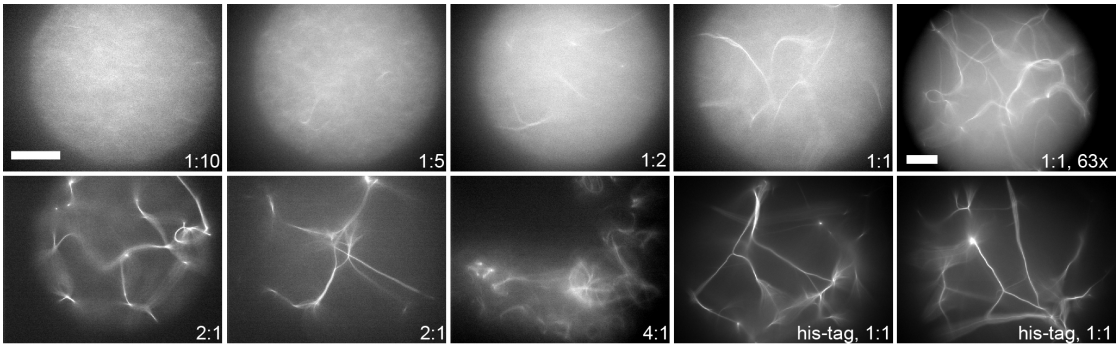

Figure 4.1: Fluorescent images of actin-EPLIN networks: (a) for small molar ratios heterogeneous actin-EPLIN-flag networks are observed - in contrast to higher molar ratios where bundles dictate the network structure. For very high $R = 4$, bundle clusters are revealed. (b) EPLIN-his lays out the same network structure as EPLIN-flag - revealing no impact from different tag choices. Parts of the data are already shown in [Schaller et al., 2013] ($c_{actin} = 3$ µM, scale bar 3 µm)

In this chapter, the very first characterization of structural and mechanical properties of actin-EPLIN networks will be presented. Similar to actin-filamin networks, two pronounced regimes emerge: Low molar ratios of EPLIN to actin lead to a filamentous phase where EPLIN may cross-link single actin filaments. Here, a unique feature is seen for low actin concentration in the formation of actin-EPLIN ring-like structures. At high EPLIN concentrations, a purely bundled network is formed that exhibits branched bundles. For even higher molar ratios R_{EPLIN}, bundle clusters are observed, which depend less on the actin concentration as in the case of filamin. Rheological data is in good agreement with the bundle onset and formation, but a filamin-like structural saturation is not observed. Here, a difference in network formation processes may occur in comparison to filamin, because aggregation may not control the network formation in actin-EPLIN networks to the same extent as in actin-filamin networks.

4.1 Structure of actin/EPLIN networks

In the following, the structure of actin-EPLIN networks is investigated as a function of the actin concentration c_{actin} and the molar ratio of EPLIN to actin R_{EPLIN} with epifluorescence microscopy. The latter is varied form $R = 0.001$ to $R = 4$ and actin concentrations of $c_{actin} = 3$ µM and $c_{actin} = 10$ µM are used. By changing the concentrations, various network structures are found (fig. 4.1): low R results in networks of single filaments, which could be cross-linked similar to actin-filamin networks are assumed to do [Stossel et al., 2001]. A phase of ring-like structures for the low actin concentration is depicted in fig. 4.2. The formation of bundles occurs at a certain critical ratio R^*_{EPLIN}, which decreases only slightly for a higher actin concentration (fig. 4.3). In this bundle phase, highly static and purely bundled networks are built with no remaining single filaments. Actin-EPLIN bundling does not depend on the tag used for purification as shown in fig. 4.1b: actin-EPLIN-his networks reveal similar bundle structure to networks with EPLIN-FLAG. Because of more convenient purification and best purity concerning SDS gel results, the FLAG tag is chosen for purification in all further measurements.

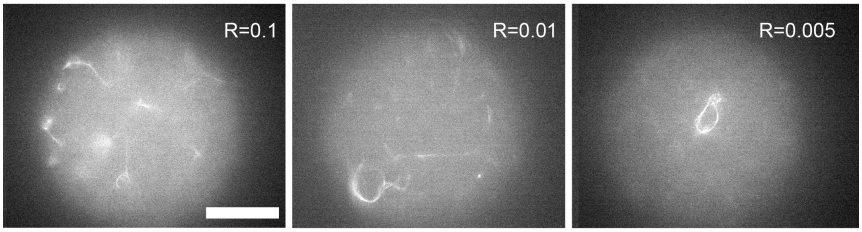

Figure 4.2: Fluorescent images of actin-EPLIN ring-like network structures for small molar ratios ($c_{actin} = 3$ µM, scale bar 3 µm)

All in all, highly curved bundles that branch and merge are observed for both actin concentrations as common structural feature (fig. 4.1). This has a striking resemblance to actin-filamin networks [Schmoller et al., 2008b]. Point-to-point cross-links are not observable with epifluorescence microscopy. Similar to actin-filamin networks, free bundle ends are not featured in these networks. At last, further commonalities to actin-filamin networks emerge: very high R_{EPLIN} induce the genesis of bundle clusters, but this seems not to be dependent on the actin concentrations as in the case of filamin [Schmoller et al., 2008b, Schmoller et al., 2008a]. These bundle clusters for filamin and EPLIN networks are evocative of the mesocopic star-shaped heterogeneities revealed in actin-α-actinin networks [Lieleg et al., 2009b]. To sum up these findings on the revealed network micro-structures, a schematic structural state diagram as a function of R and c_{actin} is shown in fig. 4.3. Overall, actin-EPLIN networks seems to be less dependent on the actin concentration than filamin. Bundle clusters do not depend on c_{actin} in the case of EPLIN - only at lower actin concentrations ring-like structures are formed.

The striking similarities to actin-filamin networks may indicate that actin-EPLIN networks exhibit internal stresses as well as observed in [Schmoller et al., 2008b]. Nev-

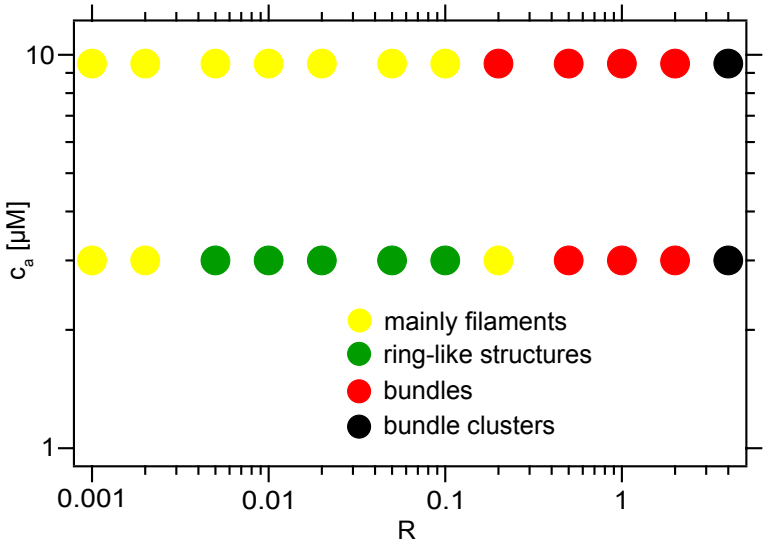

Figure 4.3: The structure of actin-EPLIN networks is revealed as a function of the actin concentration and the molar ratio of EPLIN to actin. EPLIN cross-links actin filaments at low R (yellow). For smaller R and low actin concentrations, a ring-like heterogeneous structures are formed (green). At higher R, a purely bundled network is built (red). In contrast to actin-filamin networks, less bundle clusters are observed for higher actin concentrations: Only at very high $R = 4$, bundle clusters are created.

ertheless, a hint for this assumption could be the observed ring-like structures in fluorescence images: such internal stresses may lead to these small and curved bundle phenomena. Further investigations are needed to reveal the EPLIN monomer and potential multimers structure. Then this ring formation may be revealed. How compact and how many binding sites this protein generates by dimerization could be an important parameter for actin bundling and formation of ring-like structures. A crucial role may play the potential dimerization site at the LIM domain [Maul and Chang, 1999], that exists in multiple proteins connected to mechanosensing and the cytoskeleton [Kadrmas and Beckerle, 2004]. As for filamin [Schmoller et al., 2008a], the aggregation process may be important and the bundle thickness should be investigated that depends on aggregation. Differences may be observed due to the revealed discrepancies in the structural state diagram (fig. 4.3), but similarities may prevail because of an analog non-equilibrium character of the networks resulting in a trapped state [Schmoller et al., 2008b].

To this point it has been shown that depending on the molar ratio of EPLIN to actin and the actin concentration, highly different network structures can be created. EPLIN itself has been described to be mechanosensitive [Taguchi et al., 2011] and important in cell-cell [Abe and M.Takeichi, 2008] and cell-surface adhesion [Hermann, 2011], thus it is now the next step to determine the macrorheological properties after observing pronounced differences in actin-EPLIN network structures. How single filament at low R_{EPLIN} or branched networks at high R_{EPLIN} evolve in mechanical measurements has

to be measured. In the following section of this chapter, the viscoelastic response is examined using macrorheological methods.

4.2 Viscoelastic response of actin-EPLIN networks

To characterize their linear viscoelastic properties, actin-EPLIN networks are measured in the limit of small deformations by obtaining the frequency-dependent viscoelastic moduli *G'(f)* and *G"(f)* over a frequency range of three decades. But beforehand, the polymerization is measured via *G'* while applying a small constant torque (~ 0.5 µNm). The difficult purification of EPLIN limits measurements to experimental series with a fixed actin concentration.

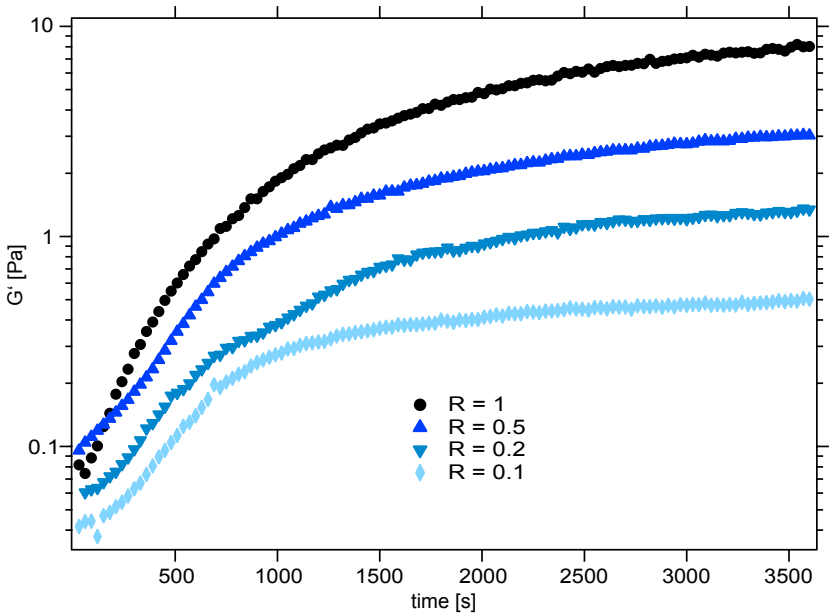

Figure 4.4: Polymerization curves for increasing molar ratios: storage modulus G' rises with increasing time due to polymerization and bundle formation. For higher ratios, G' rises faster and reaches less earlier the plateau value than the pure actin-like measurement ($R = 0.1$).

At first, as more EPLIN is initially in the sample as faster actin-EPLIN networks are formed with a higher saturation plateau in G' (fig. 4.4). For $R = 0.2$, a shoulder is observable in the G' data which could indicate a "kick-in" of bundling of actin filaments by EPLIN after following a similar course to pure actin assembly curve. Smaller ratios behave as pure actin polymerization, while higher molar ratios $R > 0.2$ show faster initial increase. In the latter case, the saturation level is reached later than in the pure actin-like measurement of $R = 0.1$, maintaining a rise in polymerization for another 1000 s. All in all, polymerization curves seem to be shifted by more EPLIN content, while the overall curve shape seems to be unchanged.

The obtained viscoelastic frequency spectra G' and G" of actin-EPLIN networks with

c_{actin} = 9.5 µM and different EPLIN concentrations are shown in fig. 4.5a. Compared to other actin-cross-linker networks with ABPs HMM [Lieleg et al., 2009b] or fascin (see fig. 3.2), these frequency spectra are entirely featureless and thereby, very similar to actin-filamin networks [Schmoller et al., 2008a]. Within the observed frequency range, this may suggest that there is no intrinsic timescale in the linear network response of actin-EPLIN networks.

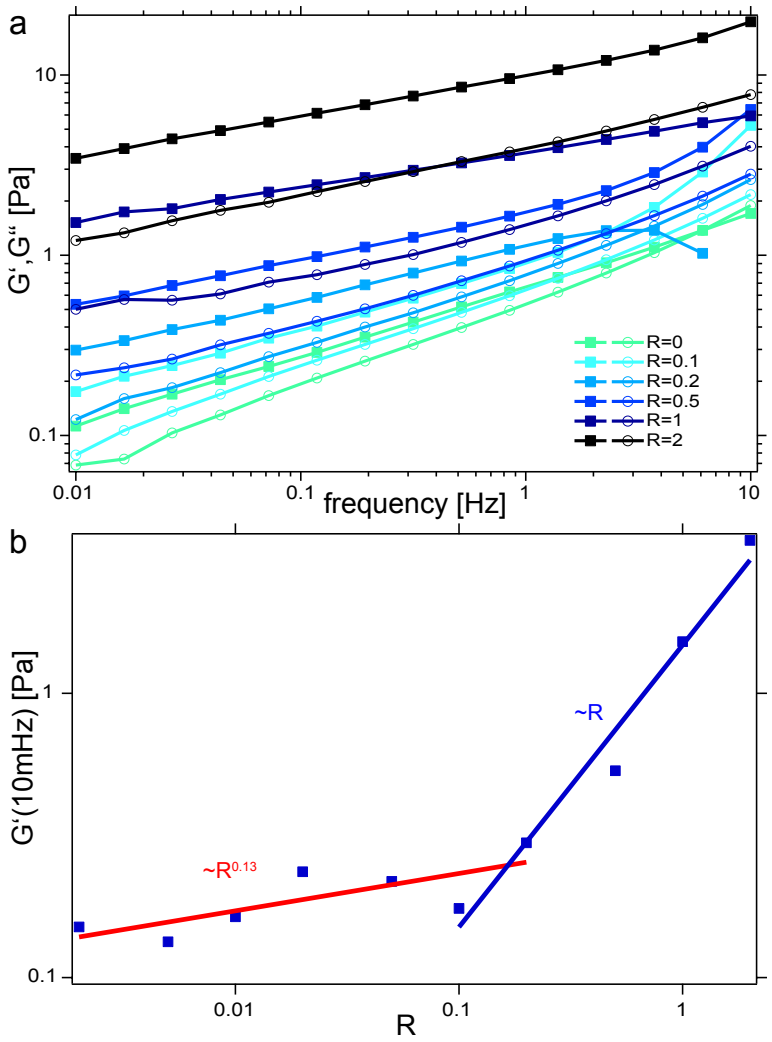

Figure 4.5: Rheological measurements of the linear regime: (a) Frequency spectrum of the viscoelastic moduli G' and G" shows featureless curves that are very similar in shape for different R. (b) Plateau moduli with rising R: until a crucial $R = R* = 0.1$, only a slow increase ($\sim R^{0.13}$ is observable. After reaching R*, G_0 rises proportional to R - marking the bundle phase.

Similar to the microscopic images, a bundling transition is observable with rheological measurements. By looking at the frequency sweep and extracting the plateau modulus $G'(10mHz) = G_0$, a transition to bundling can be seen at about R=0.2. G_0 and thereby

the stiffness increases R-dependent from $\sim R^{0.13}$ to about $\sim R$ until a maximum molar ratio $R = 2$ (fig. 4.5b). The observed clumped and sticky behavior for $R = 4$ as seen in fluorescence images could not be evaluated, because of limitations in EPLIN purification of necessary large amounts for rheological experiments. In contrast to other ABPs such as HMM [THARMANN et al., 2007], fascin [LIELEG et al., 2007] and *alpha*-actinin [TEMPEL et al., 1996], EPLIN's effect on the linear stiffness of the actin network is more weak. This resembles filamin in behavior, which was described in [SCHMOLLER et al., 2008a]. Even at high EPLIN concentrations, the G_0 rises only by an order of magnitude. Similar to filamin networks, the filamentous networks for small R could be explained by the high flexibility of individual filamin molecules [GARDEL et al., 2006], but this has to be measured with single molecule techniques. As a more compact and maybe multimer cross-linker [MAUL et al., 1999, SCHALLER et al., 2013], flexibility may differ from filamin and α-actinin. The weak increase in linear stiffness for bundled networks is a surprise and it may suggest an overall filamin-like behavior. This striking similarity to actin-filamin networks may indicate, that actin-EPLIN networks exhibit similar internal stresses as observed in [SCHMOLLER et al., 2008b]. Nevertheless, in fluorescence images observed ring-like structure may be a hint, that such internal stresses lead to these small and curved bundle phenomena. The ring-like structures are observed only at $c_{actin} = 3$ µM and therefore should not play a role at rheological measurements at $c_{actin} = 9.5$ µM.

In the limit of small deformations, the influence of filamin on the network elasticity is rather weak, but fluorescence images reveal a big impact on the structure of the network. This could lead to different effects when one leaves the linear regime. Thus, the next step is now to determine the nonlinear mechanical properties of actin-EPLIN networks. To this end, a constant shear rate $\dot{\gamma} = 5$ %/s is applied and afterwards, the differential modulus $K(\gamma) = \frac{\partial \sigma}{\partial \gamma}$ is calculated from the obtained stress-strain relation $\sigma(\gamma)$ [SEMMRICH et al., 2008]. The non-linear response of actin-EPLIN networks with $c_{actin} = 9.5$ µM is shown in fig. 4.6. By adding more EPLIN, the prototypical strain hardening of actin networks is enhanced. The dependence of the maximal non-linear network stiffness K_{max} is depicted in fig. 4.6b: With rising molar ratios R_{EPLIN}, K_{max} increases strongly. A saturation as in case for filamin [SCHMOLLER et al., 2008a] can not be observed. This may indicate that network architecture is not saturated and changes in inter-connectivity of distinct bundles created by EPLIN cross-links may not be enhanced here by pushing the degree of cross-linking between actin filaments. Furthermore, the nonlinear response $K(\gamma)$ gets broader with rising R_{EPLIN} which could be a hint to a changed network structure. In contrast, $\frac{K_{max}}{K_{lin}}$ only doubles in value from $R = 0.1$ to $R = 2$ (fig. 4.6b right inset). This reveals a strong connection of the linear to the nonlinear stiffness and only a slight dependence on R_{EPLIN}.

Finally, to characterize the transition from the linear to the nonlinear regime, the critical strain γ_c is the parameter of choice. It pins down the onset of nonlinear deformation at 5% deviation from the linear modulus. In the case of actin-EPLIN networks, a decrease of γ_c by about one order of magnitude with molar ratios rising by an order of magnitude is depicted in fig. 4.6b (left inset). Similar to G_0, only a weak dependence of R is revealed. This may imply a connection of linear stiffness to the onset of non-linearity.

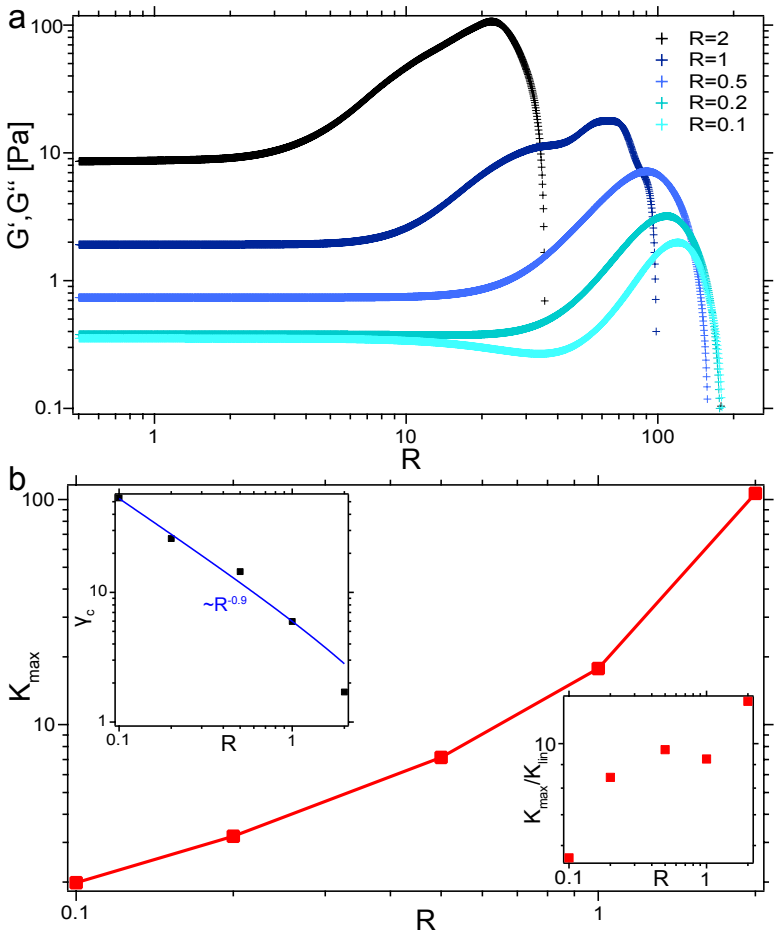

Figure 4.6: Nonlinear mechanical behavior of actin-EPLIN networks: (a) The differential modulus K is shown as a function of strain for different molar ratios of EPLIN. (b) K_{max} is plotted for different R and rises to a maximum. The inset shows the dependence of the critical strain on R_{EPLIN}.

4.3 Discussion

Together with actin, EPLIN forms branched network at high concentrations similar to those observed for filamin. At low EPLIN concentrations a filamentous phase is observed with additionally ring-like structures for a lower actin concentration. Bundle clusters are revealed for high EPLIN concentrations, but not dependent on the actin content as in case of filamin [Schmoller, 2012]. These nearly perfect similarities may suggest a similar sticky ABP phenotype as filamin, which is characterized by an internal kinetically trapped state so far not observed for actin-EPLIN structures. Structural saturation as revealed for filamin [Schmoller et al., 2008a] may occur at higher concentrations that have not been possible to measured so far. Until now, the molar ratio R_{EPLIN} is experimentally limited due to purification constraints and large quantity of protein necessary for macrorheological measurements.

In a high density motility assay, EPLIN exhibits a different behavior than other cross-linkers like filamin or alpha-actinin. It offers a more effective cross-linking in these active systems with a higher ability to stabilize actin networks under stress while maintaining the integrity of the network at low concentrations [Schaller et al., 2013]. This more sensitive behavior may stand in connection with the observed ring-like structures for low EPLIN concentration. The relatively late bundling onset of actin-EPLIN networks for $R_{EPLIN} > 0.1$ compared to filamin or α-actinin [Schmoller et al., 2008a, Lieleg et al., 2009b] suggests a less sensitive behavior. But here, the type of the systems - active or passive - may play an important role in cross-linker force dependent performances and *in vivo* duty niche.

In the future, bundle sizes have to be measured as done for filamin [Schmoller, 2008] and finally it has to be determined if multimerization occurs. A kinetically trapped state similar to filamin may be discovered with UV laser cutting as done before with photobleaching experiments of actin-filamin networks [Schmoller et al., 2008b]. Moreover, the ring-like structure has to be more closely investigated. An incorporation of EPLIN into cell mimicking active systems is another future task to build a bridge to *in vivo* properties.

The results of this chapter highlight that actin-EPLIN networks form branched bundles for high concentrations of EPLIN and a filamentous phase for low R_{EPLIN}. As the micro-structure and rheology feature many similar properties of actin-filamin networks, a structural saturation to the same extent is not seen for actin-EPLIN networks. So far, an aggregation controlled network formation process has not been observed. The findings of this chapter together with a recent *in vitro* study [Schaller et al., 2013] show differences in behavior of EPLIN in passive and active systems compared to other cross-linkers: a specific role for EPLIN in the cytoskeleton emerges now as well, which enables a cell to achieve different states for various cellular tasks. Such a case is reported for certain tumor cells, that exhibit low levels of EPLIN revealing an important role for EPLIN in cell motility [Maul and Chang, 1999, Leitner et al., 2010]. *In vivo* characterized as mechanosensitive actin bundler [Taguchi et al., 2011] that as a LIM domain containing protein locates force-dependent at focal adhesions [Schiller et al.,

2011, Karaköse, 2012], EPLIN's interaction with actin has to be further examined: How mechanical properties together with corresponding distinct micro-structures lead to mechanosensing and potentially mechanically triggers gene regulation *in vivo*. The following chapter will focus on how cells react to external forces and thereby, change their gene expression by cytoskeletal force transduction by such proteins as actin, fascin and EPLIN to adapt their cytoskeleton and regulatory proteins to enter a new cellular state.

5 Mechanotransduction and gene expression in interphase

In the previous chapter, the mechanosensitive actin cross-linker EPLIN has been characterized in terms of structure and mechanical properties of actin-EPLIN networks. EPLIN contains a potential mechanosensitive LIM domain [Kadrmas and Beckerle, 2004, Schiller et al., 2011]. Furthermore, mechanosensory machinery have been found at the interface EPLIN α-catenin which performs as a tension transmitter [Taguchi et al., 2011, Chervin-Pétinot et al., 2012]. This emphasizes bond properties which are considered important component in mechanotransmission of forces in cells [Hoffman et al., 2011]. Mechanical factors such as applied forces or the rigidity of the extracellular matrix affect form and function of cells and organisms. Mechanotransduction - the conversion of mechanical forces into biochemically relevant information - is involved in multiple developmental, physiological and pathological processes [Orr et al., 2006]. Blood flow imposes fluid shear stresses on the endothelial cells which lines the vessels in the vasculature and for example hypertension results in thickening of the arterial walls, which is a high risk criterion for cardiovascular diseases [Hahn and Schwartz, 2009]. Bone and muscle's development and pathobiology strongly relies on mechanical forces from weight and muscle contraction, while lung physiology and disease is influenced by forces from inflation [Burger and Klein-Nulend, 1999, Raisz, 1999, Orr et al., 2006, Liu et al., 2010]. Tissue stiffness influences a vast number of biological processes [Discher et al., 2005]. For example tumors can be identified by palpation due to locally increased stiffness [Hoffman et al., 2011]. The rigidity of the extracellular environment governs the differentiation of mesenchymal stem cells [Engler et al., 2006] and myotubes [Engler et al., 2004]. Muscle stem cell self-renewal is regulated by substrate elasticity [Gilbert et al., 2010]. A key process in rigidity sensing is the modulation of cellular contractility [Hoffman et al., 2011]. Structures that generate and endure cellular forces are part of force-sensing [Orr et al., 2006]. Cytoskeletal proteins such as actin with actin binding proteins for example fascin, EPLIN and tubulin are essential in the mediation of external mechanical inputs in almost all systems [Chen, 2008]. Cellular adhesion has its importance in connecting cells to neighbor cells or the extracellular matrix. Here, key players are the cadherins [Schwartz and DeSimone, 2008] and integrins [Katsumi et al., 2004] - while the interplay of all mechano-transmissive pieces and processes is still unknown.

A complete picture of mechanotransduction is still missing, although progress has been made towards a better understanding. A future concept may include force-induced changes of rates of key subcellular processes to influence cell function [Hoffman et al., 2011]: cells may function as a multiband pass filter in which time-dependent stimuli

activate individual signaling pathways that change cell fate. A better understanding of mechanotransduction and its key processes may be achieved by measuring forces and gene expression in one experiment. Although cell mechanics have been studied comprehensively over the years with various technical approaches [Evans and Yeung, 1989, Bausch et al., 1998, Pelham and Wang, 1999, Fabry et al., 2001, Trepat et al., 2004, Trepat et al., 2007, Ragsdale et al., 1997, Smith et al., 2005, Guck et al., 2001, Fernández et al., 2007, Fernández and Ott, 2008], a combination of extensive gene analysis and stress-strain measurements via dynamic shear has not been used so far in a mechanotransduction context.

In this thesis, dynamic shearing is combined with qPCR for the first time, which enables to focus on single gene responses to external forces. In contrast to 2D mechanostimulation with elastic rubber membranes, no volume changes occur in shear experiments. Furthermore, a full control of adhesive conditions is possible: albumin coated glass prevents cell adhesion during mechanostimulation. This provides a kind of integrin "knock-down" situation. Other coatings with fibronectin or other extracellular matrix compounds are also applicable. Applied frequencies and strain can be tuned to determine the hypothesized bandpass filtering of mechanotransducers. Furthermore, the qPCR method has to be refined for our mechanical purposes in terms of sample preparation, the selection of reference genes and data mining in the context of the MIQE codex [Bustin et al., 2009]. As a start, only cells in interphase are examined, because their gene expression underlies changes. Cells in mitosis have no active genetic regulation [Pollard and Earnshaw, 2008]. How forces are transduced and resonate in mitotic cells is discussed in chapter 6. In this chapter, a novel setup is introduced to characterize mechanotransduction via high throughput mechanomics: a combination of gene expression analysis with force measurements of a large amount of cells. Both techniques the mechanostimulation by dynamic shear and gene analysis method qPCR are refined. Cell monolayer rheology [Fernández et al., 2007] is used together with high quality microscopy, while qPCR data is normalized with cell culture data which enables in a unique way to extinguish influences of gene expression before experiments. β-actin the standard reference gene [Hammer et al., 2009, Engler et al., 2006] is revealed to be unsuitable as a reference due to large variations in gene expression of untreated cells. Myoblasts are sheared and tested on gene regulation and stress-strain relation but no reproducible mechano-induced signal is found. Cells seem to respond very incoherently throughout the experiments. Surprisingly, no adaption to external mechanical stimuli is revealed in terms of gene expression and mechanical properties of cells. Results, methods and pitfalls are critically discussed.

5.1 Variance of gene expression of cell lines reveals β-actin is inappropiate as reference

In the following, the variations in gene expression of standard cell types are investigated. Mouse osteoblasts, fibroblasts and myoblasts are examined. GAPDH is used as reference - "housekeeping" - gene, since its expression is supposed to be stable when pseudogenes and diseases are ruled out [Harper et al., 2003]. As a gene of interest to be analyzed

under standard cell culture conditions, β-actin is chosen. β-actin is ubiquitous expressed and one of the most abundant proteins in cells. A good reason to look at this gene is its usage as reference gene in literature. Also, it is used predominantly in cases of studies of mechanical responses of cells and regulation of actin networks [Engler et al., 2006, Hammer et al., 2009, Papaiahgari et al., 2007]. β-actin has an important function in RNA transcription [Hofmann et al., 2004], which may imply that β-actin is a bad choice for reference. Any influence of the many pseudogenes of β-actin [Raff et al., 1997] could be excluded due to the special design of the primer pairs.

Osteoblasts show large expression changes from passage 10 to passage 11 (fig. 5.1a), while fibroblasts differ within one passage but different flasks (p9-1 and 2, fig. 5.1b). Myoblasts reveal the smallest expressional variations in gene levels of all three examined cell lines (fig. 5.1c). Several studies emphasize that a careful choice of reference genes is indispensable [Bustin et al., 2009, Harper et al., 2003, Radonić et al., 2007]. Threshold cycles of GAPDH samples do not vary much, therefore GAPDH seems not to be the source of varying expression. GAPDH seems to be a reasonable choice for the following measurements over β-actin as normalizing reference gene that does not change due to mechanical measurements or cell culture conditions. Nevertheless more than one reference gene should be used in the future. The choice for an additional reference gene has to be carefully executed to find a stable reference gene for mechanostimulation purposes. Expressional variations of a major gene like β-actin is not optimal when mechanostimulation is applied - certainly in the case of using it as a reference gene. Less variation of β-actin gene levels may be recommended for gene expression studies because mRNA levels may be more stable before the experiments. Thus, myoblast cells seem to be the cell line of choice here so far. Different expression levels due to technical aspects like RNA isolation, charge of cell medium or reverse transcription reaction can be considered to be only minor differences (fig. 5.1b, c, fig. 5.2a). Nevertheless, these technical influences suggest that a fold change (see 2.3.1) of at least 1 seems to be a reasonable signal.

Another interesting property of myoblasts is the potential of multiple differentiation pathways - one way is osteogenesis, another one way is myogenesis: myoblasts transform into myotubes by adding horse serum to the cell medium or incubation of several days (see 2.1.1). This differentiation into long multicellular muscle cells can be confirmed by looking at specific myogenic markers [Engler et al., 2006, Lluís et al., 2006]: MyoG, Myf5, α-actin and p21 are all down-regulated in normal myoblasts in contrast to myotubes expression levels (fig. 5.2a, b). These results are a good proof for a working qPCR setup. Mechanics of extracellular space - for example cell-cell tension - have changed due to the confluence of the cell monolayer when myoblasts are incubated over several days (p6 (72h), fig. 5.2a). Here, Myf5 is also up-regulated. It seems to be promising to examine another way of changing the extracellular space and mechano-signaling by applying a dynamic mechanostimulation and study the effects of force and genetic response within one experiment.

All in all, the variations in gene expressions in cell culture pinpoint the need for an additional novel normalization step by incorporating cell culture data into experimental

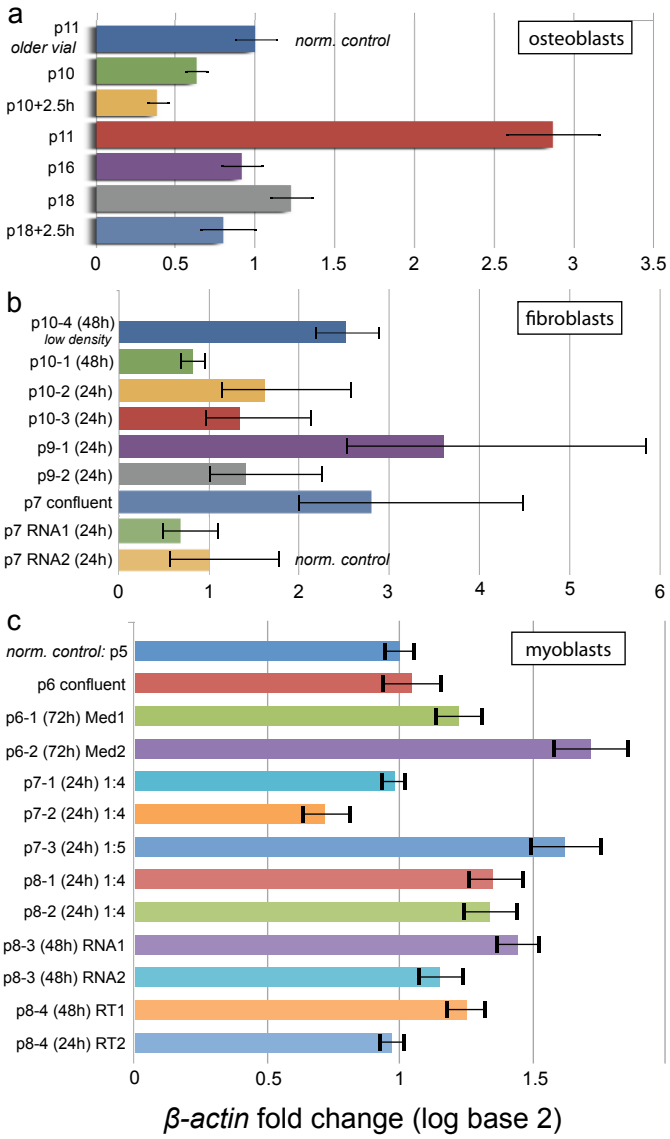

Figure 5.1: Gene expression variability across cell lines: (a) mouse osteoblasts, (b) fibroblasts and (c) myoblasts. For similar passages and splitting ratios, less variation of mRNA levels are found for myoblasts (p7/8). p indicates the passage of the corresponding cell flask. RNA isolation and reverse transcription reaction (RT) are examined but show only slight deviations. Passage age is explored (24h-72h) and reveals massive dependence on dwelling times in flasks. Different medium flasks are denoted as Med1/2.

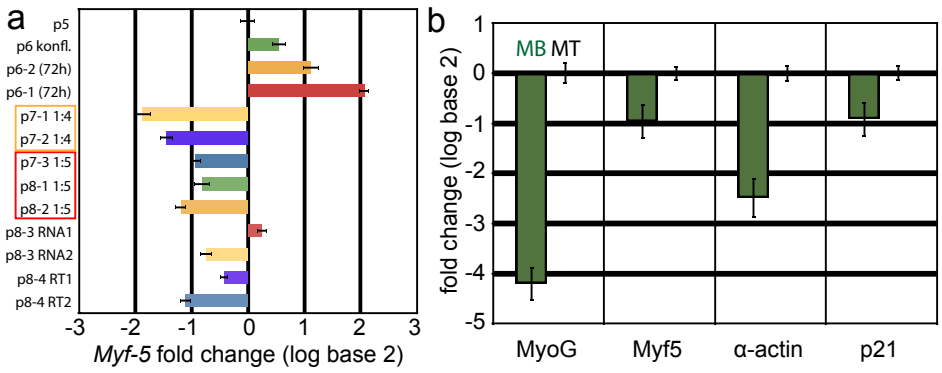

Figure 5.2: Myogenic cell marker in myoblast cell culture: (a) Myf5 regulation in cell culture of passage 7 and 8 show similar levels when split identically (1:5). Longer incubation (p6 72h) results in upregulation and thereby differentiation into myotubes. As controls, different reverse transkripase (RT) reactions and different RNA isolations (RNA) reveal dependence of gene level on technical variations. (b) Myoblasts versus Myotubes: typical gene markers for myogenesis have smaller mRNA levels in myoblasts (green) when compared with differentiated myotubes (fold change = 0)

data. Myoblasts are used from this point on because of their differentiation potential as seen with myotubes and less heterogeneity in cell culture gene expression of likewise treated culture flasks.

5.2 Culture flask normalization of experimental data

In the following, the novel cell culture flask normalization method is demonstrated with the two GOIs c-fos and Myf5. Mouse myoblasts are sheared for one hour at $f = 0.3$ Hz with a maximum strain $s = 100\%$. To ensure to cover variability of cell culture, shear (E1-4) and control experiments (C1-3) are performed at least as triplets. After mechanostimulation, qPCR is performed. GAPDH is used as reference gene, whose expression is supposed to be stable. Prior to the experiments, RNA is isolated from the same cell flask as used for the experiments afterwards. Data from pre-experimental cells are used to normalize gene expression changes of the experiments. This ensures that gene expression changes resulting from mechanostimulation are measured properly.

At first, gene levels of all shear and control experiments are examined by using only one control experiment C1 as a control (fold change = 0). Gene level data of Myf5 reveals differences of about a factor of 8 prior the experiment (fig. 5.3a). After the experiments, expression levels of the sheared cells are reduced. Control experiments have a similar gene expression before and after the experiments. Gene data of c-fos is less varied before the mechanostimulation, while shear experiments show a up-regulation due to mechanostimulation (fig. 5.3b). On the contrary, the controls C1-C3 have similar post-experimental levels and exhibit less changes during the experiment. Myf5's post experimental data would suggest that no expression is achieved without a normalization

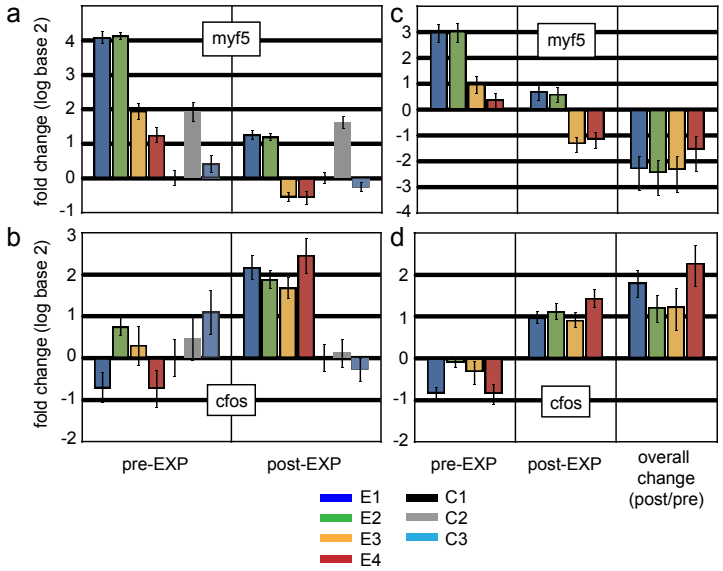

Figure 5.3: Culture flask normalization of gene expression: (a) Myf5 and (b) c-fos are examined as genes of interests before and after the shear (E1-4) and control (C1-3) experiments. Here, C1 serves as a control (fold change=0). In (c) and (d) the culture flask normalization is shown while all controls are pooled: Differences in gene levels before and after the experiments lead to consistent expression levels after the normalization with the cell flask data.

with pre-experimental data. Thus, it is necessary to take into account the mRNA level of the cells before the experiment to measure the changes gained by mechanostimulation or basically any other treatment.

High variations of gene levels before an experiment may be alerting and could evoke different expression dynamics. These dynamics may depend on the absolute expression level of a gene. A large set of experiments cannot be performed within one single cell passage, thus variations due to different passaging (see 5.1) cannot be prevented. In terms of reproducibility, gene levels may depend on the passage but a mechano-induced gene regulation should not primary depend on the passage. If this is the case, the regulation is not significant and thereby, just an useless artifact.

The next step is to pool all control experiment together (fig. 5.3c, d). Pre- and post-experimental gene level are then combined (see 2.3.1), which results in the absolute change of gene expression due to shear stimulation. Down-regulation by a factor of 4 is revealed for Myf5 in all shear experiments, while c-fos is up-regulated in all four cases within a factor of 2. Here, culture flask normalization proves to be a good instrument in revealing gene expression changes even in case with variations in pre-experimental expression patterns of multiple experiments. Different levels of gene expression before experiments may influence the overall responses. But as a proof of principle, this normalization seems to be a neccessary step in controlling gene levels of cell culture and excluding effects from pre-experimental cellular states. Especially in the case of small gene level changes in gene expression, this normalization step is a necessity.

5.3 Genetic response of cells under dynamic shear

Culture flask normalization provides the basis for studying mechano-induced changes in gene expression. qPCR enables to look at multiple sets of genes (fig. 5.4): genes related to myogenesis (a) [Engler et al., 2006, Lluís et al., 2006, Bennett and Tonks, 1997, Rohwedel et al., 1995, Guttridge et al., 2000, Perdiguero et al., 2007, Connelly et al., 2010], osteogenesis (b) [Engler et al., 2006, Valenti et al., 2008, Katagiri et al., 1994, Mansky et al., 2002, Ducy et al., 2000, Piek et al., 2010, Akune et al., 2004, Wu et al., 2006], the cytoskeleton (d) [Engler et al., 2006, Zuchero et al., 2009, Powner et al., 2011, Miano et al., 2007, Wang et al., 2006, Moritaa et al., 2007, Berg et al., 2001, Brakebusch and Fässler, 2003, Field and Alberts, 1995] and transcription factors related to the crucial AP-1 complex (d) [Shaulian and Karin, 2002, Zuchero et al., 2009, Horsley and Pavlath, 2002, Karin et al., 1997, Iavarone et al., 2003]. A major set of transcription factors known as the AP-1 complex may reveal influences on the gene regulation itself and other main cellular functions like cell cycle control. Expression levels of certain genes function as phenotypical markers for transforming myoblast cells into osteoblasts via osteogenesis [Nishimura et al., 1998, Katagiri et al., 1994] or myotubes via myogenesis [Engler et al., 2006, Lluís et al., 2006]. An adaption of the key players of the cytoskeleton may be expected to counter mechanostimulation by enhanced cell motility, stiffness or morphology due to gene levels changes. For example, the expression of the actin cross-linker EPLIN's (see 4) is regulated by actin itself via MAL-SRF signaling [Leitner et al., 2010]. In the end, results from cytoskeletal genes may then be compared to changes in cell visco-elasticity and overall rheological properties by measuring applied forces. Afterwards, mechanical data can be connected directly to gene expression adaption (see 5.4).

The overall genetic response is rather small with no clear trends in any direction of differentiation or adaption of the cytoskeleton and transcription factor of the AP-1 complex (fig. 5.4). Genes like Elk-1 and c-myc reveal different responses for the shear experiments (fig. 5.4d). No expression change of integrin is surprising (fig. 5.4c): in other studies gene regulation has been found extensively for different mechanostimulation scenarios [Engler et al., 2006, Wang et al., 2013] and overall gene regulation [Menko and Boettiger, 1987]. Only six genes show equal expression over all shear experiments: the cell cycle enhancing gene c-fos and cell cycle damping genes p53 and p21 [Shaulian and Karin, 2002, Karin et al., 1997] as well as the myogenesis enhancing genes Myf5, MEF2A and NFκB [Lluís et al., 2006, Bennett and Tonks, 1997] (fig. 5.5a). The involvement of c-fos as early response gene in mechanotransduction has been previously described [Kreja et al., 2008].

It has been shown that in standard cell culture genetic expression varies to some extent (see 5.1). This is induced by certain known stimuli for example age or unknown origins. Artifacts or cellular irregularities could lead to false results. Therefore the measurements are repeated with a different cell load from a frozen vial and the first results can not be confirmed (fig. 5.5b). Although c-fos seems to be up-regulated again, the other genes are not effectively regulated above a fold change of 1. Thus no clear trend is visible overall.

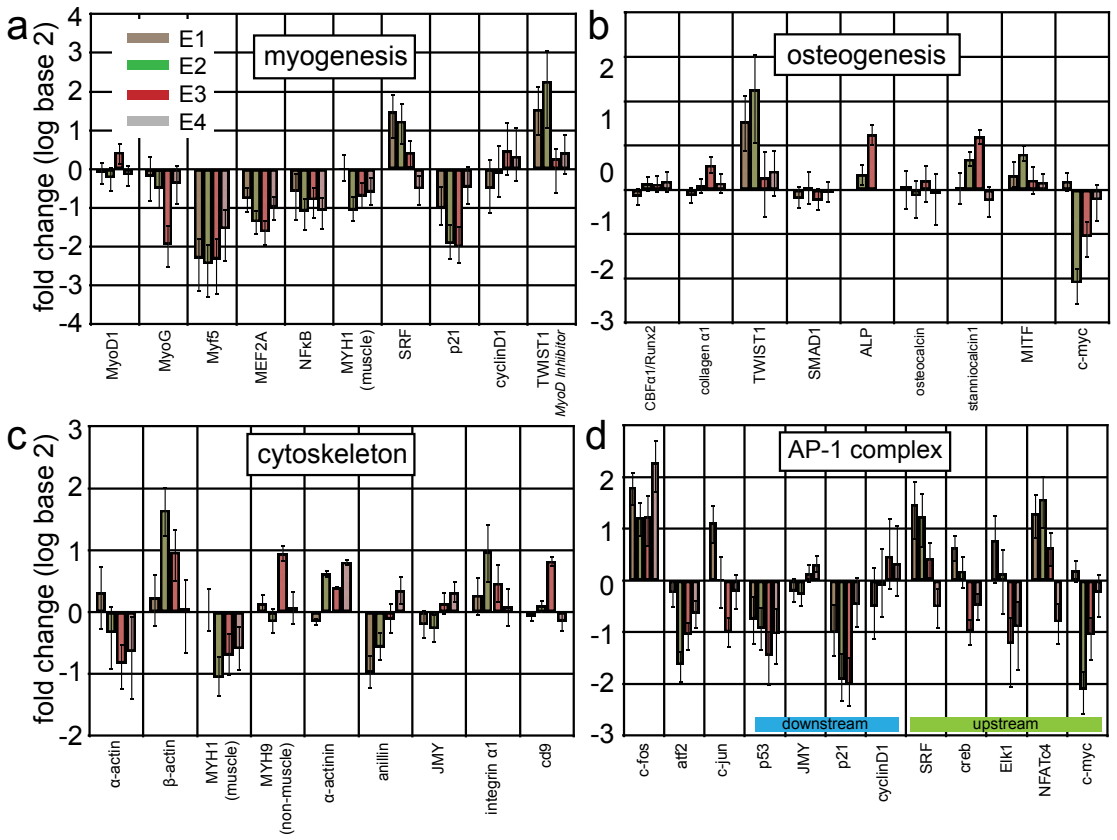

Figure 5.4: Fold changes of genes of interests: single experiments data is plotted for the gene of interests. All genes are splitted up in groups for distinct cellular functions or groups: (a) myogenesis, (b) osteogenesis, (c) cytoskeleton and (d) AP-1 complex with up- (green) and downstream (blue) targets

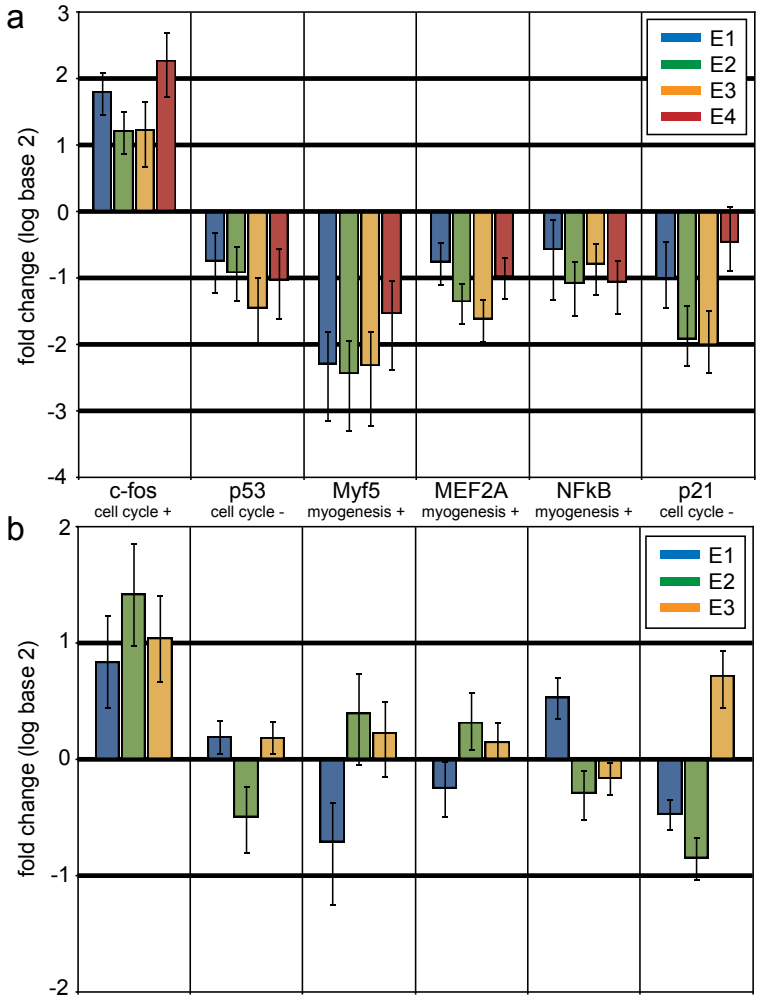

Figure 5.5: Gene response from first experiments is not reproducible: (a) Increased (c-fos) or decreased (p53, Myf5, MEF2A, NFκB, p21) gene expression due to mechanostimulation is not confirmed in experiments under identical conditions with a different myoblast charge (b). Overall, signals are reduced and noisy. c-fos may be up-regulated, but just about a factor of 2

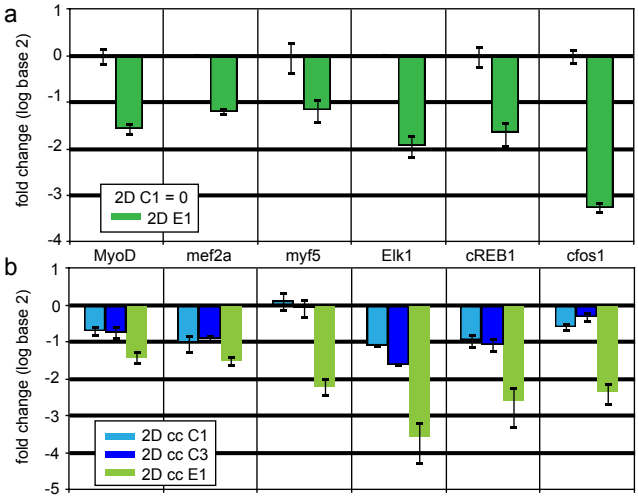

Figure 5.6: Gene expression after 2 days of incubation: (a) 2 days after shearing and (b) 2 days control cell culture (cc) with no mechanostimulation. Both groups for C1 and E1 are from the same flask in the first place. E1 shows down-regulation for all GOIs when normalized to C1 (a). (b) Cell culture data reveals extreme deviations of gene levels where no mechanostimulation is imposed (normalized to C1). cc E1 GOIs are similar down-regulated as E1, which means mechanostimulation seems not to be the reason for down-regulation in (a)

Shear stimulation for one hour during interphase [Maier, 2008] and mitosis [Fernández et al., 2011] shows effects on cell proliferation several days after the mechanostimulation. These results may suggest gene regulation may take longer times to evolve. Two days after stoppage of shear stimulation, gene expression analysis does not reveal any evidence for mechano-induced changes (fig. 5.6). Although gene data of shear experiment E1 is heavily down-regulated in contrast to the results right after the mechanostimulation, the cell culture control suggest these expression changes do not originate from external force impacts. E1 cell culture data reveals a similar down-regulation as in the shear experiment (fig. 5.6b). Thus no aftereffects after two days of shearing are accountable.

To this point it has been shown that gene regulation by dynamic mechanostimulation cannot be reproduced. Although flask normalization reduces errors from pre-experimental gene expression varieties, results show major differences in genes levels across genes and experiments. Mechano-induced gene regulation as seen in first experiments could not be repeated. Even days after the experiments, changes can not be reported other than incoherent expression patterns with no correlation to a shear stimulation.

5.4 Force measurements confirms gene expression data

Beside changes in gene expression, forces on the cell monolayer are measured dependent on the applied strain. Changes in elastic moduli could be reflected either by changes in gene expression or direct intrinsic adaption of the cytoskeleton to mechanostimulations.

No reproducible changes in gene regulation have been found so far, thus a direct adaption without detours in gene leveling may encounter. A maximum strain of 100% is applied at a frequency of $f = 0.25$ Hz. The stress-strain relation reveals two regimes: a linear (i) and a nonlinear regime (ii) (fig. 5.7). The linear elastic modulus of cell monolayer is $E \sim 0.4$ kPa. In the nonlinear response strain softening is visible which is a bit more pronounced at the end of the measurement (iv) when the drift (iii) is subtracted.

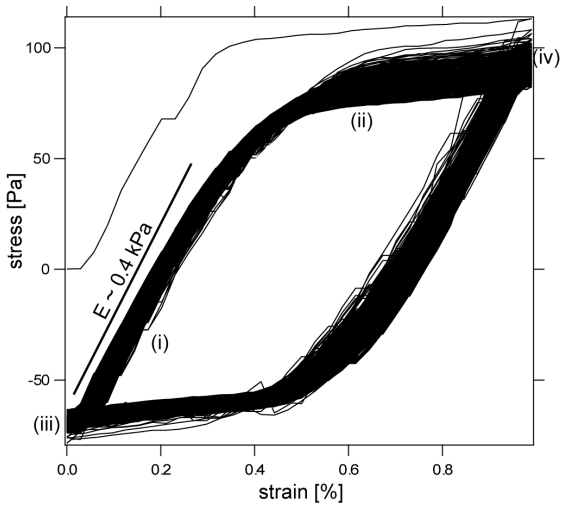

Figure 5.7: Stress-strain measurement of myoblasts($f = 0.25$ Hz, $A = 100\%$, $t_{shear} = 60$ min): Experiment E1 from set 1 shows overlay of cyclic stress-strain curves. A linear regime (i) to a strain about $s = 20\%$, the non-linear regime (ii) then emerges. Drift of the force sensor is seen to lower stress of several Pa per hour (iii). Elastic modulus of cell monolayer can be obtained by a linear fit to the linear response ($E \sim 0.4$ kPa)

Similar to the gene expression measurements, there are no obvious changes in the force data. A reason for no measurable changes could be that the exposure time to cyclic deformation is too short. Maybe it needs a higher critical cycle number to drive the cells in a different elastic regime, which is not reached within these experiments. It could be also the case that the cells counteract the deformation and changes of their mechanical parameters of their cell body by changing their adhesion to the substrate - thus no change is detectable. Limiting the adhesion area by a fibronectin or albumin pattern could be a way to limit that cellular behavior in future measurements. Another reason for no mechanical adaption may be that the measurement averages over million cells but the cellular responses could be very heterogeneous. One cell might get less elastic or reduces its adhesion - another cell could develop into the opposite direction. This could be a cybernetic survival technique to high strain mechanostimulation. This stochastic behavior could maintain more possible pathways for cells which adapt in all possible ways to certain extracellular circumstances. Here, survival rates may increase and may be of high importance for evolutionary fitness of a multicellular organism. Such heterogeneous behavior to external stimuli has been seen for example in bacteria [Maamar et al., 2007, Tyagi, 2010, Taniguchi et al., 2010].

5.5 Discussion

Although mechano-induced gene expression could not be reproduced, qPCR analysis and cell monolayer shear setup are refined in this thesis. Culture flask normalization is a must-have operation when small signals of gene expression changes by external stimuli are to be expected. β-actin is unsuitable as a reference gene due to high variations in cell culture conditions - apart from being inappropriate as a major regulator of transcription and cytoskeletal mechanotransduction.

It is a surprise that nothing is happening rheologically and genetically. Other studies [Engler et al., 2006, Engler et al., 2004] show clearly an adaption of gene expression due to changes of the external mechanical environment. For example, a myoblast could turn into non-mitotic multicellular myotubes due to various stimuli for myogenesis [Menko and Boettiger, 1987, Portier et al., 1999, Engler et al., 2004]. The observed overall changes in cell culture by no obvious stimulus revealed a heterogeneity within different cell flasks. This would lead to the assumption that gene expression may be very easy to change or to induce noise by a defined stimulus - which is not the case here.

In this thesis, gene expression analysis averages over millions of cells but maybe mechano-induced gene expression changes evoke heterogeneous cellular responses. The time from transcription to protein is estimated to be around 30 min [Pollard and Earnshaw, 2008], which should show in principal results in genetic and cytoskeletal adaption to shear stimulation. Signals could be averaged out or analyzed at the wrong moment due to previously described gene bursts behavior [Cai et al., 2008]. These bursts draw attention to the point in time of read-out and time dependence of gene regulation. qPCR in shear measurements may only capture a snapshot of highs and lows of gene bursts. c-fos and other genes may be regulated out-of-phase, thus cfos is up-regulated while other genes show no more signals.

Gene expression noise originates from fluctuations in chromatin structure [Brown et al., 2013]. Two genetically identical cells grown under the same conditions can exhibit stochastic fluctuations in gene expression - creating memories of transcription and thereby a personal history of cells [Kirchmaier, 2013]. This implies the importance of previous cellular states before mechanical stimulation. Maybe longer stimulations over days may integrate mRNA signals over multiple generation of cells. Thereby, cell cycle dependence of gene regulation should smear out. Cell cycle dependent gene expression noise [Zopf et al., 2013] may conflict with our analysis in this thesis and may be a source of heterogeneous responses. Cells are not synchronized in these shear experiments because healthy cells and not starved cells should be studied. Cell synchronization itself would be a huge stimulus for gene expression.

In the future, live or fixed cell imaging of single gene transcription and translation could be a way to analyze heterogeneity and time dependence of mechanoresponses at the mRNA and subsequent protein level. This may provide a good way to find genes of interest for future qPCR-mechanostimulation measurements. Maybe different genes and new key players are regulated that are not covered by these measurements. Parameters

may be further optimized to the point where cells are more sensitive to mechanostimulation.

Recent studies reveal that - beside transcription factors - microRNAs additionally steer protein production management while mRNA level stay unchanged [Baek et al., 2008]. Also DNA methylation is important in gene regulation [Suzuki and Bird, 2008]. Posttranslational modifications are reported to be a major process in protein regulation [Ahearn et al., 2012]. This shows that multiple processes other than mRNA production and degradation have high impact in protein production and activation. At last, mass spectrometry based proteomics [Ong and Mann, 2005] may provide an alternative to mRNA level analysis. The protein level output and modifications can be quantitatively analyzed by this method. In principal, all these methods could be evaluated after a shear stimulation which has been demonstrated with qPCR analysis in this thesis for the first time ever.

Pitfalls have been discovered and achievements for future considerations have been presented in this thesis. The cell monolayer shear setup and qPCR data analysis have been refined in this work. This novel cell monolayer shear setup is a superior method concerning the adhesive conditions enabling to create a potential adhesive knock-out with BSA coated glass plates. Progress has been made by combining cell monolayer shearing with full optical control by high quality microscopy, clean force measurements and cell environmental conditions by controlling oxygen, pH and nutrients supply. The inherent variability of biological systems can be reduced in qPCR by flask normalization. This normalization should be standard for all treatments concerning qPCR analysis. This work exemplifies clearly that using control experiments alone is not enough to ensure reliable data. These pre-experimental mRNA variations effects may be neglected only with high signals above 10-fold: Flask normalization seems to be important when signals are at the lower quantification limit. Accuracy of qPCR results strongly depends on exact transcript normalization using stably expressed reference genes. If this is not the case, their use as references is inappropriate [Bustin et al., 2009, Gutierrez et al., 2008]. This thesis reveals that β-actin is an odd choice as reference gene due to its high expressional variations in cell lines. Although there might be cases to use actin as reference, mechanical stimulation with qPCR analysis seems not to be a proper fit for using a key player of the cytoskeleton as reference. At last, gene expression changes could not be reproduced but understanding mechanotransduction and mechanosensing is still at large which may need other approaches to gain knowledge. Recent studies still imply the importance of mechanotransduction and the adaption of cells to external mechanical cues [Tse et al., 2012]. In the future, new studies and results may lead back to the methods that are presented here and may provide conclusions for the obtained results. The following chapter will focus on responses of the mitotic spindle and actomyosin cortex to external forces by dynamic shear. In mitosis no gene regulation is active thus only mechanoresponses at the protein level of the cytoskeleton are of importance.

6 Transducing forces in mitosis: elongation and orientation of cells and spindles under dynamic shear

In mitosis, cells round up and segregate pairs of chromosomes via mechanical processes to the nascent daughter cells. The necessary forces for these processes are generated at the molecular level by motor proteins and other cytoskeletal compounds like microtubules (MT) or actin. In the previous chapter, cells in interphase have been mechanically stimulated and analyzed. These cells are motile and are able to regulate their gene expression. This is in contrast to mitotic cells. The orientation of a mitotic spindle defines the plane of cell division [Gachet et al., 2004, Fishkind and Wang, 1995]. The daughter cells will accomplish different fates when cell-type determinants are variably distributed along the spindle axis due to intracellular polarity or asymmetric external cues [Betschinger and Knoblich, 2004]. The importance of these asymmetric cell divisions in the development of multicellular organisms has been discovered in many invertebrate and vertebrate systems [Betschinger and Knoblich, 2004, Strauss et al., 2006, Siller and Doe, 2009]. In adult organisms, they have an essential role in skin stratification [Lechler and Fuchs, 2005]. Here, polarized basal cells divide in the direction perpendicular to the basal membrane, which then generates a supra-basal daughter that differentiates and sets up the skin barrier.

The most basic cue which dictates spindle orientation is cell shape - cells division occurs along the long cell axis naturally [Honda, 1983]. When cell morphology influences spindle orientation, it appears to suffice to explain diverse cell fate potential in the *Xenopus* blastula. Here, fate is dictated by cell divisions perpendicular to the surface of the embryo, which correlates with a perpendicular long axis [Strauss et al., 2006]. Spindle position and orientation is achieved via a complex balance of mechanical forces that still lacks understanding. Dynein motors, which dynamically couple the actin cortex and the astral microtubules, are commonly thought to control spindle positioning [O'Connell and Wang, 2000, Grill et al., 2003] and to induce spindle oscillations [Grill et al., 2005, Pecreaux et al., 2006]. When the cell shape is altered with a micro-pipette, the spindle supervises and responds to externally inflicted variations [O'Connell and Wang, 2000]. However, biochemical cues are thought to be more dominant than the cell shape cue in several systems [Tsou et al., 2002]. This has been extensively studied *in vitro* applying fibronectin-coated patterns [Thery et al., 2005, Thery et al., 2007]. When these fibronectin-coated substrates are stretched, they evoke spindle orientation into external force directions [Fink et al., 2011]. So far, two mechanisms are known that control the orientation of the division axis in presence of external forces: alterations

in cell shape and mechanosensitive reactions triggered at certain adhesion spots. It is poorly understood how cells integrate these mechanical cues. They could antagonize or act together - essentially, it may rely on the interplay of adhesive conditions, geometry and timescale of the mechano-stimulus.

In metaphase, not only spindle orientation but also spindle length is controlled in diverse ways. Spindle length determination is far from being solved and multiple mechanisms are postulated in literature for systems like yeast, C. elegans, Xenopus and others [Dumont and Mitchison, 2009b, Goshima and Scholey, 2010]. There are some quantitative length control models like slide-and-cluster models for anastral Xenopus spindles [Burbank et al., 2007] or force-balance models for astral spindles of Drosophila embryos [Goshima et al., 2005] and mammalian cells [Ferenz et al., 2009]. Mitotic cells in tissues are constantly under external forces, thus it is natural to think of experiments, which impose external forces on mitotic cells to mimic *in vivo* scenarios and to evoke cellular responses. Self-organization of microtubules into bipolar spindles in *Xenopus* egg extracts [Heald et al., 1996] creates a valuable system for mechanical perturbations via micro-needles [Gatlin et al., 2010, Itabashi et al., 2009]. A recent study with step-like compression gives insight in dependencies of microtubule and motor protein dynamics in confined spaces [Dumont and Mitchison, 2009a]. Here, passive and active processes are revealed in spindle length determination. After compression, the spindle reaches a steady state again - which reveals the importance of mechanical coupling in spindle length control. Investigations in a more dynamic external context are missing so far and could provide more insight into the mechanical coupling of actomyosin cortex to the mitotic spindle and therewith, into the organization of length and orientation of cells and their corresponding spindles.

In this chapter, shear deformations are imposed via a monolayer shear apparatus (see chapter 5), which allows a novel kind of mechanical stimulation of cells in mitosis. This suffered deformation without volume changes - opposed to other techniques like compression or stretch - is combined with high resolution fluorescence microscopy for direct observation of cell and spindle responses of a large quantity of cells. A cell can only avoid shear by perfect dilatation - a scaling in all directions. In a physiological context, it is very unlikely that strains are experienced by cells in this ideal nature, thus they are subject to shear in one way or another by being encapsulated in a strained tissue. The shearing method provides a different spatial location of adhesion points when compared to more traditional approaches: parallel plates allow a simple realization of dynamic 3D confinement for mitotic cells. Ordinary approaches use for example a single flat substrate in a 2D context [Fink et al., 2011]. In the end, a large quantity of cells can here be analyzed and is subjected to molecular inhibitors, which allows interfering at the molecular level to gain further insight in mechanical coupling of the spindle to the actomyosin cortex, and moreover, cell to spindle morphology.

In the following, cell division of mitotic RPE1, MDCK and MC3T3 cells is revealed to be perpendicular to the external force. The preferred orientation of the division axis seems to be a direct result of force-induced cell and spindle elongation. These coupled elongation processes are mechanically nonlinear, time- and actomyosin-dependent. In

addition, spindle elongation depends on microtubule dynamics. Cell elongation of 15% already suffices to align mitotic spindles and particularly, it can be uncoupled from spindle elongation by abolishing microtubule dynamics. Spindle elongation seems to lead to a direct coupling of the actomyosin cortex to the spindle poles with astral microtubules being vanished. Here, a previously proposed mechanical coupling model is refined with inclusion of contractile actions by the actin cortex. External forces may propel actin cortex remodeling - which is indicated by higher myosin II intensity in immunofluorescence images at the cell pole than at the cell equator. All in all, cell division under external forces stays uncompromised and proceeds normally, which may imply that these phenomena uncover biological tasks - even it may be utilized to guide in-vitro buildup of artificial tissues and replacement organs in the future.

6.1 Cell shearer approach to exert external forces on mitotic cells

To learn more about the role of external forces as a tool to steer spindle morphology, it is necessary to impose forces to deform the stiff and slightly adherent mitotic cells. Furthermore, it has to be possible to image the mitotic spindle and the cell itself. To this end, a cell monolayer shear setup is combined with standard epifluorescence and phase contrast microscopy. Prominent feature of this shear stimulation is a zero-force direction - no force acting in direction perpendicular to the shear plane - and strong adhesion is not necessary [Fernández et al., 2007]. Moreover, the volume stays unchanged during stimulation. Volume variations would induce alterations of intracellular pressures and concentrations.

By combining shear rheology with epiflourescence microscopy and using mCherry-tubulin labeled MDCK cells, a large quantity of mitotic cells can be analyzed. Between two uniform glass plates used as substrates, fresh medium ($t = 37°C$) is flowing slowly (0.53 µl/s) past the cells to ensure supply of oxygen and nutrients. In addition, pH stays constant over the course of the experiment. The cells are smoothly compressed ($20 - 30\%$) with a micrometer screw and a piezo motor on the upper plate to a certain gap $h = 10$ µm. This is conducted slowly (~ 5 µl/min) to minimize convective dispersion of the cells. Another piezo moves the top plate, performing the shear stimulation on cell cycle synchronized cells (fig. 2.5a). A x-y translation stage allows recording of fluorescent images at different spots of interest to cover a large amount of cells. All is set up on a standard fluorescence and phase contrast microscope. Post processing for data analysis is managed with FIJI and Matlab algorithms (see 2.4). It is necessary to use long-distance objectives with tunable working distance to acquire cells on different positions because a thick and stable glass plate has to be used that is able to withstand the compression forces. This leads to a reduced resolution of spindle images. The contrast of the fluorescent spindle micro-graphs is limited due to fluorescent tubulin monomers - which on the other side make it possible to gain cell morphological data.

After careful compression and an adaption time of 20 minutes, a maximum strain $s = dy/h = 100\%$ for a corresponding amplitude dy is applied at a certain frequency

for 10 or 30 minutes (fig. 2.5b). When mechanical stimulation is stopped, cells are left compressed for relaxation studies of spindle and cell morphology.

6.2 Mitotic spindle orientates perpendicular to the shear force direction

6.2.1 Mitotic cells elongate actomyosin-dependent in zero-force direction

Mitotic RPE1 and MDCK cells change in their morphology in a well-defined way under external dynamic strain. They exhibit elongation perpendicular to the plane of shear direction - the direction of zero force (fig. 6.1a, b). These metaphase cells have a shape close to an ellipse which enables easy tracking of the cell contour and cell elongation quantification. Cell elongation is calculated by the ratio R of major to minor cell axis as $(R-1)\star 100\%$. A round cell has thereby a cell elongation of 0, 100% cell elongation means the major axis is two times the minor axis. Control cells have an elongation of about 10% (fig. 6.1c). All in all, cell elongation is a nonlinear response to imposed shear strain (fig. 6.1c). A time-dependence is seen when the frequency of the mechanostimulation is altered: a larger cell elongation is found for higher frequencies (fig. 6.1d). Although cell elongation is also observable with albumin and fibronectin coated glass plates, the degree of elongation is reduced compared to the uncoated substrates (fig. 6.1e, f).

The main regulator of the cell shape is the actomyosin cortex of which myosin can be inhibited by the ROCK (Rho-associated coiled kinase) inhibitor Y-27632. At a concentration of 10 µM, the tension of the actin cortex is reduced by about 50% in L929 fibroblasts [Tinevez et al., 2009]. With this obstruction of myosin activity, cell elongation is heavily decreased when shear strain is applied (fig. 6.1e, f).

6.2.2 Orientational adaption of the mitotic spindle to dynamic shear

The division axis of cells is mainly steered by the cell shape which results in alignment of the mitotic spindle along the long cell axis when no other adhesive cues are present [O'Connell and Wang, 2000]. Thus cell elongation due to external shear may steer the spindle orientation. To this end, the angular position of cells θ_{cell} and spindles θ_{spin} is measured and the angular difference $[\theta_{cell} - \theta_{spindle}]$ is plotted versus the cell elongation. Cell elongation below 10% leads to random spindle positions relative to the cell axis in control cells and low frequency sheared cells (fig. 6.2). A significant bias is achieved only with cell elongations higher than 10%: spindles orient toward the cell axis. A higher frequency of 0.3 Hz leads to a large decrease of angular difference and large increase of cell elongation for RPE1 and MDCK cells (fig. 6.2). Here, the spindle orientation shows a complete bias. This reveals an intrigued sensitivity of the mitotic spindle to the aspect ratio of the cell. This in good agreement with a recent study which uses static conditions [Minc et al., 2011].

The causal relationship between cell form and spindle angle can be further analyzed by

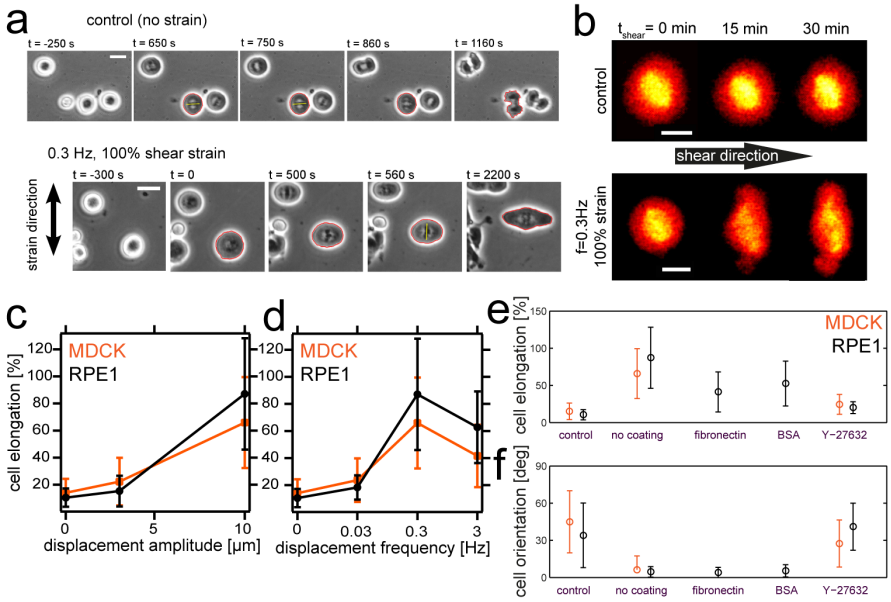

Figure 6.1: Actomyosin-dependent elongation of sheared mitotic cells along the zero-force direction: (a) Non-sheared RPE1 cells divide isotropically, while sheared RPE1 cells elongate and divide in zero-force direction. (b) Non-strained MDCK cells synchronized in metaphase stay round, sheared MDCK cells elongate along the zero-force direction perpendicular to the shearing. (c) RPE1 (black) and MDCK (orange) cell elongation as a function of amplitude for a constant frequency of 0.3 Hz. (d) Cell elongation as a function of frequency for a constant amplitude (100% strain). Glass plates are not coated in (a)-(d). (e) Albumin-passivated and fibronectin coated glass plates reveal cell elongation of RPE1 cells. Inhibition of ROCK by Y-27632 (10 µM) dimishes cell elongation of RPE1 and MDCK cells. (f) Cell orientation (major cell axis angle) of RPE1 and MDCK cells for all plate coatings and ROCK inhibition. (all scale bars 10 µm; parts of the data taken from [Fernández et al., 2011])

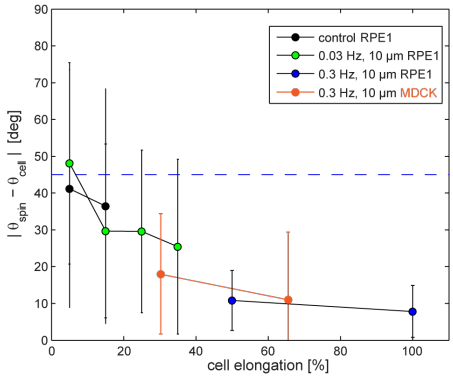

Figure 6.2: Shear elongation by 15% is enough to align the mitotic spindle: Angular difference of mitotic spindle to major cell axis vs. cell elongation. Black: RPE1, non-strained cells. Green: RPE1, low frequency 0.03 Hz, large amplitude 100% strain. Blue: RPE1, $f = 0.3$ Hz, 100% strain. Orange: MDCK cells, $f = 0.3$ Hz, 100% shear strain. Glass substrates are un-coated. (parts of the data taken from [Fernández et al., 2011])

an abrupt change of shear direction. RPE1 cells are sheared for 8 minutes in x-direction, afterwards stimulated in the perpendicular y-direction (fig. 6.3). The cells turn round due to directional switching in a first response (fig. 6.3b, control). Within 5 minutes about 95% of the cells elongate in zero-force direction x. At the same time, spindles orientate away from the imposed strain (fig. 6.3c).

Although biochemical inhibitors could provide insight into the role of molecular key players, one has to be assured that the mitotic system does not lose its bipolarity [Fernández et al., 2011]. The ROCK inhibitor Y-27632 completely diminishes cell elongation and spindle re-orientation (fig. 6.3d), while the cortical tension seems not to be fully abolished when the smooth and round shape is still abode (fig. 6.3b). Similar results are seen for direct inhibition of myosin II with blebbistatin (50 µM) and the actin polymerization inhibitor cytochalasin D (10 µM) (fig. 6.3b, [Fernández et al., 2011]).

Finally, it has been shown that cells react in an active way to external forces created by dynamic shearing. Within minutes, the actin cortex adapts morphologically to a change in shear strain direction. The mitotic spindle shows an instant response by re-orientation, which may imply that the spindle rotation process could be quicker than the re-organization of the actomyosin cortex. In the next section, the spindle length is examined while cells elongate and provoke spindle re-orientation under external shear strain.

6.3 Metaphase spindles elongate under dynamic shear

6.3.1 Length increase of metaphase spindles by dynamic shear forces

We now turn to fluorescent cells with labeled tubulin. Solely compressed control cells show no change in shape, orientation or spindle morphology under equal conditions as sheared cells (fig. 6.4a). When cells are sheared at a frequency of $f = 0.3$ Hz with a maximum applied strain $s = 100\%$, they show increased cellular and spindle elongation with orientation shifting perpendicular to shear direction together over time (fig. 6.4b). The average absolute spindle length of cells from three independent experiments increases from about 12.8 µm to about 15 µm for sheared cells, while control cells show no length changes (fig. 6.4c). Within few minutes, mitotic spindles of sheared cells elongate fast, afterwards a slower steady increase is maintained. Displayed graphs show quartiles (25th and 75th percentiles, edges of boxes), median (central line) and mean average (circle). The notch reveals the 5% significance level of the median. Fixed human RPE1 cells that are stained for tubulin exhibit similar spindle elongations after 30 min of shearing: compressed control cells stay round ($l_{spin,median} = 10.0$ µm) while sheared cells had elongated together with their spindles in combination with orientational alignment ($l_{spin,median} = 15.3$ µm, fig. 6.4f, g).

Spindles elongate, thus it is of interest how the cell shape may change along the way. With *cell elongation* defined as before (see 6.2.1), we see a steady rise for MDCK cells up to about 60% after 25 min (fig. 6.4d) in good agree with results using RPE1 cells (see fig. 6.1). When the length increase per spindle is normalized with spindle length

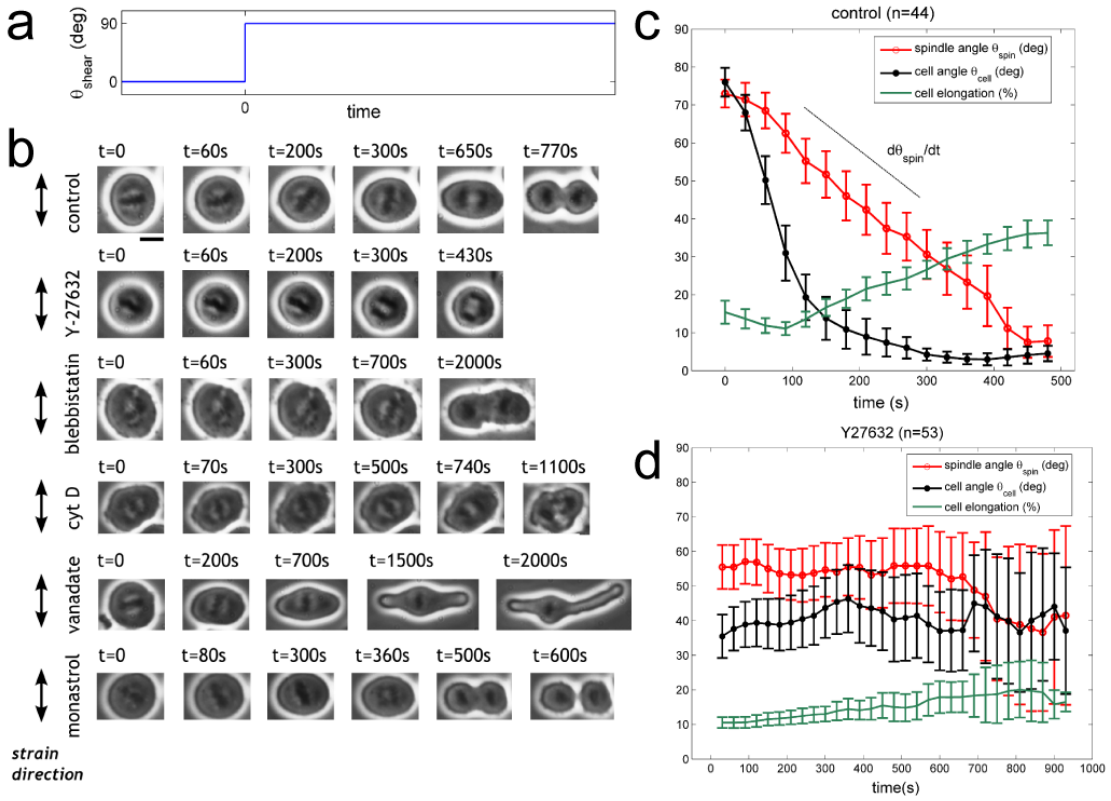

Figure 6.3: The spindle adapts to time-varying forces via actomyosin: (a) RPE1 cells are stimulated along the x-axis at frequency 0.3 Hz and strain amplitude 100%. After 10 min ($t = 0$), the direction of shear is changed by 90° from x- to y-axis and the resulting response of cell morphology and spindle angle is analyzed. (b) Immediately after switching the external force direction, control (un-treated) cells round up and elongate in x-direction afterwards. At the same time, the spindle rotates from the y- to the x-direction. ROCK inhibited cells (Y27632) do not elongate or re-orientate their spindles. In a similar way, cells incubated with blebbistatin or cytochalasin D have no spindle re-orientation ongoing. Inhibition of motor protein dynein with vanadate (0.3 mM) shows a rotation of the spindle in zero-force direction just as untreated cells, but often failed in anaphase with collapsing spindles. Cell elongation reaches abnormal values - maybe due to longer duration of the metaphase. (c) Mean average over 44 RPE1 cells as a function of time (± standard deviation). (d) RPE1 cells under the influence of Y27632 ($c = 10$ µM). (figure taken from [Fernández et al., 2011])

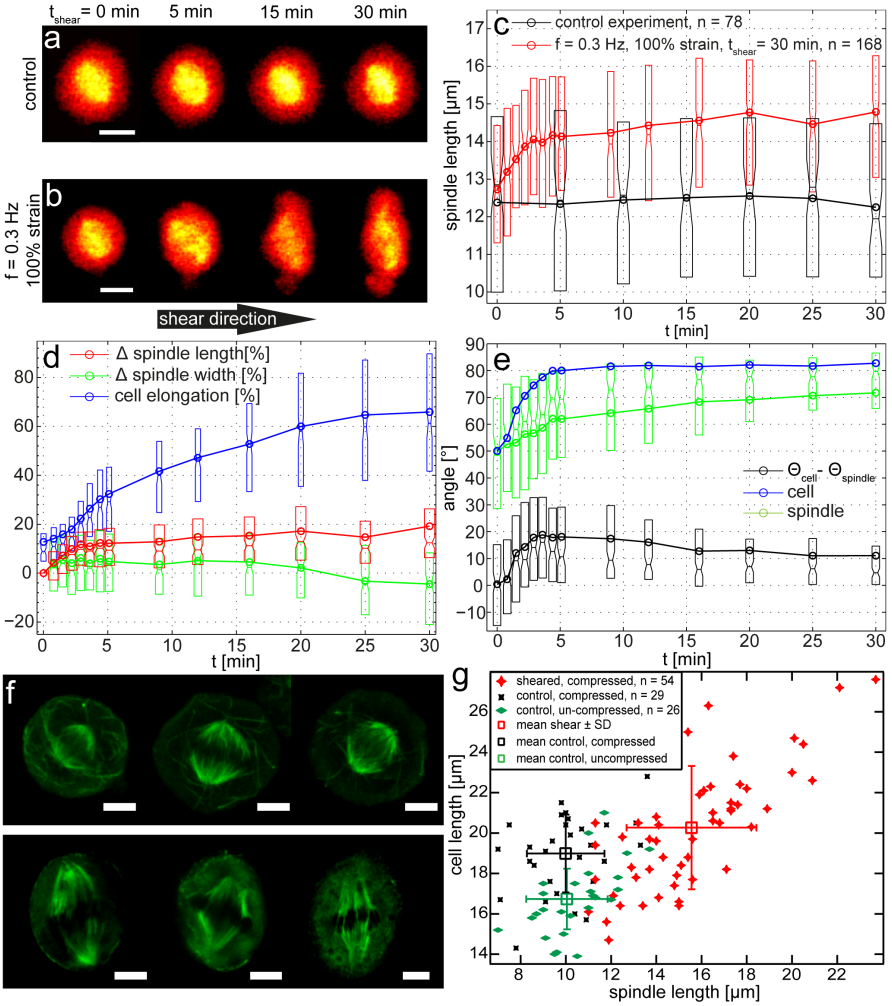

Figure 6.4: Spindle elongation is imposed by forces of dynamic shear: (a) Compressed control cell shows no length increase in contrast to a mechanically stimulated cell ($t_{shear} = 30$ min, $f = 0.3$ Hz, 100% strain). (b) Length increases of spindle and cell body are observed perpendicular to the shear direction. (c) Absolute spindle lengths of control ($n = 78$) and sheared cells ($n = 168$) show a fast length increase only for sheared cells, which slows down after five minutes (notched box-plots with median (line), mean (circle) and quartiles (boxes)). (d) Comparisons of spindle lengths and widths reveal less growth for widths in the beginning and a small decrease after 25 min of shearing. Cellular elongation rises less sharp at the beginning than spindle length. While mean spindle lengthening slows down past $t_{shear} = 5$ min, cell elongation saturates later. (e) Alignment perpendicular to the shear direction is revealed for major cell axes. The angular difference between cell and spindle increases fast, but relaxes slowly with t_{shear}. This is due to slower, out-of-phase spindle rotation where the spindle steadily approaches the cell angle. (f) Immunofluorescence images of sheared and non-sheared RPE1 cells with stained microtubules: Sheared cells reveal spindle elongation (down, $n = 54$), compressed control cells stay round (top, $n = 29$). Cells are in metaphase arrest. (g) Quantification of tubulin stain: Plotting spindle lengths vs. cell lengths reveals mean spindle lengthening of sheared RPE1 cells. (scale bars 10 µm)

at $t_{shear} = 0$, a fast increase up to 10% is seen at the beginning and a slower phase afterwards. At the end, a length boost of about 20% is achieved. Spindle lengthening is very dynamic on the single cell level and always combined with cell elongation in the single cell case (see B.2) as well in cell averaged data revealed before. Spindle widths show only a slight increase in the beginning (fig. 6.4d). Thereafter, the average spindle width shrinks after $t_{shear} = 20$ min and ends up below zero percent.

Spindles elongate faster than the cells which reveals a difference in timescales. The average of angular differences $[\Theta_{cell} - \Theta_{spindle}]$ shows a fast increase similar to the boost in elongation and spindle length in the first minutes of stimulation, but afterwards it differs: the angular difference decreases slowly to about 10°, which means that spindle re-orientation into zero-force direction kicks in. This reduces the angular difference to the cell angle. Cell and spindle orientation are therefore out of phase maybe due to different timescales of cell and spindle elongations. Slow orientation may be connected with ongoing cell elongation while spindle elongation saturates (fig. 6.4d, e).

6.3.2 Dependence of spindle length on frequency and amplitude

The next step is to reveal how linear and time-dependent the process of spindle elongation is in terms of amplitude and frequency. When the displacement amplitude is varied, spindle lengthening is seen for high amplitudes, while for small amplitudes of $A = 3$ µm no effect is visible (fig. 6.5a, box-plots show whiskers which extend to the most extreme data points not considered outliers). This reveals that shear-induced spindle elongation is a nonlinear feature just as found previously for cell elongation (see fig. 6.1c). A time-dependent response is revealed when different frequencies are examined: for middle frequencies, the effect peaks, while for low frequencies (0.03 Hz) no significant length change after 30 min is present (fig. 6.5b). Here, a putative reversible passive process - as found for spindle widening in compression studies [Dumont and Mitchison, 2009a] - may lead to an elastic response: spindles are fast enough to counter external forces and therefore, lengths remain unchanged. High frequency stimulation at 3 Hz also leads to a length increase, but not as drastic as for 0.3 Hz. Comparing now these two regimes over long shearing times, the lengthening for 3 Hz (fig. 6.5c, blue curve) is less sharp and more slowly than for $f = 0.3$ Hz (dotted red line, mean average values, see fig. 6.4). Furthermore, saturation is reached at 20 minutes. The angular difference is less for 3 Hz experiments in the beginning with a saturation after a few minutes, a decrease follows afterwards (fig. 6.5d). Here, spindle rotation seems to kick-in earlier for high frequencies and is interestingly almost as fast as cell re-orientation, while cell elongation rises slower to a maximum of about 40% (fig. 6.5e). Thus, the angular phase shift between cell and corresponding spindle is also a frequency-dependent nonlinear phenomenon.

6.3.3 Shear-induced spindle elongation depends on microtubule and actomyosin cortex dynamics

After confirming non-linearity and time-dependence in spindle morphological responses, we want to clarify the molecular basis of these dynamic behaviors. It was shown earlier

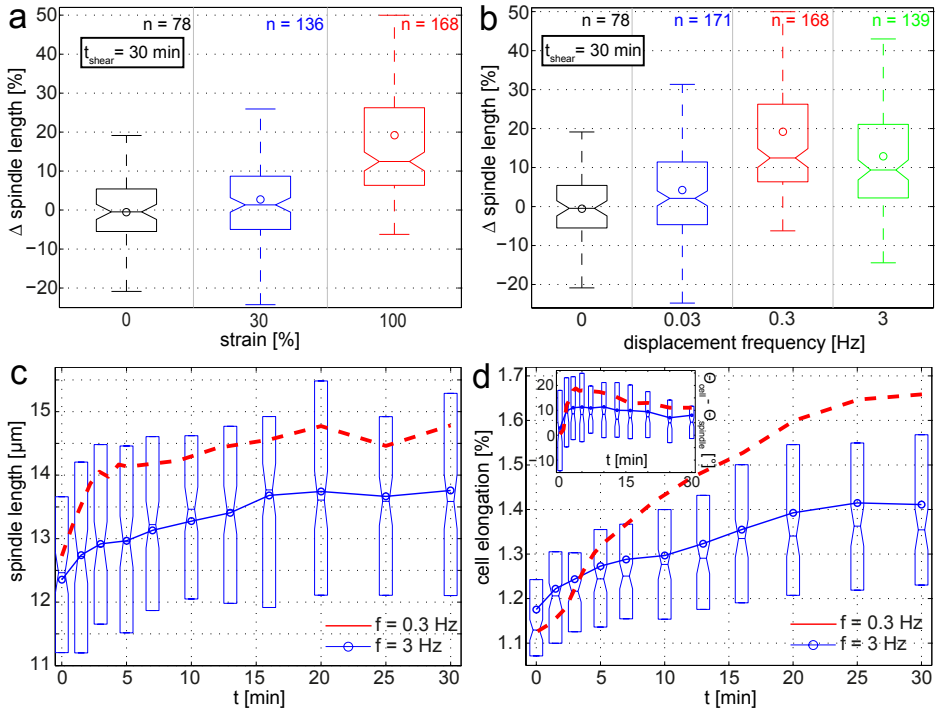

Figure 6.5: Amplitude and frequency dependence of spindle length increase reveals a nonlinear time-dependent response: (a) Box-plots for control ($n = 78$, black) and small amplitudes of 3 µm ($n = 136$, blue) reveal no changes in length after 30 minutes of shearing at $f = 0.3$ Hz in contrast to 10 µm amplitude experiments ($n = 168$, red), where a mean length increase of 19.2% is visible. (b) For low frequencies of 0.03 Hz ($n = 171$, blue) only a small increase is detectable. For 0.3 Hz a maximum value is attained ($A = 10$ µm, $t_{shear} = 30$ min). High frequencies ($f = 3$ Hz, $n = 134$, green) show lengthening of spindles, but it is reduced in comparison to frequencies of the middle range (red). (c) Comparing spindle lengths of 0.3 Hz (mean, red) and 3 Hz (blue) over time displays a less sharp increase for high frequencies. (d) Reduced cell elongation is found for cells sheared at 3 Hz. The angular difference is less pronounced for high frequencies at the beginning of stimulation (d, inset) (notched box-plots with maximal and minimal values (whiskers in (a), (b)) without outliers; median (line), mean (circle) and quartiles (boxes)

that there is a dependence of cell elongation on the re-organization of the actin-myosin cortex (see 6.2). Together with findings of time-dependent parallel boost in cell and spindle elongation of sheared cells, one has to identify the role of key players in the coupling of the actomyosin cortex to the mitotic spindle by using inhibitor experiments. Moreover, how MT contribute is to be resolved. Fluorescent images of cells show diverse responses to various inhibitors blocking actin cortex coupling, reducing cortex stiffness or MT dynamics (fig. 6.6a). Quantification of spindle elongation is shown in fig. 6.6b. Shear experiments with a high DMSO concentration of 0.1% for control - much higher than in all other inhibitor experiments - reveal cell and spindle elongation is comparable to standard conditions.

For taxol treated cells, the length is a bit reduced after $t_{shear} = 30$ min, but spindle orientation towards zero force direction is observed together with rising cell elongation. In compression experiments [Dumont and Mitchison, 2009a], abolishment of MT dynamics also leads to stable spindle lengths. Length reduction, which emerges after a long stable phase at the very end of stimulation, may be due to irreversible structural damage by shearing, while no dynamic repairs of spindle MT are possible. Therefore, cells treated with taxol are able to elongate their cell bodies and orientate their spindles, but cannot grow the latter (fig. 6.7b). Thus, the spindle elongation is not the driving force behind cell elongation and re-orientation responses of a cell and its spindle. These processes can be uncoupled in this direction, but is it possible to uncouple fast spindle elongation from cell elongation?

As described before in 6.2, this shape and orientation feature due to dynamic shear depends only on actomyosin. Nocodazole and ROCK inhibitor Y27632 obstructs cortex coupling to the spindle: nocodazole by depolymerizing astral MT and Y27632 by interfering with myosin activity and therefore reducing stiffness of the cortex. A reduction of about 50% at $c = 10$ µM was measured in L929 fibroblasts [Tinevez et al., 2009]. Only Y27632 is used here, since it delivers the identical effects to spindle orientation and cell elongation during shearing of mitotic RPE1 cells as direct inhibition of actin by cytochalasin D or myosin by blebbistatin (see 6.2). During the influence of the Y27632, cellular shape is nearly unchanged after 30 min of shearing (see fig. 6.8a). Spindles only slightly elongate, which is also the case for nocodazole treated cells (fig. 6.8b). Cell elongation reveals only sparse elevation and early saturation for both inhibitors (fig. 6.8a). Only small increments of absolute spindle lengths are apparent, when nocodazole is used for abolishment of astral MT (fig. 6.8b). A similar effect is seen for Y27632. Interestingly, spindle lengths are reduced prior to shearing.

Usage of vanadate (0.3 mM), an unspecific inhibitor of the spindle motor protein dynein, generates highly elongated cells with a spindle length increase under 10%. At higher concentrations, vanadate is able to block kinesins additionally [Abal et al., 2005]. This motor protein, which runs to the MT plus end in contrast to dynein, seems not to play a leading role in spindle length control during compression of metaphase cells [Dumont and Mitchison, 2009a]. Furthermore, kinesin-5 is connected to spindle shortening and monopolarization when inhibited [Goshima and Scholey, 2010], thus implying being less important in lengthening processes. Therefore, inhibition of this motor protein

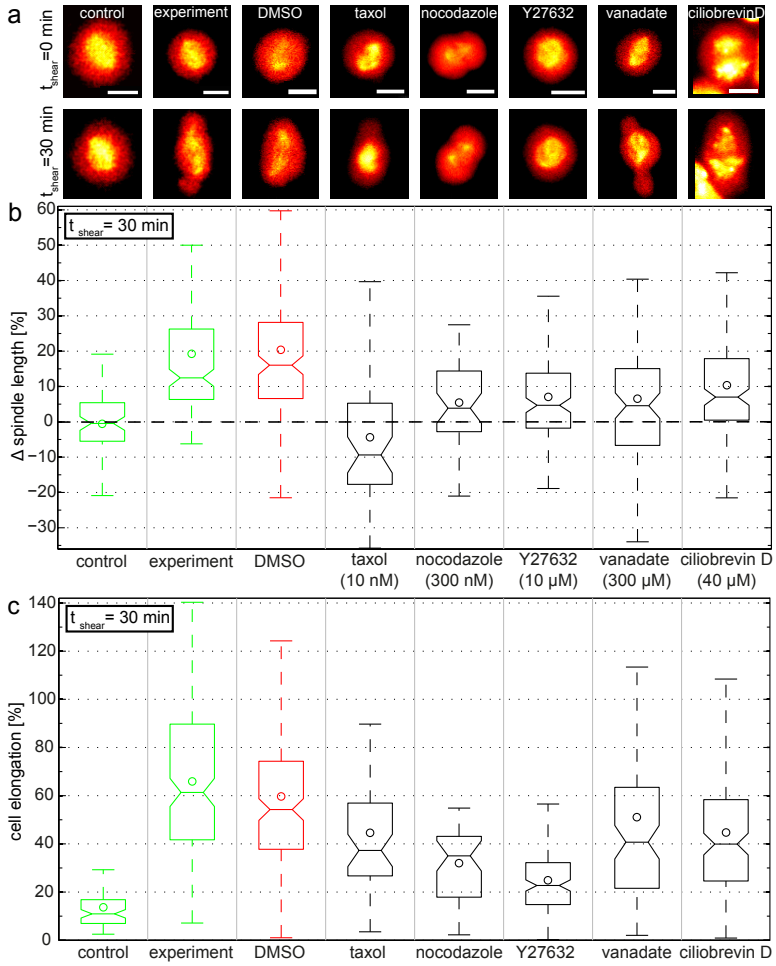

Figure 6.6: Inhibitors reduce spindle and cell dynamics: (a) Control cells show no changes in spindle parameters or cell shape. Under shear, cells elongate and spindle grow longer even in presence of high concentrations of DMSO (0.1%) in contrast to taxol (10 nM, $n = 51$) treated cells, which exhibit no spindle length increase. Nocodazole (300 nM, $n = 40$) and the ROCK inhibitor Y27632 (10 µM, $n = 139$) lead to only small increase of spindle lengths after 30 min of shear stimulation. Using the dynein inhibitors vanadate (unspecific, 0.3 mM, $n = 92$) and ciliobrevin D (specific, 40 µM, $n = 140$) show elongated cells, but spindle lengthening is reduced. (scale bars 10 µm) (b) Usage of different inhibitors show reduced length changes for all scenarios. In the case of taxol, a spindle shortening shows the importance of microtubule dynamics for the process of spindle lengthening. Getting rid of astral microtubules (nocodazole) or reducing the cortex-spindle linkage by dynein inhibition (vanadate, ciliobrevin D) leads to spindle lengthening of less than 10%. Similar behavior is observable for the ROCK inhibitor Y27632, which reduces the strength of the cortex. (c) Using chemical pertubations, cell elongation is reduced, especially in a dramatic way for nocodazole and Y27632 treated cells

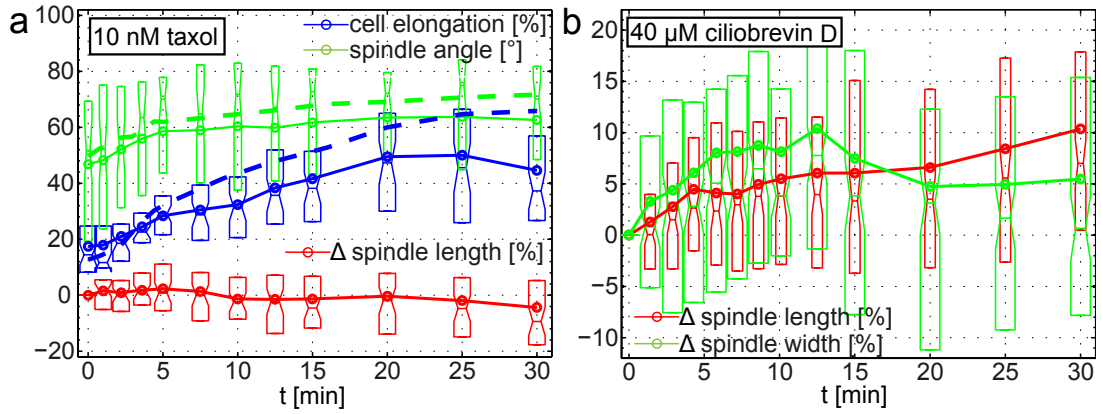

Figure 6.7: Decoupling of cell from spindle elongation and induced spindle widening: (a) Addition of taxol (10 nM) abolishes the spindle length increase completely. On the contrary, cell elongation and spindle angle rise almost as in normal experiments. This reveals that forced spindle lengthening relies on microtubule dynamics and is not a passive effect. Spindle orientation and cell elongation do not depend on it. (b) 40 µM ciliobrevin D reveals a mean width increase of about 10% after 10 minutes and dropping to about 5% after 30 min of shearing. Meanwhile, mean lengths increase steadily over time with no fast initial spindle elongation

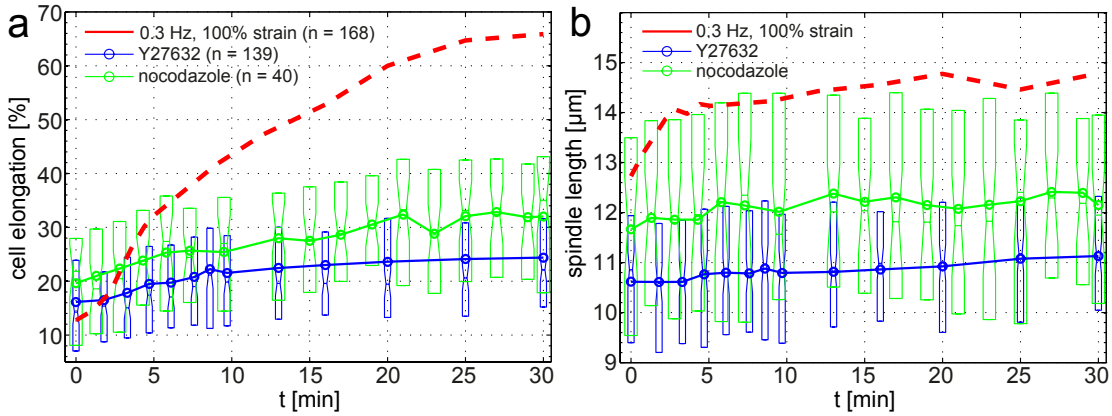

Figure 6.8: De-coupling of the actin cortex and the spindle abolishes fast initial spindle elongation: (a) Cell elongation rises only marginally in presence of Y27632 (blue) and nocodazole (green) by about 10%. (b) Actin cortex relevant drug Y27632 (ROCK inhibitor, 10 µM, blue) and astral MT depolymerizing inhibitor nocodazole (300 nM, green) show reduced absolute spindle lengths and only small spindle elongation over 30 min of shearing

is not examined. Nevertheless, to exclude any effects on kinesins, a novel specific dynein inhibitor called ciliobrevin D (40 µM) [Firestone et al., 2012] is used. It causes width and slow length increases (fig. 6.7a) with the spindle lengthening being comparable to results from vanadate experiments (fig. 6.7a). Dynein focuses spindle poles [Firestone et al., 2012] but also sits at astral MT and couples the spindle to actin cortex and cell membrane by astral pulling activity [Grill et al., 2001]. This importance of linking the actin cortex to the spindle apparatus for an initially fast spindle elongation process is seen by the abolishment of this quick elongation when ciliobrevin D is used. The slow increase must be due to MT dynamics, which are in turn abandoned by blocking them with taxol as seen here before. Spindle widening may be due to a passive process - similar to a recent study [Dumont and Mitchison, 2009a]: the spindle poles are less focused (see fig. 6.6a) and therefore, it is possible to widen the spindle more easily without reconstructing the MT bundles actively. Together with findings in chapter 6.2 on the connection of cell elongation and spindle rotation, external shearing seems to impose tangential forces on the spindle poles. How the spindle-to-cortex coupling may have to be adapted to impose these forces is still unknown. This tangential force may explain spindle widening when ciliobrevin D is used. Widening is reversed by rotation due to elongation of the cell, which may lead to a kind of refocusing again since the elongating, rotating cell cortex-membrane ensemble pushes the MT bundles together: elongated cells are more pointed and hence, less space is available. This may also result in spindle pole focusing simply due to pole confinement despite having dynein motors blocked.

6.3.4 Changing the height aspect ratio: Low cell compression results in slow spindle elongation at constant cell elongation

We showed the important dependence on MT and actomyosin cortex dynamics and furthermore, a potential role of cortex coupling to the spindle. The cortex defines the cellular shape, which is in case of the mitotic cells very stiff [Théry and Bornens, 2008]. Cell and fast spindle elongation have different timescales and can be uncoupled by biochemical treatments. The aspect ratio of cells in the x-y-plane is therefore important for spindle elongation and orientation - but how depends spindle elongation on the cellular aspect ratio in the x-z- respectively y-z-plane? Different height geometry should change the cortex dynamics and its coupling to the spindle with more three-dimensional rotational freedom. To this end, the compression is reduced by 30% to $h = 13$ µm, while shearing the cells under the same conditions as before. Here, mechanostimulation is still in the mechanical nonlinear regime. Comparison of spindle elongation over time for high and low compression shows less compressed cells having no fast increase and a rather constant boost in length of about 14% over 30 min (fig. 6.9a). Concerning the spindle angle, angular difference and cell elongation, little to no change is attained by low compression of mitotic cells (fig. 6.9b). No elongation of less compressed cells reveals that the cell shape remains unchanged when the cell height aspect ratio is reduced. Thus, spindle elongation is possible without basic changes in the cell aspect ratio in the x-y-plane, even though being more slowly.

A reason for shape-independent spindle elongation could be changes in gradients of

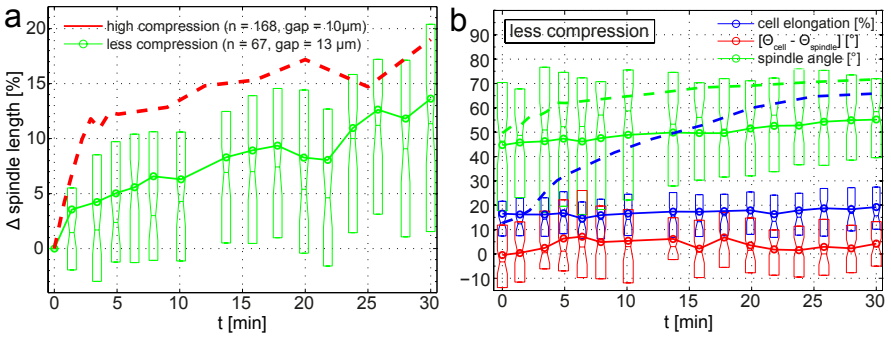

Figure 6.9: Reduced compression abolishes fast initial spindle lengthening while the cell shape stays unchanged: (a) Comparing low (green, gap $h = 13$ µm) to high compression (red, mean average, $h = 10$ µm) shows no initial fast and only slow overall spindle elongation for less compressed cells. (b) Low compression results in diminished cell elongation (blue), while spindles show only a narrowing in their angle distribution over time (green). Angular differences (red) show no shear-induced change (dotted lines: mean average high compression, see fig. 6.4)

MT severing enzyme katanin [McNally et al., 2006, Loughlin et al., 2011] by shear induced internal, cytoplasmic flows due to recently described differences in cortical tensions [Mayer et al., 2010]. This may lead to a chemical signaling model for spindle length determination. A hint for potential differences in cortical tensions is shown in 6.4.

6.3.5 Stoppage experiments reveal preserved spindle lengths in longtime stimulations

We have seen effects of different degrees of compression and hence, the cell shape and key proteins have on the spindle elongation. But what happens to the elongated spindles after stoppage of shear? Are the spindles able to relax to the original state or have they reached a new steady state? To this end, we sheared cells for 10 or 30 min and then stopped to compare their relaxing behaviors and spindle morphologies. After $t_{shear} = 30$ min and $t_{relax} = 15$ min (fig. 6.10a, red), mean spindle length get marginally reduced and the median length is more or less preserved. This is in contrast to short time (fig. 6.10a, blue) experiments: the spindles double in length increase to about 20% since the start of shear. After $t_{relax} = 10$ min, cell elongation goes down to 40% for long stimulations but for short times it remains at about 40% (fig. 6.10b). Interestingly, the angular difference between cell and spindle shows rotational relaxation for $t_{shear} = 10$ min experiments in contrast to longtime stimulation, where only a small drop can be observed (fig. 6.10c). Spindle orientation towards the cellular angle - driven by the cortex - could therefore be the driving force of post-stimulation length increase in short-time stimulations. A direct coupling of the actomyosin cortex to the spindle poles may encounter and push this scenario.

How does spindle structure change during relaxation? Images of relaxed cells with $t_{shear} = 10$ min show morphological changes: long pointed bipolar geometry, less an-

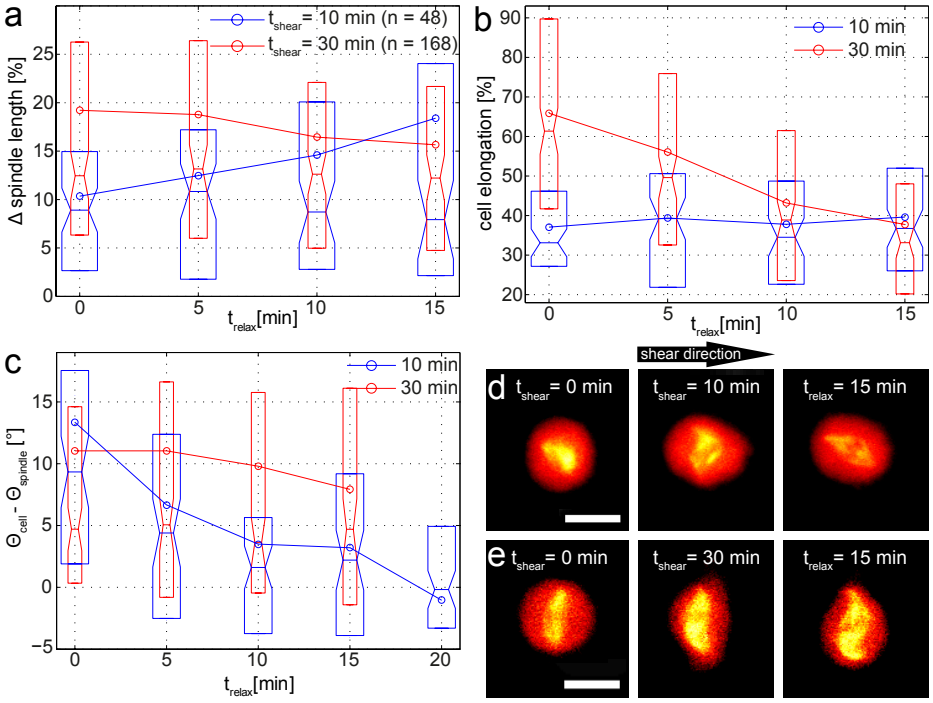

Figure 6.10: Stoppage experiments reveal prolonged spindle elongation and spindle shape depends on shear duration due to angular relaxation: (a) Cells with $t_{shear} = 30$ min (red) show only slight relaxation of spindle lengths. $t_{shear} = 10$ min (blue) leads to slow spindle increase after stoppage of shear for 15 min. Furthermore, the distribution gets broader. (b) Looking at cell elongation reveals vast relaxation for $t_{shear} = 30$ min. On the contrary, less stimulated cells do not change their elongation after shear stimulation. (c) Angular differences reveal small relaxation for longtime shear in contrast to $t_{shear} = 10$ min, where a relaxation is seen from $\theta_{cell} - \theta_{spindle} = 10^{\circ}$ to zero degrees. (d) 10 min sheared cells exhibit longer and straighter spindles after a relaxation of $t_{relax} = 15$ min than at shear stoppage. This illustrates the observed angular relaxation in (c). (e) Images of a mCherry-tubulin labeled cell with $t_{shear} = 30$ min reveal S-like spindle shape and reduction of cell elongation during relaxational processes of the cell body (scale bars 10 µm)

gular difference and only marginally cellular shape change ($t_{relax} = 15$ min, fig. 6.10d). This illustrates the continued spindle elongation combined with a rotational relaxation. Here, an enhanced coupling of spindle orientation and length seem to encounter, where rotational relaxation drives the spindle elongation. On the contrary, cells with $t_{shear} = 30$ min exhibit a S-like spindle shape and a reduced cell elongation after $t_{relax} = 15$ min (fig. 6.10e). This S-like shape could indicate that spindle elongation is much faster than a potential process concerning spindle shortening. Spindles seem to buckle only at the poles and no absolute length reduction is taking place. A direct coupling of the cortex to the spindle poles may be at hand due to less space between a pole and the cell edge. This intriguing small distance leaves no space for astral MT. A steady state of length could be reached as observed in compression studies [Dumont and Mitchison, 2009a]. Furthermore, the rounding of cells after shear stoppage is a faster process than potential spindle shortening opposed to the observed dynamics at initial shear stimulation in fig. 6.4d where spindle dynamics are fast than the cell dynamics.

The observed widening for ciliobrevin D (fig. 6.7b) treated cells reveals tangential forces on the spindle. When the cell-spindle angular difference is more pronounced, pulling forces on the spindle could be higher. This may be even enhanced by the myosin re-distribution found in 6.4. Taken together, it may explain the behavior after mechanostimulation of 10 min sheared cells. When the actin cortex pulls on the spindle, the angular difference creates a specific torque on the mitotic spindle due to enhancing cell elongation while the spindle with its increasing length serves as a steady strengthening lever. This torque may be reduced due to saturation of cell elongation and less angular difference. Thus a maximum at about 20% length increase for long and short stimulations is achieved: the force-balance is accomplished again. This would suggest that the decreasing angular difference would drive the spindle elongation in the case of 10 min sheared cells.

6.4 Shear-elongated cells have more myosin at the poles

So far, it has been shown that actomyosin is necessary for mitotic cell elongation perpendicular to the external forces and fast initial spindle elongation. An underlying mechanism for this behavior may be shear-induced myosin re-distributions. A way to get to the bottom of this prospect, immunofluorescence imaging is accomplished with confocal microscopy. To this end, shear-elongated and non-sheared RPE1 cells are fixed and stained using standard protocols (see B.1). Cells are treated with the proteasome inhibitor MG-132 to arrest cells in metaphase and block mitotic progression to anaphase. Spindle morphologies are not significantly altered by this treatment [Fernández et al., 2011]. An even distribution of myosin II is found within a ~ 2 µm periphery at the cell edge of control cells (fig. 6.11a, b), while shear-elongated cells exhibit enhanced heterogeneity in myosin stainings (fig. 6.11c, d). Furthermore, a significant portion of myosin is found in the spindle region in the case of sheared cells.

The next step is a quantitative image analysis to capture changes in intensities and distributions of myosin signals. Since cell morphology is dictated by the actomyosin

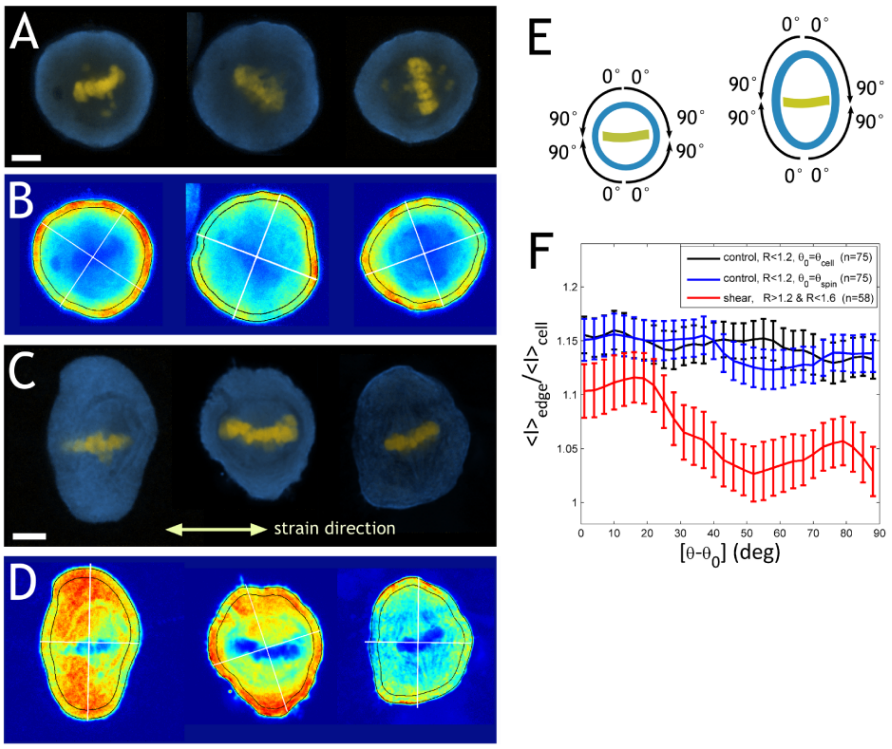

Figure 6.11: Shear-elongated cells have more myosin at the poles: (a) Immunofluorescence images of non-sheared, control RPE1 cells. (b) Color-coded intensity of myosin stain of cells from (a). The white lines flag the minor and major cell axis calculated by a matlab algorithm. The outlined cell edge region is the region of choice for myosin intensitiy quantification. (c) Immunofluorescence images of sheared RPE1 cells (100% strain, $f = 0.3$ Hz). (d) Color-coded myosin intensity of cells from (c). (e) Angular distribution of myosin intensity is averaged over several cells ($n_{control} = 75$, $n_{sheared} = 58$). Since there are no signs of polarity or chirality in the images, each cell is split into four quadrants and the data is averaged over them. For the reference angle θ_0 two possibilities are considered, the cell orientation and the chromosome plate orientation. (f) Mean myosin signal intensity throughout the periphery as a function of angle $\theta - \theta_0$, normalized by the mean intensity over the whole cell body ($\theta_0 = \theta_{cell}$, black curve) and the spindle orientation ($\theta_0 = \theta_{spin}$, blue curve). For sheared cells (red curve), this distinction plays no role since the difference between the two orientations is at most 20°. Error bars: ±2 S.E. Sheared cells show higher myosin intensity around the poles ($\theta = \theta_0$) than close to the equatorial plane (scale bars 5 µm; figure taken from [Fernández et al., 2011])

cortex [Tinevez et al., 2009], the myosin intensity is quantified in a 1 µm wide cell boundary region (fig. 6.11b, d). A reference angle θ_0 is defined for each single cell to average over several cells. In fig. 6.2, a well-defined unique axis is seen for modestly elongated cells as the cell axis is parallel to the spindle axis within 20°. In contrast, it depends on the image analysis algorithm when round control cells have an ill-defined cell orientation θ_{cell}. In this regard, the following data is analyzed via the spindle orientation axis θ_{spin} - the direction perpendicular to metaphase chromosome plate - as angular reference. Each cell is split into four quadrants running from $\theta = 0°$ (cell poles) to $\theta = 90°$ (chromosomal plate, fig. 6.11e). The data from each quadrant is then pooled. Only cells with elongations below 60% are considered (fig. 6.11f) for the purpose of reducing potential artifacts coming from desperately elongated cells. The average elongation of sheared cells used in the analysis is $32\% \pm 10\%$ and that of control cells $10\% \pm 1\%$. No significant angular dependence of myosin intensity is found in control cells - no matter what angular reference - cell or spindle - is used. However, more significant myosin signals are found at the poles than at the equator for shear-elongated cells. This is an indication for shear force-induced myosin II re-distribution, which may be the causal factor that leads to cell elongation.

6.5 Shear-elongated cells lose astral microtubules and couple directly to the cortex - mechano-contractile coupling model

We have revealed a plethora of responses of mitotic cells to external shear. Taken together, how does this may influence the force balance in a mitotic cell and therewith, the mechanical coupling of the spindle to the actomyosin cortex?

To address this question, RPE1 cells are fixed and immuno-stained for myosin II and microtubules. Whereas compressed control cells show astral microtubules reaching out of the spindle poles into the cortex, immunofluorescence images of myosin II and microtubules reveal a new coupling of the mitotic spindle to the actomyosin cortex (fig. 6.12, fig. 6.4f). No astral MT are found in the shear elongated cells - but MT intensity is enriched in the background and directly at the cell membrane - indicating tubulin monomer concentration has risen at these certain areas. The spindle poles stick now directly in the cortex and show bent shapes - similar to the shapes observed in stoppage experiments (see 6.3.5). The shortest distance of spindle pole to cell edge is heavily reduced in shear-elongated cells (1.5 µm ± 0.63 (standard deviation, SD), $n = 54$) opposed to control cells (4.0 µm ± 1.3 (SD), $n = 29$). This reduced value for sheared cells implies that the spindle pole lies now in the cortex region. The cortex thickness is around 50 nm to 1 µm [Salbreux et al., 2012]. Due to the re-organization of the myosin (see 6.4), the cortex may also thicken at the cell poles. This spindle-pole-cortex distance looks to be a more promising parameter than a simply comparison of cell to spindle length where the ratio is nevertheless changed: for sheared cells the ratio is $L_{cell}/L_{spin} = 0.66 \pm 0.22$ (SD), while control cells have a length ratio of 0.51 ± 0.13 (SD).

A reason for spindle elongation and re-orientation under shear may be an enhanced attachment to a contractile actomyosin cortex with depleted astral MTs. Similar as described in the mechanochemical switch model for compressed mitotic cells [Dumont and Mitchison, 2009a], spindle poles may act as force integrators which sense external force fields (fig. 6.13b). Tension is transmitted on kinetochore MTs at the poles by mechanical coupling at spindle poles. An elastic linker element - several candidates possible - leads to force-dependent regulation of the activity of a depolymerase or direct effect of force on depolymerization. In [Dumont and Mitchison, 2009a], the cortex was excluded as a potential elastic element. This is in contrast to the mechano-stimulated cells that are presented in this thesis. Here with sheared cells, the actin cortex and the astral microtubules are of importance for the spindle elongation process (see 6.3.3) - suggesting they could be promising candidates as elastic linker for force integration at the spindle poles. By direct coupling of cortex to spindle, this force integration of the spindle is enhanced with the cortex having direct control via its contractile skills - maybe by adjusting the degree of contractility. Shear-elongated cells have more myosin II at the poles (see 6.4) which may indicate gradients of contractility being available for spindle length determination via the actin cortex. Such a mechano-contractile coupling may contribute to successful cell division by pinpointing the spindle axis in major cell axis direction - emphasizing that contractility is of eminent importance for these processes.

When the spindle is already aligned into zero-force direction, one may expect a spindle elongation mechanism similar to the scenario described by [Dumont and Mitchison, 2009a]. Although there is only a step-like height decreasing stimulus, all cell axes depart from the spindle perspective. This is mimicked when the spindle already lies in perpendicular direction to the imposed strain: the long cell axis departs from the spindle poles and may induce a similar de-polymerization stop as seen in Ptk2 cells [Dumont and Mitchison, 2009a]. Note that in this scenario, the myosin distribution is not homogeneous. However, in the case of sufficient angular difference between cell and spindle, the actomyosin cortex is able to directly stick and couple to the spindle poles - as seen in fig. 6.12b and fig. 6.13a. The main reason is the constantly reducing width of the cell which leads to an approaching of cortex and spindle poles - constricting the space for astral microtubules. The subsequent spindle rotation could be due this width constriction and direct coupling of spindle to cortex. By this coupling, the actomyosin cortex is able to impose a corresponding torque on the spindle which may stimulate further spindle elongation. Astral microtubules are already gone and thus, only the spindle can execute elongation which is necessary for the rotation in an shear-elongated cell. A reason for vanishing astral MT could also be destructive forces by the imposed dynamic shear that directly induces depolymerization.

How does the cortex impose this torque on the spindle? This may achieved through contraction that is stimulated through the shear-elongation of the cell. In 6.4 was shown, that myosin redistributes at the cell poles with higher stain signals being found. While this staining does not show active myosin, it could be a hint that there is a contraction force acting towards the poles - which may be the reason for the cell elongation. The contractility may be tuned by the cell or adjusted via mechanosensing processes.

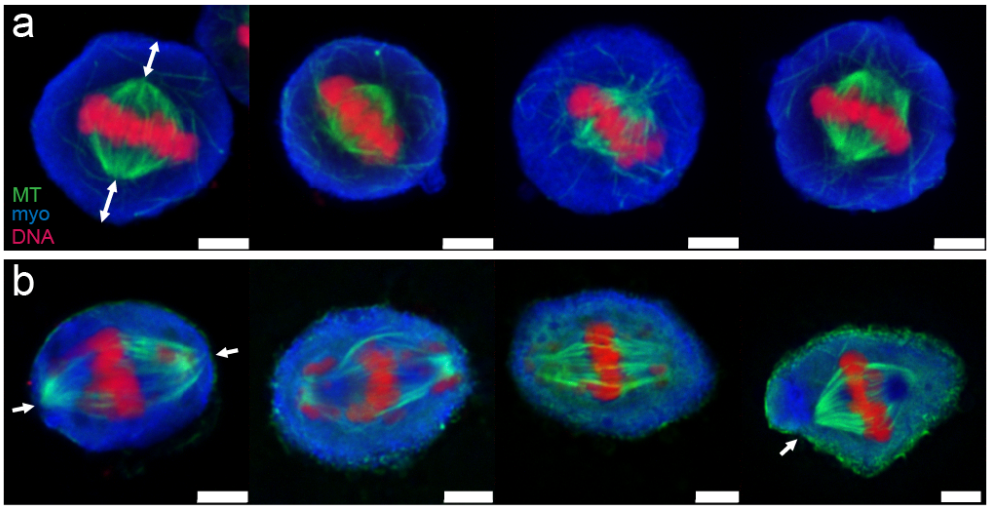

Figure 6.12: Direct coupling of spindle and actomyosin cortex: fixed RPE1 (a) compressed control and (b) shear-elongated cells (green: MT, blue: myosin II, red: DNA). Pole to membrane distance is heavily reduced in sheared cells compared to control cells (white arrows). No astral microtubules are visible for sheared cells - in contrast to control cells (scale bars 5 µm)

This extended mechanical coupling model may explain several observations already made in this thesis. In 6.3.5, the S-like spindles - that emerge after $t_{shear} = 30$ min and 15 min relaxing - show no astral MT and direct attachment to the cortex. This may imply that another steady state is reached and further spindle shortening is not possible due to the missing elastic element of astral MT to enhance MT depolymerization at the spindle pole and obstruct polymerization in the kinetochore region. This direct coupling of spindle poles to the actomyosin cortex seems to stabilize elongated spindles and thereby, ensuring this force-induced cell division plane. If the angular difference is minimized for 10 min sheared cells via a spindle elongation after stoppage of shear seems to be a mechanism to define the division axis properly. Further spindle elongation helps to ensure the correct divisional plane along the long axis. Here, the spindle poles may act as the corresponding force integrators by steering the spindle re-orientation and elongation for successful division. The direct coupling to the cortex may be necessary in this scenario to directly sense the cell shape and orientation. The putative torque created by the cortex via contraction processes - which results in cell elongation - may be the starting point for mechano- and orientation-sensing of the mitotic spindle.

Although taxol treated MDCK cells showed no spindle elongation with MT being stabilized, spindle rotation and cell elongation in zero-force direction is still possible (see 6.7). Here, a simple coupling of cortex to spindle via astral MT as a preserved elastic element proves to be sufficient. Taken together, spindle elongation with direct coupling to the cortex may provide a parameter for mitotic spindles to ensure proper division axis in certain scenarios and therewith, divisional success.

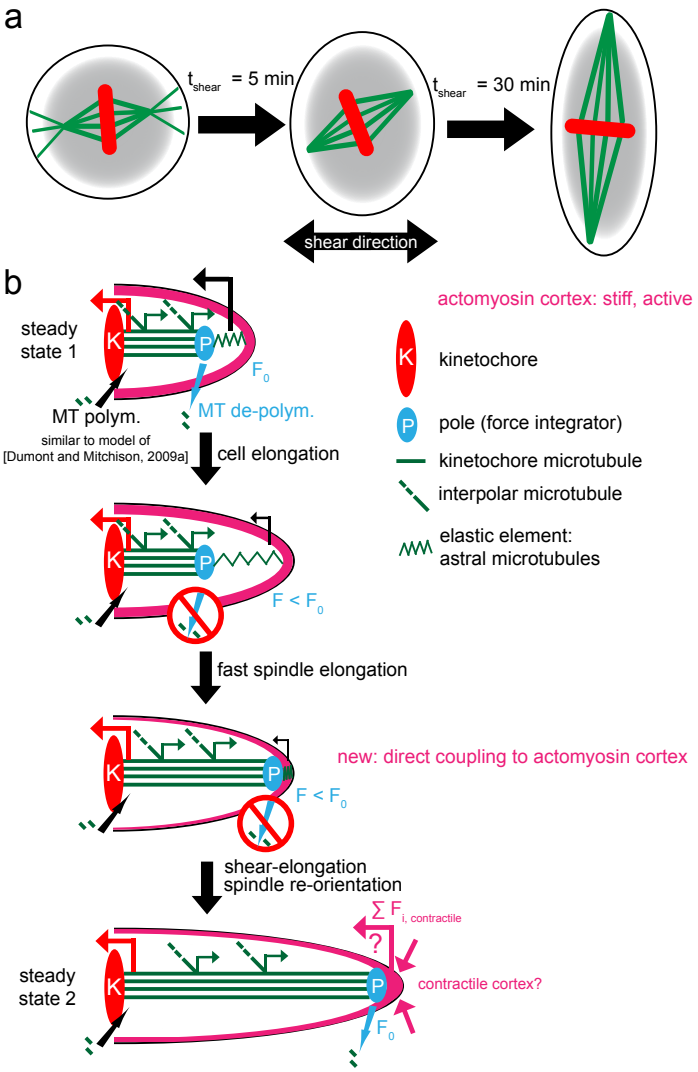

Figure 6.13: External dynamic forces regulate spindle size: (a) Cartoon of the response of a mitotic spindle to external dynamic forces and subsequent shear-elongation. Spindles initially elongate until they contact the actomyosin cortex. Further shear-elongation of mitotic cells leads to a reduction of the angular difference of cell to spindle and longer spindles by direct attachment to the cortex. (b) Mechanical contraction-dependent coupling model for spindle length regulation based on coupling model postulated by [Dumont and Mitchison, 2009a]: Length of the kinetochore MTs and thereby the spindle is dictated by force-dependent depolymerization at the spindle poles. It is further postulated that the depolymerization rate responds to the sum of all the forces acting on the kinetochore MTs. These forces can be divided into pulling on plus ends by kinetochores (red arrow), an outward sliding force acting along the length of the kinetochore MTs (green arrows) and pushing on minus ends by others elements of spindle or the cell (black arrow). K-MTs elongate at the sliding rate until the standard F (F_0) is re-established: depolymerization continues again and a new steady state is achieved. With direct coupling to the actin cortex (purple), the contractile forces of the cortex - emerging by shear-elongation - determine the end-point and new steady state length of the spindle.

6.6 Shear-induced spindle elongation is time-dependent on cell-cell adhesion

Epithelial cells form a cell layer *in vivo* and exhibit orientated cell division steered by cell-cell adhesion protein cadherin [DEN ELZEN et al., 2009]. Cell-cell adhesion is a major pivotal point in cell-cell communication, tissue management and development and considered of high importance in mechanotransduction [SCHWARTZ and DESIMONE, 2008]. How does shear-induced orientation and elongation of cells and spindles evolve in context of cell-cell connections? To this end, cell-cell contacts are examined by pure counting of cell-cell contacts for each cell with three groups: no neighbor (NB = 0), one neighbor (NB = 1) and more than one neighbor (NB > 1). This may not be the best parameter to quantify cell-cell contacts, but it is a fast and easy measure to attain. For MDCK cells with more than one neighbor, spindle elongation is less fast and shows a slight relaxation after 10 min of shearing (fig. 6.14a). Only after $t_{shear} = 15$ min, spindles from cells with NB > 1 elongate to about 20% length increase. Cells with one neighbor are only slightly slower than cells with no neighbors and they show no elongation relaxation. However, cell elongation is not neighbor dependent (fig. 6.14b). In contrast, the angular difference of cell to spindle is enhanced in the NB > 1 case: it rises up to 30° but fast relaxes to 10° when spindles elongate (fig. 6.14c).

As seen in 6.4, myosin intensities change due to external forces. To see whether cell-cell contacts interfere with the myosin distributions, the myosin intensities are analyzed again. Non-strained RPE1 cells with no neighbors show homogeneous myosin intensities (fig. 6.15a, 6.4). Otherwise, all non-strained control cells with cell-cell contacts ($n = 23$, not used for analysis in 6.4) have reduced myosin signal intensities at the cell-cell interface (fig. 6.15b). When absolute intensities are compared between contact and non-contact areas, a reduction of about 35%±16% (SD) is revealed in a preliminary analysis.

Surprisingly, this pre-experimental myosin heterogeneity in RPE1 cell-cell aggregates does not affect cell elongation in strained MDCK cells (fig. 6.14b) - which one may have expected due to the results in 6.4. Only the re-orientation of the spindle is postponed as seen in the angular difference data (fig. 6.14c, inset). This may result from the heterogeneous myosin distribution. The high angular difference diminishes after 12 min - which has to be the result of cell orientation in spindle direction. Therefore myosin signal heterogeneity weakens cell rotation perpendicular to the strain direction while not interfering with cell elongation. Cells may not be able to feel the strain direction anymore. Another reason might be pure steric hindrance of cell elongation and rotation due to neighbor cells which use up extracellular space for proper cell orientation induced by external forces. Furthermore, reduced intracellular space due to angular differences of cells and spindles leads to a postponed spindle elongation: spindles are only able to elongate if the cell orientates in spindle direction or vice versa. After 15 min of shear, this seen in fig. 6.14a with a slow spindle elongation while the angular difference dropped from 30° to a 10° level (fig. 6.14c). This behavior is illustrated in the spindle images in fig. 6.14f: a cell with two neighbors needs more than 10 min to re-orientate its spindle perpendicular to the imposed strain direction while the cells elongates just as in the non-

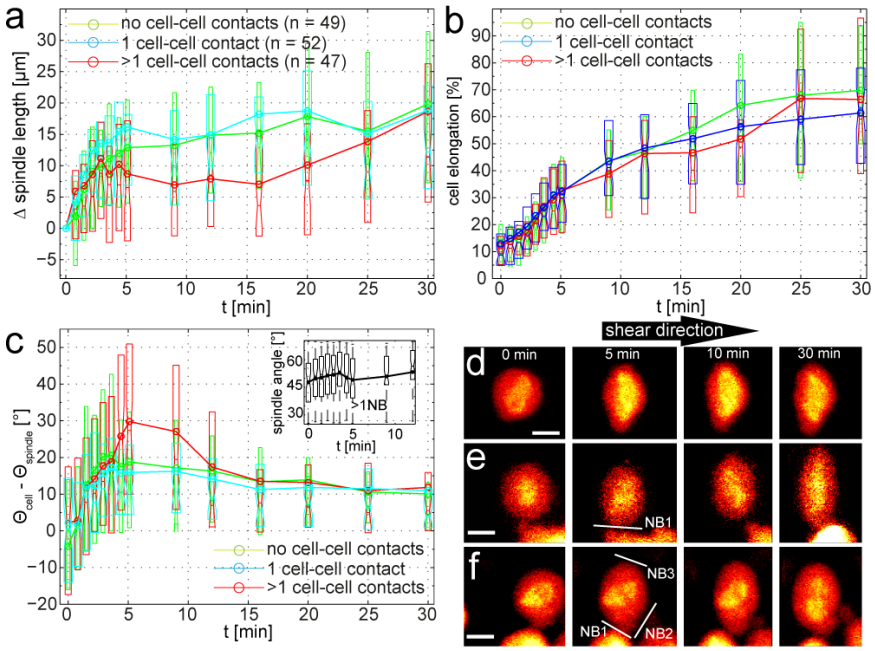

Figure 6.14: Cell-cell contacts lead to postponed slow spindle length increase: (a) Cell-cell contacts change spindle lengthening process time-dependent. With no neighbors (NB), cells exhibit intial fast then slow length increase ($n = 49$). Cells with one neighbor ($n = 52$) show similar behavior - in contrast to cells with more-than-one-neighbor ($n = 47$), which show less length after 5 min combined with a small relaxation. A late slow spindle elongation starts at about 15 min of shearing. At the end, all groups achieve similar lengths elevations. (b) Cell elongation is only marginally reduced for NB > 1. (c) $\theta_{cell} - \theta_{spindle}$ raises to 30° after $t_{shear} = 5$ min for a high number of cell-cell contact cells (red) and relaxes after 12 min. This seems to be caused of less spindle rotation (black) and cell orientation back towards the spindle (angular difference reduced). Cells with no neighbor (d), one neighbor (e) and more than two neighboring cells (f) show cell and time-dependent spindle elongation

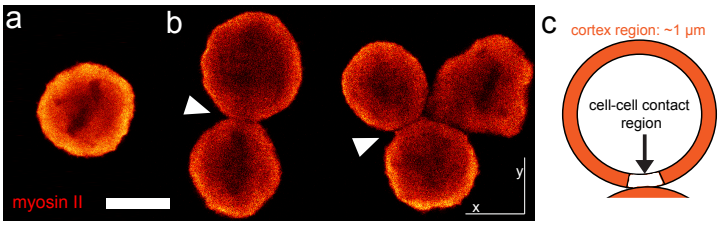

Figure 6.15: Myosin intensities are reduced at cell-cell contacts: (a) Myosin II intensities of stained control cell show homogenous distribution of motor proteins. (b) Control cells with cell-cell contacts show regions of reduced intensity (white arrows) (scale bar 5 µm). (c) Schematic representation of myosin II intensity analysis in cell-cell contact and normal cortex region (~ 1 µm from outer cell boundary).

neighbor case. Therefore, heterogeneities of myosin distributions only affect the spindle re-orientation and elongation process and not the overall cell elongation. Spindle elongation and re-orientation seems to be directly coupled here. Cell elongation may be a more indirectly uncoupled background process which is of course still necessary in lagged spindle re-orientation.

Note that cell-cell contacts may lead to less counteraction of actomyosin cortex to withstand intracellular pressure at the contact point, because this is balanced by the neighbor cell's intracellular pressure. Thus the myosin signal intensity is reduced at the contact site because the myosin concentration is diminished due to less cortical activity. This results in cell elongation only in a direction with high myosin signal intensity - which is neither the contact point with the neighbor cell nor necessarily the perpendicular direction to the imposed strain direction. A mixture of extracellular steric hindrance and passive actomyosin cortex at cell-cell contact area leads to a deficit in cell re-orientation. Cells and their spindles adapt to this behavior by correcting the angular difference and postponed spindle elongation. Whether myosin is actually active or not would be a better measure for further investigations of dependence of spindle parameters on the myosin activity and distribution. Furthermore, a better control of cell-cell adhesion in terms of strength and geometry has to be achieved to reveal the dynamics behind symbiotic cell-cell management of external mechanical stimuli.

6.7 Shear forces orient the division axis without comprising mitosis

So far, the observations made in this thesis concerned cellular behavior in the early stages of mitosis - prophase and metaphase. Proper assembly of the mitotic spindle is required for further progression through mitosis. Therefore, error-free segregation of genetic material has to be guaranteed. Contrariwise, the initiation of the spindle assembly checkpoint will postpone anaphase onset for several hours [Musacchio and Salmon, 2007]. Thus, the next task is to reveal whether cells divide properly in an environment of imposed shear.

At first, the capability of RPE1 cells to divide in static conditions is examined by a control experiment with smoothly compressed cells without shearing. 99% of mitotic cells ($n = 218$) divide with success under the imposed conditions. These control cells divide isotropically as expected: the division axis is uniformly distributed within the plane of the substrate surface (fig. 6.16a, control). Next, dynamic forces are imposed and the divisional destiny of single cells is monitored over two hours. Similar to previous observations, cells align their mitotic spindles and divide perpendicularly to the strain direction (fig. 6.16a). Altogether, a remarkable efficiency at large amplitudes is seen for the alignment process, which is revealed by narrowly peaked distributions (fig. 6.16a). At large shear amplitudes of 100% and a slow frequency 0.03 Hz, 92% of all mitotic cells ($n = 136$) successfully divide - 90% of them divide perpendicular to the shearing forces within a 30° range. This window is condensed to a width of 10° when the frequency is raised up to 0.3 Hz (fig. 6.16a). A different cell line, the osteoblast cell line MC3T3,

shows identical behavior: cells divide in direction perpendicular to the external force - for all imposed frequencies from 0.3 Hz to 10 Hz and large strain of 100% (fig. 6.16b).

Because the spindle assembly checkpoint is believed to depend on mechanical cues [Musacchio and Salmon, 2007, Bloom and Yeh, 2010], one may think that external forces would impede the metaphase to anaphase progression. So it should be now examined if imposed dynamic forces affect the efficiency and timing of the RPE1 cell division. An experimentally well-defined measure of division time is provided by the elapsed time from the start of the experiment until the anaphase onset. The starting time is defined when the setup temperature is raised to 37°C, while the anaphase onset time is specified by the fast process of chromatides separation - which could be resolved in time within 20 s. Anaphase onset is not influenced by most experimental framework parameters, but a significant delay is found specifically when large strains of 100% and the intermediate frequency 3 Hz are used (fig. 6.16c, d) - none the less, 88% of the cells divide within two hours ($n = 213$).

How spindle re-orientation alters the cell viability is addressed by monitoring cell culture for multiple days after imposing external strain. The RPE1 cells are harvested directly after the experiments, re-suspended into the fresh medium and the cell growth is monitored over three days. Cells with force-oriented spindles (100% strain, 0.03 Hz) grow at a rate indistinguishable from control cells (fig. 6.16e), which implies that no widespread cellular apoptosis occurred as a result of strain or chromosome mis-segregation. Although strained cells re-orientate their spindle and partially postpone the anaphase onset, their competence for successful division and further mitotic progression stays unaffected. Lastly, one has to pay attention to excessive strain cycles can irreversibly harm cells, as seen in observations of slightly slower growth after mechanical perturbation at fast $f = 3$ Hz (fig. 6.16e).

6.8 Discussion

It has been shown that mitotic eukaryotic cells under dynamic shear divide perpendicular to the external force. A similar behavior was observed in mouse MC3T3 osteoblasts, human RPE1 and dog MDCK epithelial cells. The orientation of the division axis seems to be a consequence of the fact that sheared mitotic cells and their spindles elongate along the zero-force direction. This duet of cell and spindle elongation is actomyosin-dependent since it could be fully obstructed by inhibition of myosin or ROCK activity. The spindle elongation seems to be partly a consequence of the fact that sheared mitotic cells couple the actomyosin cortex directly to the spindle poles with astral MT being vanished. This may influence a mechano-chemical switch at the spindle poles which has been recently proposed [Dumont and Mitchison, 2009a]. Spindle re-orientation and cell elongation can be uncoupled from spindle elongation by blocking MT dynamics. Moreover, an exceptional sensitivity of the mitotic spindle to the cell shape has been found: aspect ratios as low as 1.15 are sufficient to bias the spindle towards the long axis in RPE1 cells. This confirms recent results where cell shape is altered by a static confinement [Minc et al., 2011]. The drastic shear-induced cell elongation at high frequencies explains their

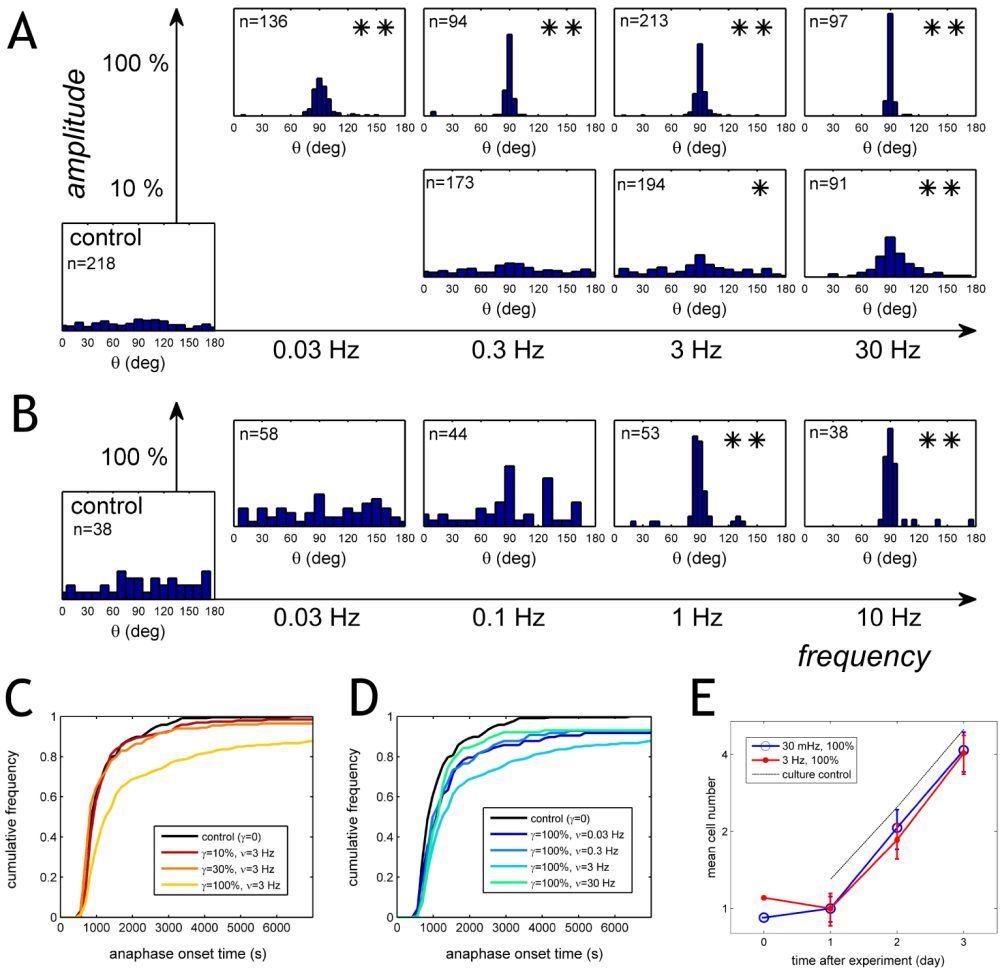

Figure 6.16: Shear forces orient the division axis without compromising mitosis: (a) Division angle distributions for different amplitudes and frequencies for RPE1 cells. Small amplitudes ($\gamma = 10\%$): anisotropic division requires a high frequency of 30 Hz. Large amplitudes ($\gamma = 100\%$): very slow stimulations (0.03 Hz) are enough to align the division axis in principal in all cells. Statistical significance relative to the control is tested via a Mann-Whitney U-test on the reflected angles $|\theta - 90°|$ (*: $P < 0.01$, **:$P < 10^{-8}$). (b) MC3T3 osteoblasts show similar behavior. (c) Cumulative histograms of anaphase onset times when RPE1 cells are shear-stimulated (one curve = one experiment, various amplitudes, $f = 3$ Hz). (d) Cumulative histograms of RPE1 anaphase onset times (various frequencies, constant strain of 100%). Strain alignment of the division axis delays division only marginally. A significant delay is seen at 3 Hz; note that mitotis is fast again at 30 Hz. (e) RPE1 growth after force-alignment of the spindle. After day 1, an exponential cell growth is seen. Cell number is divided by its value at day 1. Normally cultured cells serve as a control (black line). No significant difference in growth rate can be observed after mechanical stimulation at 0.03Hz, 100% strain. Increased cell death is seen within the first day following shear at 3 Hz, 100% strain - indicating potential damage by a non-physiological stimulation. (figure taken from [Fernández et al., 2011])

striking efficiency to bias cell division.

Why do shear-stimulated cells in mitosis elongate into the zero-force direction? To resolve this, one has to learn what dictates the cell shape at first and in which way external stimuli modify it. Cell morphology is mostly destined by the whole cytoskeleton - while in slightly adhered mitotic cells the actin cortex is seen as the crucial ingredient [Théry and Bornens, 2008]. When mean curvature C and cell membrane tension σ and of the actin cortex are set in relation, the Laplace law provides the pressure difference $\Delta p = \sigma C$. For cells here in this thesis, the hydro-static pressure is expected to be homogeneous since the oscillation period is in fact long compared to pressure equilibration times. Hence in the shear-elongated cell scenario, the spatial anomaly of the cortical curvature should coincide to active force gradients carried by the actomyosin cortex. Force gradients could derive from multiple causes, for example aberrations in myosin II activity, in cortical density or thickness. Myosin II immunofluorescence experiments and subsequent analysis displays that the intensity is higher by about 10% at the poles than at the equator of shear-elongated cells. But honestly, this outcome appears to be not enough to justify with a simple prospect of a Laplace law with constant pressure. One may anticipate detecting more myosin II at the equator when just the curvature in x-y plane is taken into account. Because the ellipse curvature ratio of maximal to minimal value goes as the cube of the axes ratio, the pole-curvature C_p of a 30% elongated cell would be approximately the doubled value of the equator-curvature C_e, $C_p = (1.3)^3 C_e \sim 2C_e$. This shows that just myosin signal intensities could not elucidate the elongated cell shapes. Note that the curvature along the z-direction cannot be quantified properly. Hence, one may suggest that on the one hand myosin activity, on the other hand actomyosin cortex structure or both scenarios alter along the cell contour. Enhanced mitotic spindle lengths may push this shear-induced cell elongation to even higher levels. While at the same time longer spindles in a steady state and properly coupled to the actomyosin cortex may stabilize cell elongation to a certain degree as seen in the stoppage experiments. This may reduce the overall workload for the actin cortex.

How do external dynamic shear forces accomplish the duet of cell and spindle elongation? It may be possible that mechanosensing and related cellular responses are part of this process. For example, mitotic *Dictyostelium* cells inherit a mechanosensoric system that controls cell morphology during anaphase via myosin-II recruitment to seize equal-sized daughter cells [Effler et al., 2007]. Otherwise, the mechanically-induced cellular response in this thesis is time-dependent and non-linear (fig. 6.2.1c), which is in agreement with a mechanical restructuring of the mitotic spindle and the actomyosin cortex - maybe similar to the re-organization of bundled actin networks [Schmoller et al., 2010]. A systematic knockout of mechanosensing pathways and likewise live cell imaging of the actomyosin system may be essential tasks to answer this question. Maybe a separate pathway acts for spindle elongation, which is found to be initially faster than cell elongation. A hint on this may give the possibility to uncouple spindle re-orientation and cell elongation from spindle elongation by inhibition of the MT dynamics with taxol. For spindle elongation, it is of eminent importance to have a functional actomyosin cortex and a proper initial coupling via astral microtubules (see nocodazole experiments in

6.3.3).

All in all, it has been shown that mitotic RPE1 and MDCK cells under dynamic shear exhibit actomyosin-driven elongation and division along the direction perpendicular to the external forces. External shear further stimulates fast spindle elongation. Observations of reduced myosin II immunofluorescence signals at the equator of elongated cells imply that the external strain induces gradients in actomyosin structure. Moreover, the mitotic spindle couples directly to the cortex and astral microtubules vanish. More work will be necessary to unravel if these observed processes are caused by purely mechanical remodeling or by more complicated mechanosensing responses. In the end, these stunning findings provide a novel approach to study the intricate connections between the mitotic apparatus, the actomyosin system and the extracellular environment.

7 Outlook

In recent decades, reconstituted cytoskeletal systems proofed to be a powerful tool to unmask properties and mechanisms of cell mechanics. Moreover, *Xenopus* extracts are used for several years now to study mitotic and meiotic spindles in a more *in vitro* like scenario, which has a reduced complexity compared to standard mitotic mammalian cells [Heald et al., 1996, McNally et al., 2006, Gatlin et al., 2010, Shimamoto et al., 2011]. But these *Xenopus* extracts are missing a key element in comparison to human or mouse cells as used in this thesis: they lack astral microtubules and therefore a functioning coupling to an actin cortex. Here, a new *in vitro* system may be developed by combining these two fields and approaches to achieve more than just the sum of its single parts: *In vitro* spindle from *Xenopus* extracts or purified proteins could be combined with a reconstituted cytoskeleton and the interactions may then be studied (fig. 7.1a). By adding PEG and the subsequent compression of the system to the surface, it may be possible to study a more two-dimensional system as seen with an *in vitro* cortex created in a recent study [Carvalho et al., 2013]. Cortex to spindle coupling could be deeply analyzed and the effects as seen in chapter 6 better understood. With diverse actin-binding proteins like fascin, α-actinin or filamin and related motor proteins, one may be able to study the contribution of each protein to the forces created or felt by a mitotic spindle. Another protein presented in this thesis which may be a good target to add to this *in vitro* cocktail could be EPLIN. It is essential in divisional success in mitosis because of its location in the cortex and structural impact in the contractile ring during cytokinesis [Chircop et al., 2009].

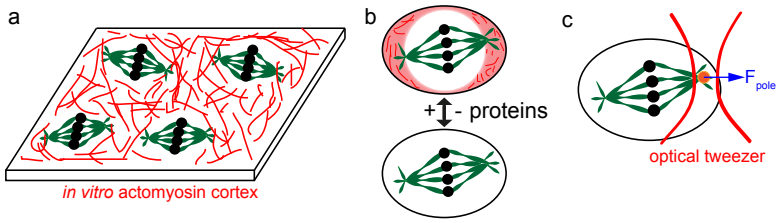

Figure 7.1: Combination of reconstituted actin networks and *in vitro* mitotic spindles creates new valuable system: (a) *in vitro* spindles from *xenopus* extract or purified proteins selectively placed by an imposed pattern could be embedded in an *in vitro* actomyosin cortex environment. This can be used to study the cortex-spindle coupling in a scenario with reduced complexity compared to a living cell. (b) More cell-type *in vitro* system: combination of recent vesicle technology with *in vitro* spindle from cell extracts or purified proteins and to the inner-membrane attached is an *in vitro* actomyosin cortex. (c) Due to this building block system, it would be easy to add proteins at will, but also it is possible to incorporate functionalized beads for example direct force measurements at the spindle with optical tweezers.

Even one step further, this new reconstituted spindle system may be packed in a vesicle or liposome. Due to the technical advancements in vesicles production and control, this could be combined with an artificial cortex that is attached to the vesicle's inner membrane [Carvalho et al., 2013]. Confinement is known as an important parameter - cell size has been already described as an essential cue in spindle length determination [Dumont and Mitchison, 2009b, Goshima and Scholey, 2010]. This paves the way for a building block system where different proteins like myosin X which directly resides at spindle fibers [Woolner et al., 2008] from your protein toolbox of your freezer can be incorporated into the vesicle (fig. 7.1b). This building block system of a vesicle enclosed mitotic spindle enables the simple use of modern bio-techniques: incorporating mutations in key proteins, add and subtract purified proteins to study interactions or posttranslational modification like phosphorylation or glycosylation should all be straightforward possibilities (fig. 7.1b). Thereby, a better understanding of mechanical and biochemical interactions between key components could be achieved. One may learn more about interplay and by full control of components, one could test models and adapt to certain species-like structures and configurations. Here, conserved mechanisms and information processing in diverse organisms may lead to a better understanding of mitotic regulation dynamics not only for a species of one kind, but for all kinds. Moreover, the usage of motor protein mutants of dynein, kinesin-5 or the spindle fiber related myosin X [Woolner et al., 2008] could be helpful. Here, one may test spindle length controlling process which consists of polymerization and depolymerization at certain spindles spots [Dumont and Mitchison, 2009a]. This could lead the way to more enhanced cancer therapeutic targets in spindle structure and force generation.

If interests shift into more time-dependent analysis of this systems, photoactivatable proteins via a LOV domain in motor proteins or actin related proteins [Wu et al., 2009] could provide insight into dynamic processes. To photo-activate spindle elongation may result in discovery of further biological relevance of mitotic key parameters. High resolution microscopy methods like STED and PALM - that inevitably use high laser power which is bad for living cells - may be perfect for this new reconstituted system where your system dies less easily. The *in vitro* mitotic vesicle system are a good candidate for these imaging techniques by less relying on healthy cellular state controlled by parts of the cell that are not connected in the first line of mitotic spindle mechanics and in large parts only biochemically steered. With this flexible *in vitro* type of system and ultra-precise microscopy, kinetochores may be examined by using recently developed tension FRET-based bio-sensor [Grashoff et al., 2010]. This technique may also be useful at other sites for example spindle poles, where microtubules are thought to depolymerize force-dependent. Moreover in combination with direct force measurements, it could provide more insight into the spindle and cytoskeletal mechanics. This *in vitro* artificial cortex-spindle-vesicle system is way easier to be mechano-stimulated due to less concerns on cell viability and overall sterility. Because of this building block design, optical trapping is even possible by simplified incorporation of beads and again, less concerns on cellular viability. Thus forces could be directly measured that are needed for spindle rotation or obstruction of microtubule poly- and depolymerization (fig. 7.1c).

A List of qPCR primers

These oligo(dT) primers were self-designed using *Primer3* and *NCBI Blast* search engine using following basic principles: reverse and forward primer on neighboring exons (estimate genomic DNA contamination), amplified fragment length of about 100-250 bp in 3' area of the gene, annealing temperature of about 55-60°C (right and left should be similar), GC content less than 60 percent of the amplified fragment and no blasting results of the gene fragment other than the target gene itself. Alphabetical order of qPCR-used Primers all in 3' to 5' direction with fragment length in base pairs and used annealing temperatures (purchased at *Metabion international AG*, Germany, all *mus musculus* except where noted):

- ATP-binding cassette G2 (ABCG2): 132bp, GTC CGT TAC ATT GAA TCC TGG (right), GTG AAT CTC AGA ACC ATT GGG (left) (T_m=55°C)
- ALP (alkalic phosphatase): 211bp, CTG GTA GTT GTT GTG AGC GTA ATC (right), AAG ACA CCT TGA CTG TGG TTA CTG (left) (T_m=55°C)
- alpha-actinin (ACTN1): 180bp, GG GTC GTT GCC AAT ATC ATA ACC (right), GAC CAT CAA TGA AGT GGA GAA C(left) (T_m=55°C)
- alpha-actin: 107bp, CAT GAC GTT GTT GGC ATA CAG (right), CTT CCT TTA TCG GTA TGG AGT CTG (left) (T_m=55°C)
- ATF2: 207bp, C TTG AAG CTG CTG CTC TAT TTC (right), CAG TGG ATT GGT TAG GAC TCA G (left) (T_m=55°C)
- anillin: CTG GGA AGC AAA GGA GTA GC (right), GCA GGA CAC CGT AAC ATT TG (left) (T_m=55°C)
- beta-actin: 226bp, GC ATA GAG GTC TTT ACG GAT GTC (right), CTC TAG ACT TCG AGC AGG AGA TG (left) (T_m=55°C)
- beta-actin(*h.sapiens*): 141bp, CCT GCT TGC TGA TCC ACA TC (right), AGA AGG AGA TCA CTG CCC TG (left) (T_m=52°C)
- CBFa1/Runx2: 221bp, G ATC TGT AAT CTG ACT CTG TCC TTG (right), TCT GAT TTT ACT TCC ACC TGG C (left) (T_m=55°C)
- cd9 antigen (p24): 112bp, GAG ATA AAC TGC TCC AAA GGA C (right), GAG TTT TAC AAG GAC ACC TAC C (left) (T_m=55°C)

- c-fos: 263bp, A AGA AGT CAT CAA AGG GTT CTG (right), CTG CTG AAA GAG AAG GAA AAA C (left) (T_m=52°C)
- c-jun: 220bp, TAA CGT GGT TCA TGA CTT TCT G (right), CCT ATC GAC ATG GAG TCT CAG (left) (T_m=50°C)
- c-myc: 277bp, C TCG TCG TTT CCT CAA TAA GTC (right), CTG AAG CAG ATC AGC AAC AAC (left) (T_m=55°C)
- collagen a1 (Col1a1): 202bp, CTG AGT AGG GAA CAC ACA GGT C (right), C CTG AGT CAG CAG ATT GAG AAC (left) (T_m=55°C)
- cREB1: 258bp, G CTT TTA GCT CCT CAA TCA ATG (right), CTC AGG CGA TGT ACA AAC ATA C (left) (T_m=52°C)
- cyclin-D1: 118bp, GAT GGT CTG CTT GTT CTC ATC (right), AA ATG GAA CTG CTT CTG GTG (left) (T_m=55°C)
- cyclophilin(*HK*): 209bp, CTC AAA TTT CTC TCC GTA GAT GG (right), AGA CAA AGT TCC AAA GAC AGC AG (left) (T_m=55°C)
- E2F: 268bp, CAG TTG GTC CTC TTC CAT AGG (right), GA TCT CCC TTA AGA GCA AAC AAG (left) (T_m=52°C)
- Elk1: 204bp, G CTG TGT TCT CTG TTA GGA TGG (right), AAA CCA GAA ATC CGA AGA GTT G (left) (T_m=52°C)
- GAPDH: 237bp, T ACT CCT TGG AGG CCA TGT AGG (right), CAT CAA GAA GGT GGT GAA GCA G (left) (T_m=55°C)
- integrin a1 (ITGA1): 141bp, TAT CTG AAT AGC CAG CTC TCG (right), GAA TGT CTC ACT CAT CTT GTG G (left) (T_m=55°C)
- JMY: AC TGT AAA CTG GGT CCA GCA (right), CT CCA GCT GGC ATT TTA GTG (left) (T_m=55°C)
- MAD2 (*h.sapiens*): 250bp, TAG TAA ATG AAC GAA GGC GGA C (right), GAG TGT GAC AAG ACT GCA AAA G (left) (T_m=52°C)
- MAPT (Tau): 112bp, T CTG ATT TTA CTT CCA CCT GGC (right), GTG TGC AAA TAG TCT ACA AGC C (left) (T_m=55°C)
- MEF2A: 121bp, GTA ATC AGT GTT GTA GGC TGT C (right), GAT AAG CAG TTC TCA AGC CAC (left) (T_m=55°C)
- MITF: CTG CTC TTG GAT CTC TCC ATC (right), TC TTT TGG ACC AGC ACT GAC (left) (T_m=55°C)
- Myf5: 103bp, CAA CCC TAA CCA GAG ACT CCC (right), TGT AAT AGT TCT CCA CCT GTT CCC (left) (T_m=55°C)

- Myf6: 275bp, CT GAA GAA ATA CTG TCC ACG ATG (right), CA TCA GCT ACA TTG AGC GTC TAC (left) (T_m=55°C)
- MYH1/MHC (muscle): 150bp, CTC AGC TTG TCT CTT GTA GGC (right), GTG GAA GCT ATC AAG GGT CTG (left) (T_m=55°C)
- MYH9 (NMMIIa): 107bp, G CCT TGT ATT TGG ACT TGA CAG (right), CAC GCA CAG AAG AAT GAG AAT G (left) (T_m=55°C)
- MyoD1: 100bp, AGC ACC TGA TAA ATC GCA TTG G (right), CAT CCC TAA GCG ACA CAG AAC (left) (T_m=55°C)
- MyoG: 189bp, CTG TAG GCG CTC AAT GTA CTG (right), AAG GTG TGT AAG AGG AAG TCT GTG (left) (T_m=55°C)
- NFATc4: 299bp, TGA TAC CCT GGA TAG GTA CAC TG (right), CCT ACC TTC AGT CTC TTT CCT TC (left) (T_m=52°C)
- NFkB: 138bp, G CTC ATA CGG TTT CCC ATT TAG (right), ACT TTG AGC CTC TCT ATG ACC (left) (T_m=55°C)
- osteocalcin: 234bp, CAT ACT GGT CTG ATA GCT CGT CAC (right), AGG ACC ATC TTT CTG CTC ACT C (left) (T_m=55°C)
- p21: 114bp, GA AGT CAA AGT TCC ACC GTT CTC (right), AAA GTG TGC CGT TGT CTC TTC (left) (T_m=55°C)
- p53 (TRP53): 295bp, TAA CTC TAA GGC CTC ATT CAG C (right), TAC CAT CAT CAC ACT GGA AGA C (left) (T_m=55°C)
- Shugoshin-like 2: GAT GAA AAC TGC TCC ATC TCC (right), CTT CTG CAC TAG CTC CAT GC (left) (T_m=55°C)
- SMAD1: 161bp, CAG AAG CGG TTC TTA TTG TTG G (right), ATC AGC AGA GGA GAT GTT CAG G (left) (T_m=55°C)
- SRF (serum response factor): 215bp, GTG AAG CTG AAC TGC AGA GAC (right), GCC ACA TGA TGT ACC CTA GTC (left) (T_m=52°C)
- stanniocalcin1: 216bp, AGG CTG TCT CTG ATT GTA CTG ACC G (right), CAT TCG GAG GTG TTC GAC TTT CCA G (left) (T_m=55°C)
- tubulin beta3 (TUBB3): 140bp, CAT TGA GCT GAC CAG GGA ATC (right), CAT CGA CAA TGA AGC CCT CTA C (left) (T_m=55°C)
- TWIST1: 150bp, AGA CGG AGA AGG CGT AGC TG (right), CGG ACA AGC TGA GCA AGA TTC (left) (T_m=55°C)

B Cell culture protocols and controls

B.1 Fixation and staining of cells

This protocol using standard routines was used for all cell staining experiments:

- Add 10 vol% fresh prepared 30% paraformaldehyde (PFA) in PBS
- Pre-warm PFA solution to 37°C and fix the cells for 5 min at 37°C
- Wash 3-4 times with PBS and cells are permeabilized with 0.5% Triton X100 for 10 min at room temperature (RT)
- Wash 2 times with PBS and block with 5% FBS/0.3% Triton X100/PBS in humid environment for 30min
- Incubate first antibody for one hour at RT
- Wash 2 times with PBS
- Incubate with 1x PBS + 400 mM NaCl for 5 min at RT
- Wash one time PBS
- Incubate second antibody/phalloidin/YO-PRO for 45 min at RT
- Wash 2 times with PBS
- Wash one time with PBS + 400 mM NaCl for 5 min at RT
- Wash one time with PBS
- Put 10 µm glass beads in PBS solution onto the sample and seal it gently with grease and a slide
- Following second antibody dyes for different targets were used: DNA: YO-PRO1-488 (*Life technologies*), myosin II: Alexa647n (*Life technologies*), actin: phalloidin-atto647n (*Sigma-Aldrich*), MT: atto555 (*Sigma-Aldrich*)
- Dilutions: MT: 1. antibody (AB) 1:100 (*Sigma-Aldrich*), 2. AB 1:500; actin: phalloidin 1:100; DNA: AB 1:500; myosinII: 1. antibody (AB) 1:50, 2. AB 1:500;

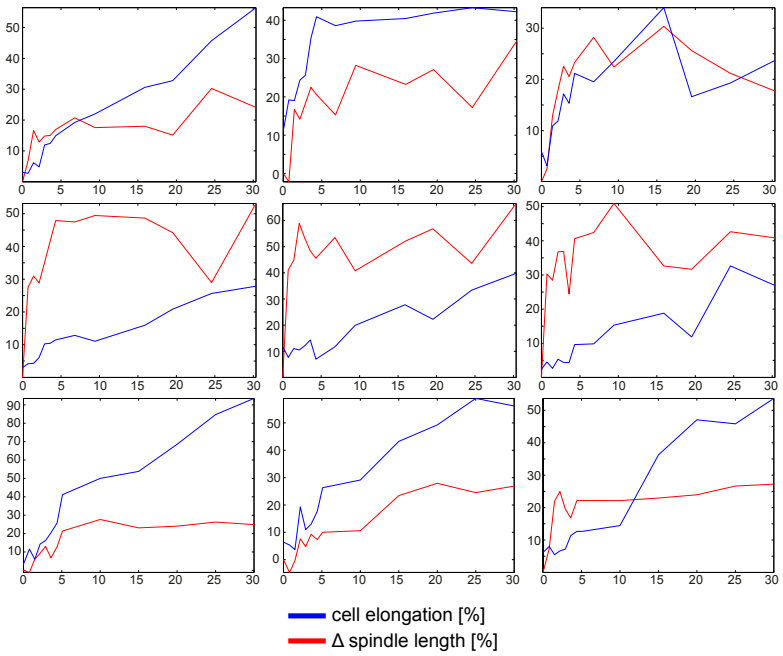

Figure B.1: Single cell and spindle curves: Dynamic cell behavior is revealed by plotting length increase [%] (red) and cell elongation [%] (blue).

B.2 Metaphase cells under dynamic shear: single cell curves

9 single cell curves with plotted length increase [%] (red) reveals dynamic cell behavior dependent on cell elongation [%] (blue).

B.3 DMSO control for mitotic cells under dynamic shear

Cells are treated with DMSO with higher concentration of 0.1% than in any of the drug-experiments. The images show shear elongated cells with increased spindle length by external shear forces over time (fig. B.2).

In fig. B.3, averaged cell data ($n = 163$) show no overall deviations in angle adaption, spindle and cell elongation from standard experiments without high DMSO content.

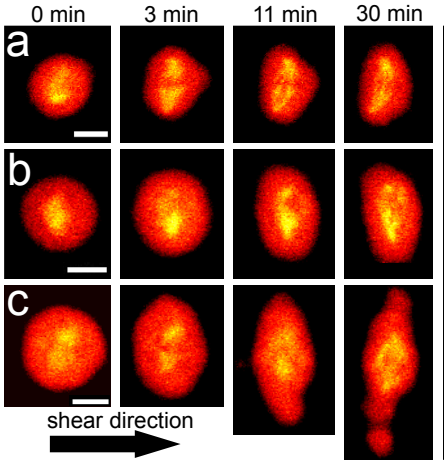

Figure B.2: DMSO (0.1%) control: Normal cell elongation and spindle lengthening is observed for high DMSO concentrations (higher than in all other inhibitor experiments) of metaphase cells under external shear forces. (scale bar 10 µm)

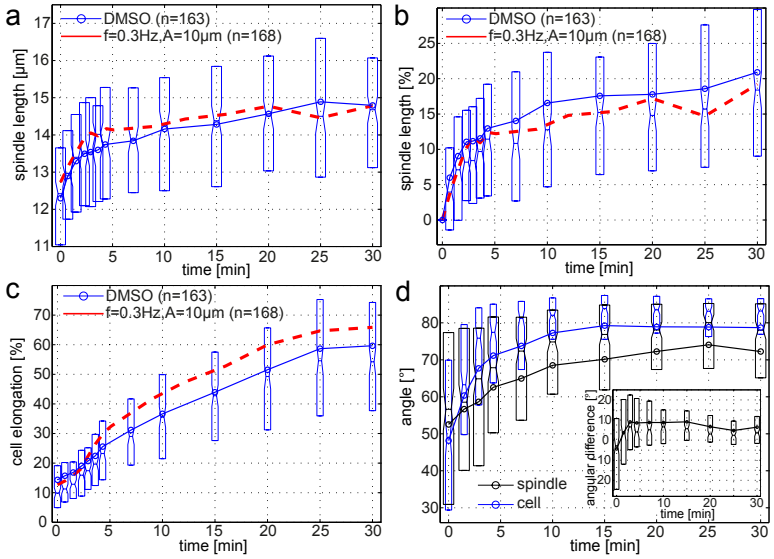

Figure B.3: DMSO (0.1%) shear experiments ($n = 3$, $f = 0.3$ **Hz**, $A = 10$ **µm**, $t_{shear} = 30$ **min):** Normal cell and spindle elongation is observed for high DMSO concentrations (higher than in all other inhibitor experiments) of metaphase cells under external shear forces. Furthermore, cell and spindle angle rotate in direction perpendicular to the shear direction just as in normal experiments without high DMSO content.

Bibliography

[Abal et al., 2005] Abal, M., G. Keryer and M. Bornens (2005). *Centrioles resist forces applied on centrosomes during G2/M transition.* Biology of the Cell, 97:425–434.

[Abe and M.Takeichi, 2008] Abe, K. and M.Takeichi (2008). *EPLIN mediates linkage of the cadherin-catenin complex to F-actin and stabilizes the circumferential actin belt.* Proc. Natl. Acad. Sci., 105:13–19.

[Ahearn et al., 2012] Ahearn, I.M., K. Haigis, D. Bar-Sagi and M. Philips (2012). *Regulating the regulator: post-translational modification of RAS.* Mol. Cell Biol., 13:39–51.

[Akune et al., 2004] Akune, T., S. Ohba, S. Kamekura, M. Yamaguchi, U. Chung, N. Kubota, Y. Terauchi, Y. Harada, Y. Azuma, K. Nakamura, T. Kadowaki and H. Kawaguchi (2004). *PPARγ insufficiency enhances osteogenesis through osteoblast formation from bone marrow progenitors.* J. Clin. Invest., 113:846–855.

[Aratyn et al., 2007] Aratyn, Y.S., T. Schaus, E. Taylor and G. Borisy (2007). *Intrinsic Dynamic Behavior of Fascin in Filopodia.* Mol. Bio. Cell, 18:3928–3940.

[Astroem et al., 2008] Astroem, J.A., P. Kumar, I. Vattulainen and M. Karttunen (2008). *Strain hardening, avalanches, and strain softening in dense cross-linked actin networks.* Phys. Rev. E, 77:0519131–6.

[Baek et al., 2008] Baek, D., J. Villèn, C. Shin, F. Camargo, S. Gygi and D. Bartel (2008). *The impact of microRNAs on protein output.* Nature, 455:64–71.

[Bausch et al., 1998] Bausch, A. R., F. Ziemann, A. A. Boulbitch, K. Jacobson and E. Sackmann (1998). *Local measurements of viscoelastic parameters of adherent cell surfaces by magnetic bead microrheometry.* Biophys. J., 75:2038–2049.

[Bausch and Kroy, 2006] Bausch, A.R. and K. Kroy (2006). *A bottom-up approach to cell mechanics.* Nature physics, 2:231–238.

[Bennett and Tonks, 1997] Bennett, A.M. and N. Tonks (1997). *Regulation of distinct stages of skeletal muscle differentiation by mitogen-activated protein kinases.* Science, 278:1288–1291.

[Berg et al., 2001] Berg, J.S., B. Powell and R. Cheney (2001). *A Millennial Myosin Census.* Mol. Biol. Cell, 12:780–794.

[Betschinger and Knoblich, 2004] Betschinger, J. and J. Knoblich (2004). *Dare to be different: Asymmetric cell division in Drosophila, C-elegans and vertebrates.* Curr. Biol., 14:23–31.

[Bloom and Yeh, 2010] Bloom, K. and E. Yeh (2010). *Tension management in the kinetochore.* Curr. Biol., 20:R1040–R1048.

[Brakebusch and Fässler, 2003] Brakebusch, C. and R. Fässler (2003). *The integrin-actin connection, an eternal love affair.* The EMBO Journal, 22:2324 – 2333.

[Brown et al., 2013] Brown, C.R., C. Mao, E. Falkovskaia, M. Jurica and H. Boeger (2013). *Linking stochastic fluctuations in chromatin structure and gene expression.* PLoS Biology, 11:1–15.

[Burbank et al., 2007] Burbank, K.S., T. Mitchison and D. Fisher (2007). *Slide-and-cluster models for spindle assembly.* Curr. Biol., 17:1373–83.

[Burger and Klein-Nulend, 1999] Burger, E.H. and J. Klein-Nulend (1999). *Mechanotransduction in bone-role of the lacuno-canalicular network.* FASEB, 13:101–112.

[Bustin et al., 2009] Bustin, S.A., V. Benes, J. Garson, J. Hellemans, J. Huggett, M. Kubista, R. Mueller, T. Nolan, M. Pfaffl, G. Shipley, J. Vandesompele and C. Wittwer (2009). *The MIQE guidelines: Minimum information for publication of quantitative real-time PCR experiments.* Clinical Chemistry, 55:611–622.

[Cai et al., 2008] Cai, L., C. Dalal and M. Elowitz (2008). *Frequency-modulated nuclear localization bursts coordinate gene regulation.* Nature, 455:485–490.

[Carvalho et al., 2013] Carvalho, K., F.-C. Tsai, E. Lees, R. Voituriez, G. Koenderink and C. Sykes (2013). *Cell-sized liposomes reveal how actomyosin cortical tension drives shape change.* Proc. Natl. Acad. Sci., 110:16456–16461.

[Chen, 2008] Chen, C.S. (2008). *Mechanotransduction - a field pulling together?.* JCS, 121:3285–3292.

[Chervin-Pétinot et al., 2012] Chervin-Pétinot, A., M. Courçon, S. Almagro, A. Nicolas, A. Grichine, D. Grunwald, M.-H. Prandini, P. Huber and D. Gulino-Debrac (2012). *Epithelial Protein lost In Neoplasm (EPLIN) Interacts with alpha-catenin and actin filaments in endothelial cells and stabilizes vascular capillary network in vitro.* JBC, 287:7556–7572.

[Chircop et al., 2009] Chircop, M., V. Oakes, M. G. M. Ma, C. Smith, P. Robinson and K. Khanna (2009). *The actin-binding and bundling protein, EPLIN, is required for cytokinesis.* Cell Cycle, 12:757–764.

[Claessens et al., 2008] Claessens, M. M. A. E., C. Semmrich, L. Ramos and A. Bausch (2008). *Helical twist controls the thickness of F-actin bundles.* Proc. Natl. Acad. Sci., 105:8819–8822.

[Claessens et al., 2006] Claessens, M.M.A.E., M. Bathe, E. Frey and A. Bausch (2006). *Actin-binding proteins sensitively mediate F-actin bundle stiffness.* Nature materials, 5:748–753.

[Clute and Pines, 1999] Clute, P. and J. Pines (1999). *Temporal and spatial control of cyclin B1 destruction in metaphase.* Nat. Cell Biol., 1:82–87.

[Connelly et al., 2010] Connelly, J.T., J. Gautrot, B. Trappmann, D. W.-M. Tan, G. Donati, W. Huck and F. Watt (2010). *Actin and serum response factor transduce physical cues from the microenvironment to regulate epidermal stem cell fate decisions.* Nat. Cell Biol., 12:711–723.

[Conti and MacKintosh, 2009] Conti, E. and F. MacKintosh (2009). *Cross-linked networks of stiff filaments exhibit negative normal stress.* Phys. Rev. Lett., 102:0881021–4.

[Courson and Rock, 2010] Courson, D.S. and R. Rock (2010). *Actin cross-link assembly and disassembly mechanics for a-actinin and fascin.* JBC, 285:26350–26357.

[Discher et al., 2005] Discher, D.E., P. Janmey and Y. Wang (2005). *Tissue cells feel and respond to the stiffness of their substrate.* Science, 310:1139–1143.

[DSMZ, 2010] DSMZ, Leibnitz Institute (2010). *Catalogue of human and animal cell lines.*

[Ducy et al., 2000] Ducy, P., T. Schinke and G. Karsenty (2000). *The osteoblast: a sophisticated fibroblast under central surveillance.* Science, 289:1501–1504.

[Dumont and Mitchison, 2009a] Dumont, S. and T. Mitchison (2009a). *Compression regulates mitotic spindle length by a mechanochemical switch at the poles.* Curr. Biol., 19:1086–1095.

[Dumont and Mitchison, 2009b] Dumont, S. and T. Mitchison (2009b). *Force and length in the mitotic spindle.* Curr. Biol., 19:R749–R761.

[Effler et al., 2007] Effler, J.C., P. Iglesias and D. Robinson (2007). *Role of cortical tension in bleb growth.* Cell Cycle, 6:30–35.

[den Elzen et al., 2009] Elzen, N. den, C. Buttery, M. Maddugoda, G. Ren and A. Yap (2009). *Cadherin adhesion receptors orient the mitotic spindle during symmetric cell division in mammalian epithelia.* Mol. Biol. Cell, 20:3740–3750.

[Engler et al., 2006] Engler, A. J., S. Sen, H. L. Sweeney and D. E. Discher (2006). *Matrix elasticity directs stem cell lineage specification.* Cell, 126:677–689.

[Engler et al., 2004] Engler, A.J., M. Griffin, S. Sen, C. Bönnemann, H. Sweeney and D. Discher (2004). *Myotubes differentiate optimally on substrates with tissue-like stiffness: pathological implications for soft or stiff microenvironments.* JCB, 166:877–887.

[Evans and Yeung, 1989] Evans, E. and A. Yeung (1989). *Apparent viscosity and cortical tension of blood granulocytes determined by micropipette aspiration.* Biophys. J., 56:151–160.

[Fabry et al., 2001] Fabry, B., G. Maksym, J. Butler, M. Glogauer, D. Navajas and J. Fredberg (2001). *Scaling the microrheology of living cells.* Phys. Rev. Lett., 87(14):148102.

[Faix and K.Rottner, 2006] Faix, J. and K.Rottner (2006). *The making of filopodia.* Curr. Opin. Cell Biol., 18(1):18–25.

[Ferenz et al., 2009] Ferenz, N.P., R. Paul, C. Fagerstrom, A. Mogilner and P. Wadsworth (2009). *Dynein antagonizes Eg5 by crosslinking and sliding antiparallel microtubules.* Curr. Biol., 19:1833–1838.

[Fernández et al., 2007] Fernández, P., L. Heymann, A. Ott, N. Aksel and P. Pullarkat (2007). *Shear rheology of a cell monolayer.* New Journal of Physics, 9:1–28.

[Fernández et al., 2011] Fernández, P., M. Maier, M. Lindauer, C. Kuffer, Z. Storchova and A. Bausch (2011). *Mitotic spindle orients perpendicular to the forces imposed by dynamic shear.* PLoS ONE, 6:1–10.

[Fernández and Ott, 2008] Fernández, P. and A. Ott (2008). *Single cell mechanics: stress stiffening and kinematic hardening.* Phys. Rev. Lett., 100:2381021–4.

[Field and Alberts, 1995] Field, C. M. and B. M. Alberts (1995). *Anillin, a contractile ring protein that cycles from the nucleus to the cell cortex.* JCB, 131:165–178.

[Fink et al., 2011] Fink, J., N. Carpi, T. Betz, A. Betard, M. Chebah, A. Azioune, M. Bornens, C. Sykes, L. Fetler, D. Cuvelier and M. Piel (2011). *External forces control mitotic spindle positioning.* Nat. Cell Biol., 13:771–U401.

[Firestone et al., 2012] Firestone, A.J., J. Weinger, M. Maldonado, K. Barlan, L. Langston, M. O'Donnell, V. Gelfand, T. Kapoor and J. Chen (2012). *Small-molecule inhibitors of the AAA+ ATPase motor cytoplasmic dynein.* Nature, 484:125–129.

[Fishkind and Wang, 1995] Fishkind, D.J. and Y. Wang (1995). *New horizons for cytokinesis.* Curr. Op. Cell Biol., 7:23–31.

[Gachet et al., 2004] Gachet, Y., S. Tournier, J. Millar and J. Hyams (2004). *Mechanism controlling perpendicular alignment of the spindle to the axis of cell division in fission yeast.* EMBO J., 23:1289–1300.

[Garcia-Cardena et al., 2001] Garcia-Cardena, G., J. Comander, K. Anderson, B. Blackman and M. Gimbrone (2001). *Biomechanical activation of vascular endothelium as a determinant of its functional phenotype.* Proc. Natl. Acad. Sci., 98:4478–4485.

[Gardel et al., 2002] Gardel, M.L., F. Nakamura, J. Hartwig, J. Crocker, T. Stossel and D. Weitz (2002). *Prestressed F-actin networks cross-linked by hinged filamins replicate mechanical properties of cells.* Proc. Natl. Acad. Sci., 24:350–361.

[Gardel et al., 2006] Gardel, M.L., N. Nakamura, J. H. Hartwig, J. Crocker, T. Stossel and D. Weitz (2006). *Prestressed F-actin networks cross-linked by hinged filamins replicate mechanical properties of cells.* Proc. Natl. Acad. Sci., 103(6):1762–1767.

[Gatlin et al., 2010] Gatlin, J. C., A. Matov, G. Danuser, T. J. Mitchison and E. D. Salmon (2010). *Directly probing the mechanical properties of the spindle and its matrix.* JCB, 188:481–489.

[Gilbert et al., 2010] Gilbert, P.M., K. Havenstrite, K. Magnusson, A. Sacco, N. Leonardi, P. Kraft, N. Nguyen, S. Thrun, M. Lutolf and H. Blau (2010). *Substrate elasticity regulates skeletal muscle stem cell self-renewal in culture.* Science, 329:1078–1081.

[Goshima and Scholey, 2010] Goshima, G. and J. Scholey (2010). *Control of mitotic spindle length.* Annual Review of Cell and Developmental Biology, 26:21–57.

[Goshima et al., 2005] Goshima, G., R. Wollman, N. Stuurman, J. M. Scholey and R. D. Vale (2005). *Length control of the metaphase spindle.* Curr. Biol., 15:1979–1988.

[Grashoff et al., 2010] Grashoff, C., B. Hoffman, M. Brenner, R. Zhou, M. Parsons, M. Yang, M. McLean, S. Sligar, C. Chen, T. Ha and M. Schwartz (2010). *Measuring mechanical tension across vinculin reveals regulation of focal adhesion dynamics.* Nature, 466:263–266.

[Grill et al., 2001] Grill, S.W., P. Gonczy, E. Stelzer and A. Hyman (2001). *Polarity controls forces governing asymmetric spindle positioning in the Caenorhabditis elegans embryos.* Nature, 409:630–33.

[Grill et al., 2003] Grill, S.W., J. Howard, E. Schaffer, E. Stelzer and A. Hyman (2003). *The distribution of active force generators controls mitotic spindle position.* Science, 301:518–521.

[Grill et al., 2005] Grill, S.W., K. Kruse and F. Jülicher (2005). *Theory of mitotic spindle oscillations.* Phys. Rev. Lett., 94:108104–1–4.

[Grote et al., 2003] Grote, K., I. Flach, M. Luchtefeld, E. Akin, S. Holland, H. Drexler and B. Schieffer (2003). *Mechanical stretch enhances mRNA expression and proenzyme release of matrix metalloproteinase-2 (MMP-2) via NAD(P)H oxidase-derived reactive oxygen species.* Circ. Res., 92:e80–e86.

[Guck et al., 2001] Guck, J., R. Ananthakrishnan, H. Mahmood, T. Moon, C. Cunningham and J. Käs (2001). *The optical stretcher: a novel laser tool to micromanipulate cells.* Biophys. J., 81:767–784.

[Gulino-Debrac, 2013] Gulino-Debrac, D. (2013). *Mechanotransduction at the basis of endothelial barrier function.* Tissue Barriers, 1:1–6.

[Gutierrez et al., 2008] Gutierrez, L., M. Mauriat, S. Guénin, J. Pelloux, J.-F. Lefebvre, R. Louvet, C. Rusterucci, T. Moritz, F. Guerineau, C. Bellini and O. VanWuytswinkel (2008). *The lack of a systematic validation of reference genes: a serious pitfall undervalued in reverse transcription-polymerase chain reaction (RT-PCR) analysis in plants.* Plant Biotech. J., 475:609–618.

[Guttridge et al., 2000] Guttridge, D.C., M. Mayo, L. Madrid, C.-Y. Wang and A. Baldwin (2000). *NF-kB-induced loss of MyoD messenger RNA: Possible role in muscle decay and cachexia.* Science, 289:2363–2366.

[Hahn and Schwartz, 2009] Hahn, C. and M. Schwartz (2009). *Mechanotransduction in vascular physiology and atherogenesis.* Nat. Rev. Mol. Cell Biol., 10:53–62.

[Hammer et al., 2009] Hammer, B.E., L. Kidder, P. Williams and W. Xu (2009). *Magnetic levitation of MC3T3 osteoblast cells as a ground-based simulation of microgravity.* Microgravity Sci. Technol, 21:311–318.

[Harper et al., 2003] Harper, L.V., A. Hilton and A. Jones (2003). *RT-PCR for the pseudogene-free amplification of the glyceraldehyde-3-phosphate dehydrogenase gene.* MCP, 17:261–265.

[Head et al., 2003] Head, D. A., A. J. Levine and F. C. MacKintosh (2003). *Deformation of cross-linked semiflexible polymer networks.* Phys. Rev. Lett., 91(10):108102.

[Heald et al., 1996] Heald, R., R. Tournebize, T. Blank, R. Sandaltzopoulos, P. Becker, A. Hyman and E. Karsenti (1996). *Self-organization of microtubules into bipolar spindles around artificial chromosomes in Xenopus egg extracts.* Nature, 382:420–425.

[Hermann, 2011] Hermann, M.R. (2011). *Biomechanics of Integrin-Fibronectin Bonds and Integrin Subtype Specific Molecular Interactions at Focal Adhesions.* MPIB status report.

[Heussinger and Frey, 2007] Heussinger, C. and E. Frey (2007). *The role of architecture in the elastic response of semiflexible polymer and fiber networks.* Phys. Rev. E, 75:011917.

[Hoffman et al., 2011] Hoffman, B.D., C. Grashoff and M. Schwartz (2011). *Dynamic molecular processes mediate cellular mechanotransduction.* Nature, 475:316–323.

[Hofmann et al., 2004] Hofmann, W.A., L. Stojiljkovic, B. Fuchsova, G. Vargas, E. Mavrommatis, V. Philimonenko, K. Kysela, J. Goodrich, J. Lessard, T. Hope, P. Hozak and P. de Lanerolle (2004). *Actin is part of pre-initiation complexes and is necessary for transcription by RNA polymerase II.* Nat. Cell Biol., 11:1094–1101.

[Honda, 1983] Honda, H. (1983). *Geometrical Models for Cells in Tissues.* Int. Rev. Cyt., 81:191–248.

[Horsley and Pavlath, 2002] Horsley, V. and G. Pavlath (2002). *NFAT: ubiquitous regulator of cell differentiation and adaptation.* JCB, 156:771–774.

[Huisman et al., 2007] Huisman, E. M., T. van Dillen, P. R. Onck and E. V. der Giessen (2007). *Three-dimensional cross-linked F-actin networks: relation between network architecture and mechanical behavior.* Phys. Rev. Lett., 99:2081031–4.

[I. Spector and Groweiss, 1983] I. Spector, N.R. Shochet, Y. Kashman and A. Groweiss (1983). *Latrunculins: novel marine toxins that disrupt microfilament organization in cultured cells.* Science, 219:493–495.

[Iavarone et al., 2003] Iavarone, C., A. Catania, M. Marinissen, R. Visconti, M. Acunzo, C. Tarantino, M. S. Carlomagno, C. Bruni, J. Gutkind and M. Chiariello (2003). *The platelet-derived growth factor controls c-myc expression through a JNK- and AP-1-dependent signaling pathway.* JBC, 278:50024–50030.

[Itabashi et al., 2009] Itabashi, T., J. Takagi, Y. Shimamoto, H. Onoe, K. Kuwana, I. Shimoyama, J. Gaetz, T. M. Kapoor and S. Ishiwata (2009). *Probing the mechanical architecture of the vertebrate meiotic spindle.* Nature Methods, 6:167–172.

[Jansen et al., 2011] Jansen, S., A. Collins, C. Yang, G. Rebowski, T. Svitkina and R. Dominguez (2011). *Mechanism of actin filament bundling by fascin.* JBC, 286:30087–30096.

[Jawhari et al., 2003] Jawhari, A.U., A. Buda, M. Jenkins, K. Shehzad, C. Sarraf, M. Noda, M. Farthing, M. Pignatelli and J. Adams (2003). *Fascin, an actin-bundling protein, modulates colonic epithelial cell invasiveness and differentiation in vitro.* Am J Pathol, 162:69–80.

[Kadrmas and Beckerle, 2004] Kadrmas, J.L. and M. Beckerle (2004). *The LIM domain: From the cytoskeleton to the nucleus.* Molecular Cell Biology, 5:920–931.

[Kapoor et al., 2000] Kapoor, T.M., T. Mayer, M. Coughlin and T. Mitchison (2000). *Probing spindle assembly mechanisms with monastrol, a small molecule inhibitor of the mitotic kinesin, Eg5.* JCB, 150:975–988.

[Karaköse, 2012] Karaköse, Esra (2012). *Functional characterization of PINCH-1 in embryoid bodies and keratinocytes and identification of new interaction partners.* PhD thesis, Ludwig-Maximilians-Universität München.

[Karin et al., 1997] Karin, M., Z.-G. Liu and E. Zandi (1997). *AP-1 function and regulation.* Curr. Op. Cell Biol., 9:240–246.

[Kasza et al., 2009] Kasza, K. E., G. H. Koenderink, Y. C. Lin, C. P. Broedersz, W. Messner, F. Nakamura, T. P. Stossel, F. C. MacKintosh and D. A. Weitz (2009). *Nonlinear elasticity of stiff biopolymers connected by flexible linkers.* Phys. Rev. E, 79:041928.

[Kasza et al., 2007] Kasza, K.E., A. Rowat, J. Liu, T. Angelini, C. Brangwynne, G. Koenderink and D. Weitz (2007). *The cell as a material.* JCB, 19:101–107.

[Katagiri et al., 1994] Katagiri, T., A. Yamaguchi, M. Komaki, E. Abe, N. Takahashi, T. Ikeda, V. Rosen, J. Wozney, A. Fujisawa-Sehara and T. Suda (1994). *Bone morphogenetic protein-2 converts the differentiation pathway of C2C12 myoblasts into the osteoblast lineage.* JCB, 127:1755–1766.

[Katsumi et al., 2004] Katsumi, A., A. Wayne Orr, E. Tzima and M. A. Schwartz (2004). *Integrins in mechanotransduction.* JBC, 279(13):12001–12004.

[Köhler, 2012] Köhler, Simone (2012). *Dynamics and structure formation in active actin networks.* PhD thesis, Technische Universität München.

[Kirchmaier, 2013] Kirchmaier, A.L. (2013). *Creating memories of transcription.* Proc. Natl. Acad. Sci., 110:13701–13702.

[Kovács et al., 2004] Kovács, M., J. Tóth, C. Hetényi, A. Málnási-Csizmadia and J. R. Sellers (2004). *Mechanism of blebbistatin inhibition of myosin II.* JBC, 279:35557–35563.

[Kreja et al., 2008] Kreja, L., A. Liedert, S. Hasni, L. Claes and A. Ignatius (2008). *Mechanical regulation of osteoclastic genes in human osteoblasts.* Bioch. Biophys. Res. Com., 368:582–587.

[Kureishy et al., 2002] Kureishy, N., V. Sapountzi, S. Prag, N. Anilkumar and J. Adams (2002). *Fascins, and their roles in cell structure and function.* Bioessays, 24:350–361.

[Lechler and Fuchs, 2005] Lechler, T. and E. Fuchs (2005). *Asymmetric cell divisions promote stratification and differentiation of mammalian skin.* Nature, 437:275–280.

[Leitner et al., 2010] Leitner, L., D. Shaposhnikov, A. Descot, R. Hoffmann and G. Posern (2010). *Epithelial Protein Lost in Neoplasm (EPLIN-alpha) is transcriptionally regulated by G-actin and MAL/MRTF coactivators.* Molecular Cancer, 9:60:1–7.

[Li et al., 2010] Li, A., J. Dawson, M. Forero-Vargas, H. Spence, X. Lu, I. König, K. Andersen and L. Machesky (2010). *The actin-bundling protein fascin stabilizes actin in invadopodia and potentiates protrusive invasion.* Curr. Biol., 20:339–345.

[Lieleg and Bausch, 2007] Lieleg, O. and A. Bausch (2007). *Cross-linker unbinding and self-similiarity in bundled cytoskeletal networks.* Phys. Rev. Lett., 99:1581051–15810514.

[Lieleg et al., 2007] Lieleg, O., M. M. A. E. Claessens, C. Heussinger, L. Frey and A. Bausch (2007). *Mechanics of bundled semiflexible polymer networks.* Phys. Rev. Lett., 99:0881021–0881024.

[Lieleg et al., 2011] Lieleg, O., J. Kayser, G. Brambilla, L. Cipelletti and A. Bausch (2011). *Slow dynamics and internal stress relaxation in bundled cytoskeletal networks.* Nature materials, 10:236–242.

[Lieleg et al., 2009a] Lieleg, O., K. Schmoller, M. Claessens and A. Bausch (2009a). *Cytoskeletal polymer networks: viscoelastic properties are determined by the microscopic interaction potential of cross-links.* Biophys. J., 96:4725–4732.

[Lieleg et al., 2009b] Lieleg, O., K. Schmoller, C. Cyron, W. Wall and A. Bausch (2009b). *Structural polymorphism in heterogeneous cytoskeletal networks.* Soft Matter, 5:1796–1803.

[Limouze et al., 2004] Limouze, J., A. F. Straight, T. Mitchison and J. R. Sellers (2004). *Specificity of blebbistatin, an inhibitor of myosin II*. J. Mus. Res. Cell Motil., 25:1573–2657.

[Lindl, 2008] Lindl, Tony (2008). *Zell- und Gewebekultur*. Spektrum akademischer Verlag, Heidelberg.

[Liu et al., 2010] Liu, F., J. Mih, B. Shea, A. Kho, A. Sharif, A. Tager and D. Tschumperlin (2010). *Feedback amplification of fibrosis through matrix stiffening and COX-2 suppression*. JCB, 190:693–706.

[Lluís et al., 2006] Lluís, F., E. Perdiguero, A. Nebreda and P. Muñoz-Cánoves (2006). *Regulation of skeletal muscle gene expression by p38 MAP kinases*. Trends in Cell Biology, 16:36–44.

[Loughlin et al., 2011] Loughlin, R., J. Wilbur, F. McNally, F. Nédélec and R. Heald (2011). *Katanin contributes to interspecies spindle length scaling in Xenopus*. Cell, 147:1397–1407.

[Maamar et al., 2007] Maamar, H., A. Raj and D. Dubnau (2007). *Noise in gene expression determines cell fate in bacillus subtilis*. Science, 317:526–529.

[Maier, 2008] Maier, Matthias (2008). *Neue Methoden für die Untersuchung der Mechanotransduktion*.

[Mansky et al., 2002] Mansky, K.C., U. Sankar, J. Han and M. Ostrowski (2002). *Microphthalmia transcription factor is a target of the p38 MAPK pathway in response to receptor activator of NF-κB ligand signaling*. JBC, 277:11077–11083.

[Mattila and Lappalainen, 2008] Mattila, P.K. and P. Lappalainen (2008). *Filopodia: molecular architecture and cellular functions*. JBC, 9:446–454.

[Maul and Chang, 1999] Maul, R.S. and D. Chang (1999). *EPLIN, Epithelial protein lost in neoplasm*. Oncogene, 18:7838–7841.

[Maul et al., 1999] Maul, R.S., Y. Song, K. Amann, S. Gerbin, T. Pollard and D. Chang (1999). *EPLIN regulates actin dynamics by cross-linking and stabilizing filaments*. JCB, 160:399–407.

[Mayer et al., 2010] Mayer, M., M. Depken, J. Bois, F. Jülicher and S. Grill (2010). *Anisotropies in cortical tension reveal the physical basis of polarizing cortical flows*. Nature, 467:617–623.

[Mayer et al., 1999] Mayer, T.U., T. Kapoor, S. Haggarty, R. King, S. Schreiber and T. Mitchison (1999). *Small molecule inhibitor of mitotic spindle bipolarity identified in a phenotype-based screen*. Science, 286:971–974.

[McNally et al., 2006] McNally, K., A. Audhya, K. Oegema and F. McNally (2006). *Katanin controls mitotic and meiotic spindle length*. JCB, 175:881–891.

[Menko and Boettiger, 1987] Menko, A.S. and D. Boettiger (1987). *Occupaton of the extracellular Matrix Receptor Integrin, is a control point for myogenic differentiation*. Cell, 51:51–57.

[Miano et al., 2007] Miano, J.M., X. Long and K. Fujiwara (2007). *Serum response factor: master regulator of the actin cytoskeleton and contractile apparatus*. Am. J. Physiol. Cell Physiol., 292:70–81.

[Minc et al., 2011] Minc, N., D. Burgess and F. Chang (2011). *Influence of cell geometry on division-plane positioning*. Cell, 144:414–426.

[Mitchison et al., 2005] Mitchison, T.J., P. Maddox, J. Gaetz, A. C. Groen, M. Shirazu, A. Desai, E. D. Salmon and T. M. Kapoor (2005). *Roles of polymerization dynamics, opposed motors, and a tensile element in governing the length of Xenopus extract meiotic spindles*. Mol. Biol. Cell, 16:3064–3076.

[Moritaa et al., 2007] Moritaa, T., T. Mayanagib and K. Sobuea (2007). *Reorganization of the actin cytoskeleton via transcriptional regulation of cytoskeletal/focal adhesion genes by myocardin-related transcription factors.* Exp. Cell Res., 313:3432–3445.

[Musacchio and Salmon, 2007] Musacchio, A. and E. Salmon (2007). *The spindle-assembly checkpoint in space and time.* Nat. Rev. Mol. Biol., 8:379–393.

[Nishimura et al., 1998] Nishimura, R., Y. Kato, D. Chen, S. Harris, G. Mundy and T. Yoneda (1998). *Smad5 and DPC4 are key molecules in mediating BMP-2-induced osteoblastic differentiation of the pluripotent mesenchymal precursor cell Line C2C12.* JBC, 273:1872–1879.

[O'Connell and Wang, 2000] O'Connell, C.B. and Y. Wang (2000). *Mammalian spindle orientation and position respond to changes in cell shape in a dynein-dependent fashion.* Mol. Biol. Cell, 11:1765–1774.

[Ong and Mann, 2005] Ong, S.E. and M. Mann (2005). *Mass spectrometry-based proteomics turns quantitative.* Nat. Chem. Biol., 1:252–262.

[Ono et al., 1997] Ono, S., Y. Yamakita, S. Yamashiro, P. Matsudaira, J. Gnarra, T. Obinata and F. Matsumura (1997). *Identification of an actin binding region and a protein kinase C phosphorylation site on human fascin.* JBC, 272:2527–2533.

[Orr et al., 2006] Orr, A.W., B. Helmke, B. Blackman and M. Schwartz (2006). *Mechanisms of mechanotransduction.* Dev. Cell, 10:11–20.

[Papaiahgari et al., 2007] Papaiahgari, S., A. Yerrapureddy, P. Hassoun, J. Garcia, K. Birukov and S. Reddy (2007). *EGFR-activated signaling and actin remodeling regulate cyclic stretch-induced NRF2-ARE activation.* Am. J. Respir. Cell. Mol. Biol., 36:304–312.

[Pecreaux et al., 2006] Pecreaux, J., J. Roper, K. Kruse, F. Jülicher, A. Hyman, S. Grill and J. Howard (2006). *Spindle oscillations during asymmetric cell division require a threshold number of active cortical force generators.* Curr. Biol., 16:2111–2122.

[Pelham and Wang, 1999] Pelham, Jr., R. J. and Y. L. Wang (1999). *High resolution detection of mechanical forces exerted by locomoting fibroblasts on the substrate.* Mol.Biol.Cell, 10:935–945.

[Perdiguero et al., 2007] Perdiguero, E., V. Ruiz-Bonilla, L.Gresh, L. Hui, E. Ballestar, P. Sousa-Victor, B. Baeza-Raja, M. Jardí, A. Bosch-Comas, M. Esteller, C. Caelles, A. Serrano, E. Wagner and P. Muñoz-Cánoves (2007). *Genetic analysis of p38 MAP kinases in myogenesis: fundamental role of p38α in abrogating myoblast proliferation.* EMBO J., 26:1245–1256.

[Piek et al., 2010] Piek, E., L. Sleumer, E. van Someren, L. Heuver, J. de Haan, I. de Grijs, C. Gilissen, J. Hendriks, R. van Ravestein-van Os, S. Bauerschmidt, K. Dechering and E. van Zoelen (2010). *Osteo-transcriptomics of human mesenchymal stem cells: Accelerated gene expression and osteoblast differentiation induced by vitamin D reveals c-MYC as an enhancer of BMP2-induced osteogenesis.* Bone, 46:613–627.

[Pollard and Earnshaw, 2008] Pollard, T.D. and W. Earnshaw (2008). *Cell Biology.* Elsevier, Philadelphia, 2nd Edition ed.

[Portier et al., 1999] Portier, G.L., A. Benders, A. Ooserhof, J. Veerkamp and T. VanKuppevelt (1999). *Differentiation markers of mouse C2C12 and rat L6 myogenic cell lines and the effect of the differentiation medium.* In Vitro Cell. .Dev. Biol., 135:219–227.

[Powner et al., 2011] Powner, D., P. Kopp, S. Monkley, D. Critchley and F. Berditchevski (2011). *Tetraspanin CD9 in cell migration.* Biochem. Soc. Trans., 39:563–567.

[Radonić et al., 2007] Radonić, A., S. Thulke, I. Mackay, O. Landt, W. Siegert and A. Nitsche (2007). *Guideline to reference gene selection for quantitative real-time PCR.* Am. J. Respir. Cell. Mol. Biol., 36:304–312.

[Raff et al., 1997] Raff, T., M. van der Giet, D. Endemann, T. Wiederholt and M. Paul (1997). *Design and testing of β-actin primers for RT-PCR that do not co-amplify processed pseudogenes.* BioTechniques, 23:456–460.

[Ragsdale et al., 1997] Ragsdale, G. K., J. Phelps and K. Luby-Phelps (1997). *Viscoelastic response of fibroblasts to tension transmitted through adherens junctions.* Biophys. J., 73:2798–2808.

[Raisz, 1999] Raisz, L.G. (1999). *Physiology and pathophysiology of bone remodeling.* Clin. Chem., 45:1353–1358.

[Rohwedel et al., 1995] Rohwedel, J., V. Horák, M. Hebrok, E.-M. Füchtbauer and A. Wobus (1995). *M-twist expression inhibits mouse embryonic stem cell-derived myogenic differentiation in vitro.* Exp. Cell Res., 220:92–100.

[Salbreux et al., 2012] Salbreux, G., G. Charras and E. Paluch (2012). *Actin cortex mechanics and cellular morphogenesis.* Trends in Cell Biology, 105:536–545.

[Schaller et al., 2013] Schaller, V., K. Schmoller, E. Karaköse, B. Hammerich, M. Maier and A. Bausch (2013). *Crosslinking proteins modulate the self-organization of driven systems.* Soft Matter, 9:7229–33.

[Schiff et al., 1979] Schiff, P.B., J. Fant and S. Horwitz (1979). *Promotion of microtubule assembly in vitro by taxol.* Nature, 277:665–667.

[Schiff and Horwitz, 1980] Schiff, P.B. and S. Horwitz (1980). *Taxol stabilizes microtubules in mouse fibroblast cells.* Proc. Natl. Acad. Sci., 77:1561–65.

[Schiller et al., 2011] Schiller, H.B., C. Friedel, C. Boulegue and R. Fässler (2011). *Quantitative proteomics of the integrin adhesome show a myosin II-dependent recruitment of LIM domain proteins.* EMBO reports, 12:259–266.

[Schmoller et al., 2010] Schmoller, K.M., P. Fernández, R. Arevalo, D. Blair and A. Bausch (2010). *Cyclic hardening in bundled actin networks.* Nature comm., 1:134.

[Schmoller et al., 2008a] Schmoller, K.M., O. Lieleg and A. Bausch (2008a). *Crosslinking molecules modify composite actin networks independently.* Phys. Rev. Lett., 101:118102–1–4.

[Schmoller et al., 2008b] Schmoller, K.M., O. Lieleg and A. Bausch (2008b). *Internal stress in kinetically trapped actin bundle networks.* Soft Matter Communication, 4:2365–2367.

[Schmoller, 2008] Schmoller, Kurt M. (2008). *Composite Actin Networks.* Diplomarbeit, Technische Universität München.

[Schmoller, 2012] Schmoller, Kurt M. (2012). *Kinetics and Mechanics of Non-equilibrium Actin Networks.* PhD thesis, Technische Universität München.

[Schwartz and DeSimone, 2008] Schwartz, M.A. and D. DeSimone (2008). *Cell adhesion receptors in mechanotransduction.* Curr. Op. Cell Biol., 20:551–556.

[Semmrich et al., 2008] Semmrich, C., R. J. Larsen and A. R. Bausch (2008). *Nonlinear mechanics of entangled F-actin solutions.* Soft Matter, 4:1675–1680.

[Shaulian and Karin, 2002] Shaulian, E. and M. Karin (2002). *AP-1 as a regulator of cell life and death.* Nat. Cell Biol., 126:131–136.

[Shimamoto et al., 2011] Shimamoto, Y., Y. T. Maeda, S. Ishiwata, A. J. Libchaber and T. M. Kapoor (2011). *Insights into the micromechanical properties of the metaphase spindle.* Cell, 145:1062–1074.

[Shin et al., 2004] Shin, J.H., M. Gardel, L. Mahadevan, P. Matsudaira and D. Weitz (2004). *Relating microstructure to rheology of a bundled and cross-linked F-actin network in vitro.* Proc. Natl. Acad. Sci., 101:9636–9641.

[Siller and Doe, 2009] Siller, K.H. and C. Doe (2009). *Spindle orientation during asymmetric cell division.* Nat. Cell Biol., 11:365–374.

[Simmons et al., 2003] Simmons, C.A., S. Matlis, A. Thornton, S. Chen, C.-Y. Wang and D. Mooney (2003). *Cyclic strain enhances matrix mineralization by adult human mesenchymal stem cells via the extracellular signal-regulated kinase (ERK1/2) signaling pathway.* J. Biomech., 36:1087–1096.

[Smith et al., 2005] Smith, B. A., B. Tolloczko, J. G. Martin and P. Grütter (2005). *Probing the viscoelastic behavior of cultured airway smooth muscle cells with atomic force microscopy: stiffening induced by contractile agonist.* Biophys. J., doi:10.1529/biophysj.104.046649.

[Spudich and Watt, 1971] Spudich, J.A. and S. Watt (1971). *The Regulation of Rabbit Skeletal Muscle Contraction.* JBC, 246:4866–4871.

[Stossel et al., 2001] Stossel, T.P., J. Condeelis, L. Cooley, J. Hartwig, A. Noegel, M. Schleicher and S. Shapiro (2001). *Filamins as integrators of cell mechanics and signalling.* Nat. Rev. Mol. Cell Bio., 2:138–145.

[Strauss et al., 2006] Strauss, B., R. Adams and N. Papalopulu (2006). *A default mechanism of spindle orientation based on cell shape is sufficient to generate cell fate diversity in polarised Xenopus blastomeres.* Development, 133:3883–3893.

[Suzuki and Bird, 2008] Suzuki, M.M. and A. Bird (2008). *DNA methylation landscapes: provocative insights from epigenomics.* Nat. Rev. Gen., 9:465–476.

[Taguchi et al., 2011] Taguchi, K., T. Ishiuchi and M. Takeichi (2011). *Mechanosensitive EPLIN-dependent remodeling of adherens junctions regulates epithelial reshaping.* JCB, 194:643–656.

[Tang and Janmey, 1996] Tang, J.X. and P. Janmey (1996). *The Polyelectrolyte Nature of F-actin and the Mechanism of Actin Bundle Formation.* JBC, 271:8556–8563.

[Taniguchi et al., 2010] Taniguchi, Y., P. J. Choi, G.-W. Li, H. Chen, M. Babu, J. Hearn, A. Emili and X. Xie (2010). *Quantifying E. coli proteome and transcriptome with single-molecule sensitivity in single cells.* Science, 329:533–538.

[Tempel et al., 1996] Tempel, M., G. Isenberg and E. Sackmann (1996). *Temperature-induced sol-gel transition and microgel formation in α-actinin cross-linked actin networks: A rheological study.* Phys. Rev. E, 54:1802–1810.

[Tharmann et al., 2007] Tharmann, R., M. M. A. E. Claessens and A. R. Bausch (2007). *Viscoelasticity of Isotropically Cross-Linked Actin Networks.* Phys. Rev. Lett., 98:088103.

[Théry and Bornens, 2008] Théry, M. and M. Bornens (2008). *Get round and stiff for mitosis.* Hfsp Journal, 2:65–71.

[Thery et al., 2007] Thery, M., A. Jimenez-Dalmaroni, V. Racine, M. Bornens and F. Jülicher (2007). *Experimental and theoretical study of mitotic spindle orientation.* Nature, 447:493–U6.

[Thery et al., 2005] Thery, M., V. Racine, A. Pepin, M. Piel, Y. Chen, J.-B. Sibarita and M. Bornens (2005). *The extracellular matrix guides the orientation of the cell division axis.* Nat. Cell Biol., 7:947–953.

[Tinevez et al., 2009] Tinevez, J.Y., U. Schulze, G. Salbreux, J. Roensch, J. Joanny and E. Paluch (2009). *Role of cortical tension in bleb growth.* Proc. Natl. Acad. Sci., 106:18581–18586.

[Trepat et al., 2007] Trepat, X., L. Deng, S. An, D. Navajas, D. Tschumperlin, W. Gerthoffer, J. Butler and J. Fredberg (2007). *Universal physical responses to stretch in the living cell.* Nature, 447:592–595.

[Trepat et al., 2004] Trepat, X., M. Grabulosa, F. Puig, G. N. Maksym, D. Navajas and R. Farré (2004). *Viscoelasticity of human alveolar epithelial cells subjected to stretch.*. Am. J. Physiol. Lung. Cell. Mol. Physiol., 287:L1025–L1034.

[Tse et al., 2012] Tse, J.M., G. Cheng, J. Tyrrell, S. Wilcox-Adelman, Y. Boucher, R. Jain and L. Munn (2012). *Mechanical compression drives cancer cells toward invasive phenotype*. Proc. Natl. Acad. Sci., 109:911–916.

[Tseng et al., 2004] Tseng, Y., K. M. An, O. Esue and D. Wirtz (2004). *The Bimodal Role of Filamin in Controlling the Architecture and Mechanics of F-actin Networks*. JBC, 279:1819.

[Tseng and Wirtz, 2001] Tseng, Y. and D. Wirtz (2001). *Mechanics and multiple-particle tracking microheterogeneity of α-actinin-cross-linked actin filament networks*. Biophys. J., 81:1643–1656.

[Tsou et al., 2002] Tsou, M.F.B., A. Hayashi, L. DeBella, G. McGrath and L. Rose (2002). *LET-99 determines spindle position and is asymmetrically enriched in response to PAR polarity cues in C-elegans embryos*. Development, 129:4469–4481.

[Tyagi, 2010] Tyagi, S. (2010). *E. coli, what a noisy bug*. Science, 329:518–519.

[Tzima et al., 2002] Tzima, E., M. D. Pozo, W. Kiosses, S. Mohamed, S. Li, S. Chien and M. Schwartz (2002). *Activation of Rac1 by shear stress in endothelial cells mediates both cytoskeletal reorganization and effects on gene expression*. EMBO J., 21:6791–6800.

[Valenti et al., 2008] Valenti, M.T., L. Carbonare, L. Donatelli, F. Bertoldo, M. Zanatta and V. Cascio (2008). *Gene expression analysis in osteoblastic differentiation from peripheral blood mesenchymal stem cells*. Bone, 43:1084–1092.

[Vignjevic et al., 2006] Vignjevic, D., S. Kojima, Y. Aratyn, O. Danciu, T. Svitkina and G. Borisy (2006). *Role of fascin in filopodial protrusion*. JCB, 174:863–875.

[Vignjevic et al., 2007] Vignjevic, D., M. Schoumacher, N. Gavert, K.-P. Janssen, G. Jih, M. Lae, D. Louvard, A. Ben-Ze'ev and S. Robine (2007). *Fascin, a novel target of beta-catenin-TCF signaling, is expressed at the invasive front of human colon cancer*. Cancer Research, 67:6844–6853.

[Vogel, 2006] Vogel, Viola (2006). *Mechanotransduction Involving Multimodular Proteins: Converting Force into Biochemical Signals*. Annu. Rev. Biomol. Struct., 35:459–488.

[Wagner et al., 2006] Wagner, B., R. Tharmann, I. Haase, M. Fischer and A. Bausch (2006). *Cytoskeletal polymer networks: The molecular structure of cross-linkers determines macroscopic properties*. Proc. Natl. Acad. Sci., 103:13974–13978.

[Wang et al., 2006] Wang, J., R. Zohar and C. McCulloch (2006). *Multiple roles of α-smooth muscle actin in mechanotransduction*. Exp. Cell Res., 312:205–214.

[Wang et al., 2013] Wang, Y., Z. Huang, P. Nayak, B. Matthews, D. Warburton, W. Shi and J. Sanchez-Esteban (2013). *Strain-induced differentiation of fetal type II epithelial cells is mediated via the integrin $\alpha_6\beta_1$-ADAM17/tumor necrosis factor-α-converting enzyme (TACE) signaling pathway*. JBC, 288:25646–25657.

[Ward et al., 2008] Ward, S.M. Volkmer, A. Weins, M. Pollak and D. Weitz (2008). *Dynamic Viscoelasticity of Actin Cross-Linked with Wild-Type and Disease-Causing Mutant α-Actinin-4*. Biophys. J., 95:4915–4923.

[Wilhelm and Frey, 2003] Wilhelm, J. and E. Frey (2003). *Elasticity of stiff polymer networks*. Phys. Rev. Lett., 91(10):108103.

[Woolner et al., 2008] Woolner, S., L. L. O'Brien, C. Wiese and W. M. Bement (2008). *Myosin-10 and actin filaments are essential for mitotic spindle function*. JCB, 182:77–88.

[Wu et al., 2006] Wu, S., Y. Yoshiko and F. D. Luca (2006). *Stanniocalcin 1 Acts as a Paracrine Regulator of Growth Plate Chondrogenesis.* JBC, 281:5120–5127.

[Wu et al., 2009] Wu, Y.I., D. Frey, O. Lungu, A. Jaehrig, I. Schlichting, B. Kuhlman and K. Hahn (2009). *A genetically encoded photoactivable Rac controls the motility of living cells.* Nature, 461:104–108.

[Yang et al., 2006] Yang, L., D. Sept and A. Carlsson (2006). *Energetics and Dynamics of Constrained Actin Filament Bundling.* Biophys. J., 90:4295?4304.

[Yang et al., 2013] Yang, S., F. Huang, J. Huang, S. Chen, J. Jakoncic, A. Leo-Macias, R. Diaz-Avalos, L. Chen, J. Zhang and X. Huang (2013). *Molecular mechanism of fascin function in filopodial formation.* JBC, 288:274–284.

[Zanet et al., 2012] Zanet, J., A. Jayo, S. Plaza, T. Millard, M. Parsons and B. Stramer (2012). *Fascin promotes filopodia formation independent of its role in actin bundling.* JCB, 197:477–486.

[Zieve et al., 1980] Zieve, G.W., D. Turnbull, J. Mullins and J. McIntosh (1980). *Production of large numbers of mitotic mammalian cells by use of the reversible microtubule inhibitor Nocodazole: Nocodazole accumulated mitotic cells.* Exp. Cell Res., 126:397–405.

[Zopf et al., 2013] Zopf, C.J., K. Quinn, J. Zeidman and N. Maheshri (2013). *Cell-Cycle Dependence of Transcription Dominates Noise in Gene Expression.* PLoS Comp. Biol., 9:1–12.

[Zuchero et al., 2009] Zuchero, J.B., A. Coutts, M. Quinlan, N. L. Thangue and R. Mullins (2009). *p53-cofactor JMY is a multifunctional actin nucleation factor.* Nat. Cell Biol., 11:451–459.

List of Figures

Danke

Viele Dank an alle Personen, die zum Gelingen dieser Promotion beigetragen haben! Besonderer Dank gilt:

- Andreas Bausch für die Möglichkeit bei ihm die Doktorarbeit über spannende Zellprojekte am großartigen Lehrstuhl E27 durchzuführen!
- Pablo Fernández für die großartige Zusammenarbeit bei den Zellprojekten, vielen fruchtbaren Diskussionen, wertvollen Rat und Korrekturlesen!
- Simone Köhler für die Zusammenarbeit bei dem Fascinprojekt!
- Actin cytoskeleton group: Kurt, Christine, Martina, Schuppi, Jona, Volker, Simone, Pablo, Benni, Etienne, Rio, Carina, Katherina, Petra, Joanna, Ariane, Regi, Katharina, Katerina, Iris
- Volker Schaller, Esra Karaköse and Reinhard Fässler (MPI Biochemie) for cooperation on the EPLIN project
- C. Kuffer, Z. Storchova, C. Klingner and R. Wedlich-Sölnder (MPI Biochemie) for collaborations on the spindle projects
- Ludwig Eichinger (Universiät Köln) für die Zusammenarbeit beim Genexpressionsprojekt
- allen TAs insbesondere Gabi Chmel für die großartige Unterstützung bei der Zellkultur sowie Monika Rusp für die Aktinaufreinigung sowie für die Unterstützung beim Pipettieren der qPCR 96-Wells im biblischen Ausmaß!
- E22 und E27: danke für die Zusammenarbeit, aber insbesondere auch f́ur Fussball und Beachvolleyball sowie CCITC Meetings!
- meinen Eltern dafür, dass sie mir mein Studium der Physik überhaupt ermöglicht haben und mich immer voll unterstützten! Dank an meinem Vater fürs Korrekturlesen!

List of publications

1. P. Fernández, **M. Maier**, M. Lindauer, C. Kuffer, Z. Storchova, A.R. Bausch. Mitotic Spindle Orients Perpendicular to the Forces Imposed by Dynamic Shear. PLoS ONE 2011; 6e28965.
2. V. Schaller, K.M. Schmoller, E. Karaköse, B. Hammerich, **M. Maier**, A.R. Bausch. Crosslinking proteins modulate the self-organization of driven systems. Soft Matter 2013.
3. **M. Maier**, C. Klingner, R. Wedlich-Söldner, A.R. Bausch. The metaphase spindle elongates under dynamic shear forces. in preparation.
4. **M. Maier**, K. Müller, S. Köhler, K.M. Schmoller, O. Lieleg, A.R. Bausch. Controlling the mechanical properties of actin networks by changing the affinities of the actin binding protein fascin. in preparation.